Graduate School ETD Form 9
(Revised 12/07)

PURDUE UNIVERSITY
GRADUATE SCHOOL
Thesis/Dissertation Acceptance

This is to certify that the thesis/dissertation prepared

By Quazi Mohammed Rushaed Farooqi

Entitled
Injector Waveform Monitoring of a Diesel Engine in Real-Time on a Hardware in the Loop Bench

For the degree of Master of Science in Mechanical Engineering

Is approved by the final examining committee:

Sohel Anwar
Chair

Tamer Wasfy

Jaehwan (John) Lee

To the best of my knowledge and as understood by the student in the *Research Integrity and Copyright Disclaimer (Graduate School Form 20)*, this thesis/dissertation adheres to the provisions of Purdue University's "Policy on Integrity in Research" and the use of copyrighted material.

Approved by Major Professor(s): Sohel Anwar

Approved by: Sohel Anwar 12/5/11
Head of the Graduate Program Date

Graduate School Form 20
(Revised 9/10)

PURDUE UNIVERSITY
GRADUATE SCHOOL

Research Integrity and Copyright Disclaimer

Title of Thesis/Dissertation:

Injector Waveform Monitoring of a Diesel Engine in Real-Time on a Hardware in the Loop Bench

For the degree of Master of Science in Mechanical Engineering

I certify that in the preparation of this thesis, I have observed the provisions of *Purdue University Executive Memorandum No. C-22,* September 6, 1991, *Policy on Integrity in Research.**

Further, I certify that this work is free of plagiarism and all materials appearing in this thesis/dissertation have been properly quoted and attributed.

I certify that all copyrighted material incorporated into this thesis/dissertation is in compliance with the United States' copyright law and that I have received written permission from the copyright owners for my use of their work, which is beyond the scope of the law. I agree to indemnify and save harmless Purdue University from any and all claims that may be asserted or that may arise from any copyright violation.

Quazi Mohammed Rushaed Farooqi

Printed Name and Signature of Candidate

12/6/2011

Date (month/day/year)

*Located at http://www.purdue.edu/policies/pages/teach_res_outreach/c_22.html

INJECTOR WAVEFORM MONITORING OF A DIESEL ENGINE IN REAL-TIME ON A HARDWARE IN THE LOOP BENCH

A Thesis

Submitted to the Faculty

of

Purdue University

by

Quazi Mohammed Rushaed Farooqi

In Partial Fulfillment of the

Requirements for the Degree

of

Master of Science in Mechanical Engineering

December 2011

Purdue University

Indianapolis, Indiana

ACKNOWLEDGMENT

I would like to express my sincere gratitude to Mr. Benjamin Snyder, Dr. Sohel Anwar, Mr. Gary Salemme, for their continuous support, guidance and motivation throughout the project. I would also like to thank Mr. Matthew Butts, Mr. Perry Donnelly, Ms. Kimberly A. Walters, Mr. Jahangir Alam and the co-supervisors of my research committee Dr. Jaehwan (John) Lee and Dr. Tamer Wasfy for their support and motivation.

I appreciate the course instructors at IUPUI and Purdue University at West Lafayette for the knowledge and insight imparted to me. I'd like to thank Ms. Herrera Amanda who has provided me with the support in the administrative issues, and especially Ms. Valerie Lim Diemer and Ms. Ginger Lauderback for their support in thesis formatting and other critical administrative support.

TABLE OF CONTENTS

Page

Page

LIST OF TABLES

LIST OF FIGURES

Figure Page

Figure Page

Appendix Figure

Appendix Figure Page

Appendix Figure Page

Appendix Figure Page

ABSTRACT

Farooqi, Quazi Mohammed Rushaed. M.S.M.E., Purdue University, December 2011. Injector Waveform Monitoring of a Diesel Engine in Real-Time on a Hardware in the Loop Bench. Major Professor: Sohel Anwar.

This thesis presents the development, experimentation and validation of a reliable and robust system to monitor the injector pulse generated by an Engine Control Module (ECM) and send the corresponding fueling quantity to the real-time computer in a closed-loop Hardware In the Loop (HIL) bench. The system can be easily calibrated for different engine platforms as well. The fueling quantity that is being injected by the injectors is a crucial variable to run closed loop HIL simulation to carry out the performance testing of engine, aftertreatment and other components of the vehicle. This research utilized Field Programmable Gate Arrays (FPGA) and Direct Memory Access (DMA) transfer capability offered by National Instruments (NI) Compact Reconfigurable Input-Output (cRIO) to achieve high speed data acquisition and delivery. The research was conducted in three stages. The first stage was to develop the HIL bench for the research. The second stage was to determine the performance of the system with different threshold methods and different sampling speeds necessary to satisfy the required accuracy of the fueling quantity being monitored. The third stage was to study the error and its variability involved in the injected fueling quantity from pulse to pulse, from injector to injector, between real injector stators and cheaper inductor load cells emulating the injectors, over different operating conditions with full factorial design of experimentation and mixed model Analysis Of Variance (ANOVA). Different thresholds were experimented to find out the best thresholds, the Start of Injection (SOI) threshold and the End of Injection (EOI) threshold that captured the injector “ontime” with best reliability and accuracy.

Experimentation has been carried out at various data acquisition rates to find out the optimum speed of data sampling rate, trading off the accuracy of fueling quantity. The experimentation found out the expected error with a system with cheaper solution as well, so that, if a test application is not sensitive to error in fueling quantity, a cheaper solution with lower sampling rate and inductors as load cells can be used. The statistical analysis was carried out at highest available sampling rate on both injectors and inductors with the best threshold method found in previous studies. The result clearly shows the factors that affect the error and the variability in the standard deviations in error; it also shows the relation with the fixed and random factors. The real-time application developed for the HIL bench is capable of monitoring the injector waveform, using any fueling ontime table corresponding to the platform being tested, and delivering the fueling quantity in real-time. The test bench made for this research is also capable of studying injectors of different types with the automated test sequence, without occupying the resource of fully capable closed loop test benches for testing the ECM functionality.

1. INTRODUCTION

1.1 Background

The closed loop test in a Hardware in the Loop (HIL) bench is a very important step in the research and development, as well as, performance testing of engines. In order to carry out systems performance analysis, simulation of the model of the engine and all other components of the vehicle are run on a real-time computer. The Engine Control Module (ECM) is fed with all the sensor signals it expects in a real vehicle, in real-time, from emulated sensors using required hardware. The emulated sensor signal values correspond to the variable values being calculated in the simulation. Fueling quantity being injected in the engine is very important information for simulating the engine, which in turn affects the values of all the variable values that are sent to the ECM with emulated sensors. The ECM calculates the desired fueling quantity to be injected under current operating condition with the control algorithm downloaded into it, taking into account all the required sensor feedbacks at the previous time step. Finally the injector "ontime", the length of time the injector should inject the fuel into the cylinder, is looked up from a fuel-ontime table in the ECM. The fuel-ontime table contains the injector ontime corresponding to the fueling quantity that is to be injected and the operating common-rail pressure existing in the rail. The table is created based on the dynamics of the fuel systems. The corresponding electrical pulse is generated from the ECM to be sent to the injectors. In this research, the electrical signal is sent to the injector stators or the inductor load cells that emulates the injectors through necessary hardware to monitor the voltage signal. The signal is then converted by the Analog to Digital (A/D) converter in an Analog Input (AI) module. This research investigates whether the inductors, instead of the injectors, are appropriate to be used in a closed loop bench, if necessary correction measures can be taken to adopt this cheaper solution. It also investigates different

thresholds to find out the one that works best to capture the correct “ontime”. Analog input module NI-9205, along with Xilinx Virtex-5 Field Programmable Gate Arrays (FPGA) hardware and the Direct Memory Access (DMA) transfer capability in the Compact Reconfigurable Input-Output(cRIO) RT(Real-time) controller, have been utilized to capture the injector voltage signal generated by the ECM. Since the analog input module has a specification of +/-10V and the peak voltage of the injector signal is 12V, voltage dividers of 2V:1V ratios were used to capture the signals. The analog signals were logged at different data acquisition rates and the voltage signals were post-processed in MATLAB to obtain the ontime with various threshold approaches in the first investigation phase. The shot to shot variability, i.e. the variation of captured fueling quantity from pulse to pulse were compared with the standard deviation in different threshold approaches, as well as, different operating conditions. Different operating condition comprises different engine speed, common rail pressure, fueling quantity, injector or inductor load cells on all six injectors or inductors. In the next phase, a real-time application, along with the FPGA bitstream that imprinted the desired circuitry into the hardware, was built, compiled and deployed to the real-time target that could interpret the fueling quantity from the analog signals. The FPGA circuitry allowed generation of Engine Speed Signal(ESS) and Engine Position Signal(EPS) to be generated to simulate crank shaft rotation in the engine, corresponding to the engine speed. The real-time application used the double threshold approach, since it was concluded from the previous study that, the double threshold approach yields better accuracy and lower variability in capturing the correct fueling quantity. Finally, the error and variability present at highest sampling rate available was studied with 95 percent statistical significance with full factorial design of experimentation (DOE) and three-way, as well as, mixed model Analysis of Variance (ANOVA) on both injectors and inductors at various operating conditions. The relation between the error and the factors, as well as, the relation between the variability in standard deviation of error percent with the factors were found out with thirty six steady state operating points. Based on statistical results obtained, recommendations have been made at the end of the study.

1.2 Literature Review

The research involved use of FPGA based data acquisition system having different threshold approach with different FPGA configurations of circuitry. FPGA allows using its prebuilt logic blocks and programmable routing resources, to configure the silicon chips to implement custom hardware functionality [1] providing hardware-timed speed and reliability. The real-time HIL simulation requires hardware timed speed and reliability, which was only possible with FPGA. Reyneri, et al. [2] presented their work with a complete HIL test bench for a common rail injection system where they demonstrated the codesign techniques that integrated co-design and co-simulation of hardware(HW) and software(SW) which constitutes the HIL bench. They used eight FPGA's, one PC, one A/D, one Digital to analog(D/A) board and a data acquisition board, in the test bench, in addition to the common rail test bench and the co-simulation in CodeSimulink environment. Predefined voltage waveform computed on the basis of the required current waveform and the electrical model of the injector was sent to the injectors. Unlike this research, that aims towards testing the ECM performance, which requires the injected fueling quantity to be sensed and fed back to the software simulation running in the RT, [2] uses ad-hoc hardware signal generator implemented on FPGA and drives as many H bridges as there were injectors. They utilized 10Hz commercial A/D board into the PC, only to be displayed on the PC monitor, i.e., they have used open-loop generation of current waveform. However, they tuned the inductor load cells, i.e. R-L circuits with estimated R and L values. They employed neuro-fuzzy methodologies that characterized the injectors, i.e. the electrical parameters, in order to tune the inductor load cells that allowed them to weight the fuel injected with cheaper load cells and still obtain appreciable precision. FPGA and 8-channel A/D converter with about 20kHz sample rate was used during the injector characterization process.

Saldaña-González, G. et al. [3] presented FPGA based hardware implementation that takes the digitized voltage signals produced by the data acquisition electronics of the photo multiplier tubes and process them to allow identifying events and to determine the strength and positions of the interactions based on the logic of anger to form a planar

image that allows reconstruction of 2D image for medical diagnostics in a gamma camera in real-time. Pozniak and Krzysztof [4] presented the application of FPGA based multi-channel, distributed, synchronous measurement systems for triggering and data acquisition used in high-energy physics experiments. Turqueti et al. [5] presented design and implementation of a 52 microphone MEMS array, embedded in an FPGA platform with real-time processing capabilities.

The statistical analysis tool used in this research was Analysis of Variance (ANOVA) with fixed factors, as well as, random factors. Mixed model ANOVA, one of the ways to carry out multivariate ANOVA, was used that took into account the random factors in addition to the fixed factors. In the literature, ANOVA has been found to have been widely used to study the variation of dependent variables and the effects of factors on this variation, especially in the research in medical, dental, biomedical, biomechanical and material processing applications. One of those research done by Kulas, Anthony et al. [12], where they carried out ANOVA to observe the effects of added trunk load and corresponding trunk position adaptations on lower extremity biomechanics during drop-landings. Twenty-one recreationally active subjects were instrumented for biomechanical analysis. Subjects performed two sets of eight double-limb landings with and without 10% body weight added to the trunk. On lower extremity dependent variables, 2(condition: no load, trunk load) and 2 (group: trunk extensors vs. trunk flexors) ANOVAs were performed. Condition by group interactions at the hip showed differing responses to the added trunk load between groups where the trunk extensor group decreased hip extensor efforts (11-18%) while the trunk flexor group increased hip extensor efforts (14-19%). The trunk load increased biomechanical demands at the knee and ankle regardless of trunk adaptation group. However, the percent increases in angular impulses and energy absorption in the trunk extensor group were 14-28% while increases in the trunk flexor group were 4-9%. Given the 10% body weight added to the trunk, the 14-28% increases at the knee and ankle in the trunk extensor group were likely due to the reduced hip extensor efforts during landing. Mohammadi, Aminollah et al. [12] studied the effects of several factors on the material removal rate in the wire electrical discharge

machining process. The factors considered to carry out the Design of Experiment (DOE) were power, time-off, voltage, servo, wire speed, wire tension, and rotational speed. ANOVA, as well as, regression analysis were performed on experimental data.

1.3 Limitations of Current Systems

The current HIL bench receives the fueling quantity through CUTY (A Cummins proprietary software to communicate with the ECM) and Controller Area Network (CAN) bus that has inherent latency in delivering the data; it is also weak in terms of robustness. The other approach available is to read the fueling quantity through Nexus port, which is very expensive to implement. Besides, changing the platform will require the user to change the system to accommodate the new calibration in order to read a different memory location. Therefore, using a real injector load or an emulated load with inductors and using a data acquisition system to capture the injector signal, satisfy the purpose of HIL simulation more appropriately, which was pursued in this research.

1.4 Objective

The objective of the research is to develop a system that will be part of the closed loop HIL bench, capable to monitor the electrical injection signal generated by the ECM, interpret the signal into the corresponding fueling quantity intended to be injected and finally deliver the corresponding fueling quantity in real-time without adding much latency to the entire system. It is also important to investigate the variability and inaccuracy inherent in the injector monitoring process, across different configuration of the proposed system. It is required to determine the most cost effective and reasonably accurate configuration that can be applied to several closed loop HIL benches, provided, the benches will be using different calibrations and engine platforms. Another objective is to find out if the inductor load cells that emulate the injectors is adequate to be used on HIL bench. A statistical analysis is needed to evaluate the cost of accuracy involved, if the cheaper inductors instead of the injectors are used. It is also required to find out if the

inductor load cells or the injectors show certain offset that can be corrected on the benches through proper tuning, which in turn requires investigating the effect of factors on the error as well. It is also important to determine how much variability is present from pulse to pulse, from injector to injector and over different operating conditions. The accuracy in the system with different approaches is investigated. Finally, an automated test bench and test sequence needs to be developed in order to study the performance of the proposed system with new generation of injectors and new calibrations for different engine platforms in future.

2. EXPERIMENTAL SETUP AND SIMULATION MODEL

2.1 Diesel Engine and the Importance of Fuel Injection System

Diesel engine is an internal combustion engine that produces mechanical energy from the chemical energy stored in the fossil fuel called diesel. The property of diesel fuel is different from the gasoline used in spark-ignited (SI) engine, that allows the compression-ignition (CI) engines, known as diesel engines, to generate energy by compressing air to a high pressures then injecting a small amount of fuel into this highly compressed air. The high temperature created when air is compressed causes the small amount of highly atomized injected fuel to evaporate. Mixing with the hot surrounding air in the combustion chamber, the evaporated fuel reaches its auto-ignition temperature and goes through combustion process to release the energy that is stored in that fuel. Most diesel engines are four stroke engines, i.e. it takes four strokes for each power stroke in the four-stroke engines.

The performance of a diesel engine, both in terms of thermal efficiency and emission, is heavily dependent on the fuel system that delivers fuel into the engine cylinder; which takes care of precisely controlling the injection timing, correct pressure of injection to ensure proper mixing of air and fuel taking into account proper fuel atomization, and other critical parameters. Diesel engines such as those made by Cummins Inc. are controlled with superior control system to ensure precise control of the fuel injection into the cylinder with the advanced fuel system that constitutes common-rail, pump and high precision injectors. The necessity to reduce fuel consumption, exhaust gas emissions and engine noise has led to advanced technologies being employed in the fuel systems, replacing the mechanical injection system.

In general, the common-rail architecture employs a common pressure accumulator or high pressure storage, called rail. This rail is fed by a high pressure fuel pump that could be driven at crankshaft speed (engine or twice the camshaft speed). Sometimes high pressure radial pump, independently from the engine rate generates high pressure at the rail. High pressure injection lines connect the common rail to the fuel injectors. ECM controls the pressure at the rail through inlet metering valve (IMV). The ECM generates the injection pulse, which controls the opening of the injectors with electronic actuators. The ECM calculates the fuel quantity needed based on a predefined characteristic curve, the engine model, the driver's intentions via the accelerator position, engine speed, torque, temperature, acceleration, etc.

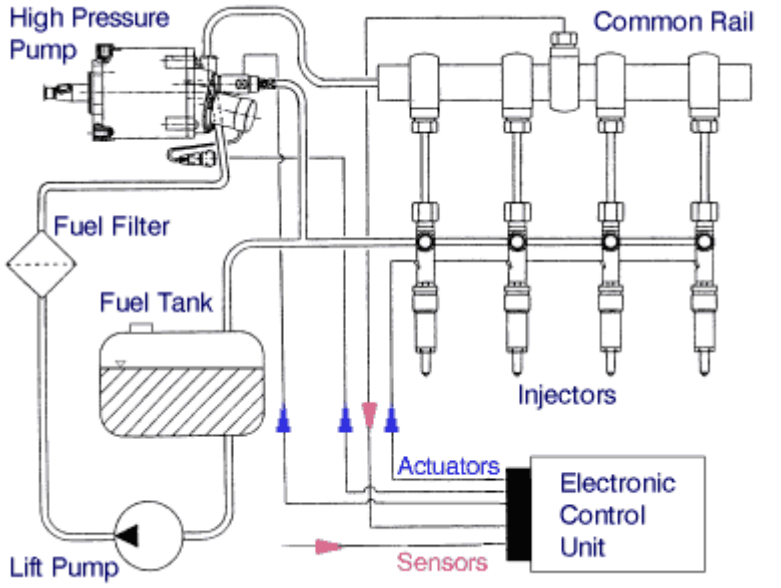

Figure 3.1 Schematic of the common-rail injection system

The electronic control facilitates flexibility in injection timing and metering control, reduced cycle-to-cycle and cylinder-to-cylinder variability, as well as, tighter control tolerances and increased accuracy over very long periods of operations. Figure 3.1 shows the layout of the common-rail architecture of the fuel injection system[6].

The common rail system includes the following components (Figure 3.1):

- High pressure fuel pump

- Rail for fuel storage and distribution
- Injectors
- Electronic control Module (ECM).

An electric or camshaft driven low pressure lift pump takes the fuel from the fuel tank, pumps it through a fuel filter and feeds the high pressure pump. A solenoid operated metering valve controls the amount of fuel entering the high pressure pump. The high pressure pump is driven by the engine and delivers fuel at a constant pressure to the rail. A pressure sensor installed in the rail monitors the fuel pressure. The signal is used by the ECM to control the rail pressure by acting on both the pressure regulator and the inlet metering valve, with excess fuel returned from the pressure regulator to the fuel tank. Other early systems used little or no inlet metering to the high pressure pump and the temperature of the fuel returning to the tank could be very high (sometimes in excess of 100°C)—an important consideration for the use of fuel additives or emulsified fuels in diesel engines.

The rail serves as a fuel accumulator to maintain a relatively constant pressure at all fueling rates used by the engine. The fuel volume in the rail also dampens pressure oscillations caused by the high-pressure pump and the injection process. From the rail, the fuel is supplied at constant pressure to the injectors via high pressure pipes. The ECM generates current pulses which energize each injector solenoid valve in sequence and define the start and the end of each injection event per engine cycle. The common rail system can generate more than one injection per engine cycle and gives more flexible control of the rate of injection compared to other injection system design.

2.2 Development of the Injector Waveform Monitoring System

This research addresses the most important attribute of the fuel injection system, i.e. metering of correct amount of fuel into the cylinder. The control system calculates the correct amount of fuel to be injected by the fuel system in terms of fuel quantity, which is implemented by converting the fuel quantity into duration in time, to inject the fuel at a given common-rail pressure and operating condition. In order to carry out HIL

simulation, the simulation model needs the accurate information of the fuel being injected, in order to carry out the accurate calculation to simulate the engine performance. The ECM generates the fueling signal in terms of electrical pulse, to the injectors. The voltage waveform constitutes a high initial boost voltage to overcome the inertia of the injector mechanics, followed by a lower constant voltage which holds the injector nozzle to open position for the desired period of time. The hardware used in this research senses this electrical pulse and real-time system that utilizes the FPGA personality and DMA transfer, converts the pulse back into the fuel quantity. The electrical signal captured by the sensors does not distinctly indicate the start of injection and end of injection, which is the critical parameter to be figured out in this research, in order to calculate the most accurate measurement of injector on-time. The injector on-time is the period of time the injector remains open to allow the fuel to be injected.

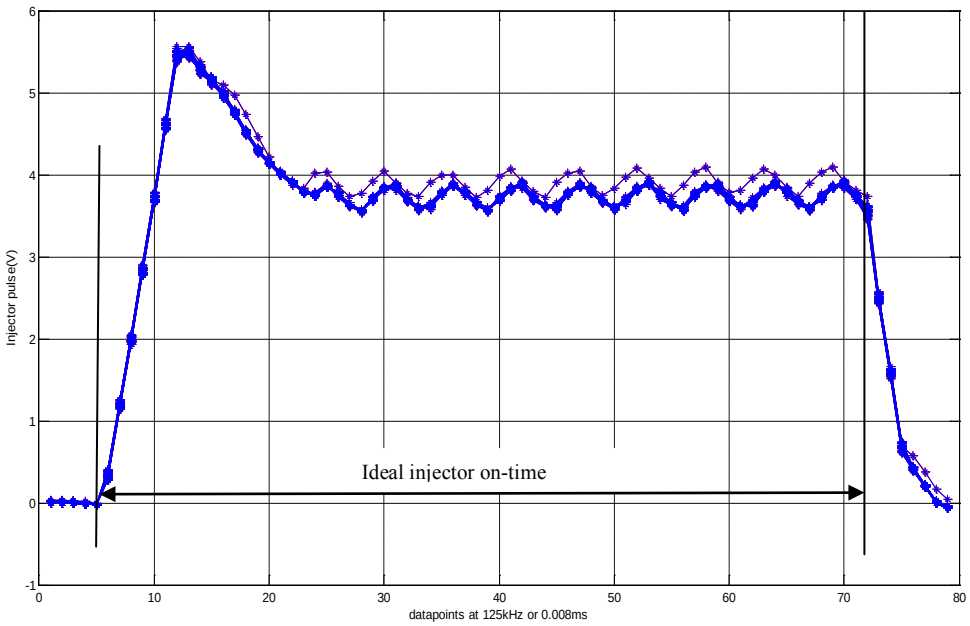

Figure 3.2 Fifty injector pulses captured by the system overlayed on each other

The injection pulse captured is shown in Figure 3.2. Ideally, the injection on-time corresponds to the length of time between the time the injector signal starts to rise from zero voltage and the time it starts to fall from the steady voltage value that is held during

the injection period. Figure 3.2 clearly delineates the challenge involved in identifying the start of injection and end of injection.

The Start of Injection (SOI) can be identified, as soon as the voltage value goes over 0V, however, the noise in the analog signal captured causes error in the identification of SOI. On the other hand, the steady value of voltage, maintained at the period of time when the injector is held open, is noisy. The approaches taken to identify the End of Injection (EOI) were to consider the slope of the voltage drop, or identify a threshold value for EOI. The latter approach turned out to be more suitable.

Another important parameter investigated in this research is the variability involved in the injector pulses captured by the proposed method. The importance of delivering the correct fuel quantity with consistency is very important in the hardware-in-the-loop test. Error in fueling quantity deteriorates the accuracy of simulation result, especially when the engine is simulated to run over a long period of time. The error may accumulate and important result, such as, fuel efficiency calculated from the simulation will become erroneous. The standard deviation in the captured ontime being held at a steady state indicated the repeatability of the injection pulse monitoring system. The fuel-quantity being injected by the ECM was overridden through the CAN bus, while the system captured the injector pulses. The fuel quantity being identified is expected to be exactly the same as the value being overridden on the ECM. However, the inherent variability was calculated by the standard deviation. Later, injection on-time was directly overridden instead of the fuel-quantity. The on-time was held at a steady value and the system logged the on-time captured by the proposed system. Different variability was obtained with different approaches of injection on-time capture.

The research aims at identifying the optimal approach, in terms of cost of implementation, the accuracy, repeatability and variability involved in capturing the correct fuel.

The simplified architecture of the HIL bench is shown in Figure 3.3. On the HIL bench, the vehicle simulation is run on the RT computer, the resulting calculated variables, the ones that are sensed by the sensors in a real world environment on a vehicle, are converted into electrical signals with emulated sensors by the appropriate hardware. These signals are sent to the ECM in real-time closed loop simulation environment.

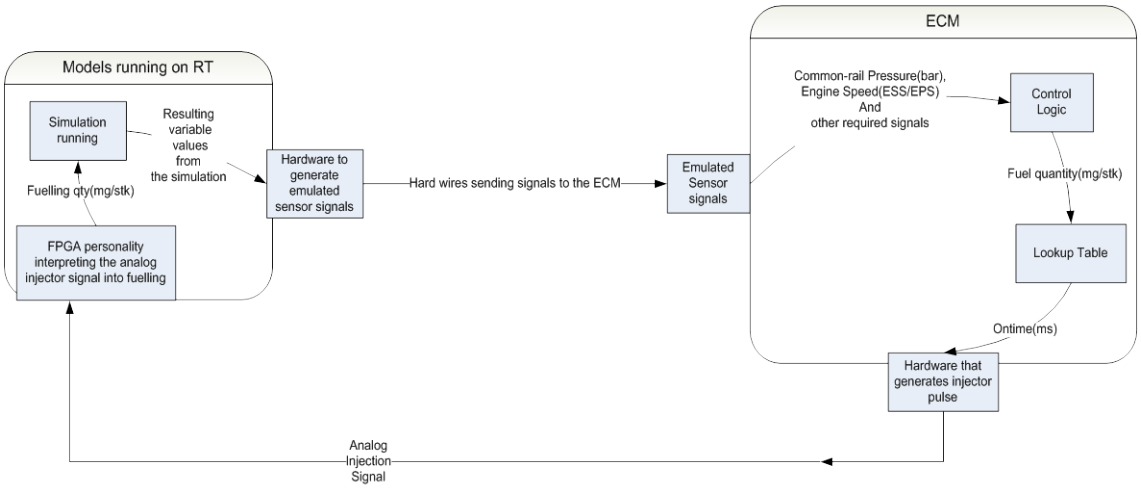

Figure 3.3 Layout of the existing HIL bench

The ECM calculates the fueling quantity to be injected, based on the sensor signals, such as, throttle position, torque requirement. Other actuator signals generated by the ECM are not shown on the diagram. The fueling quantity is converted to the duration in time for the injector to stay open. The lookup table used to obtain the injector on-time in milliseconds(ms) corresponding to the required fueling quantity is called fueling on-time table. The injector signal generated from the ECM, needs to be fed back to the RT computer to close the loop. The research investigates how the injector signal can be interpreted into the correct fueling quantity, that the control algorithm calculates, in order to be delivered to the RT computer to input to the simulation.

Since the injector signal generated by the ECM is of importance in this research and the whole HIL bench for closed loop testing is not required, a separate bench was

developed for this research, to run tests through different steady state operating points of different variables, in an open loop testing environment.

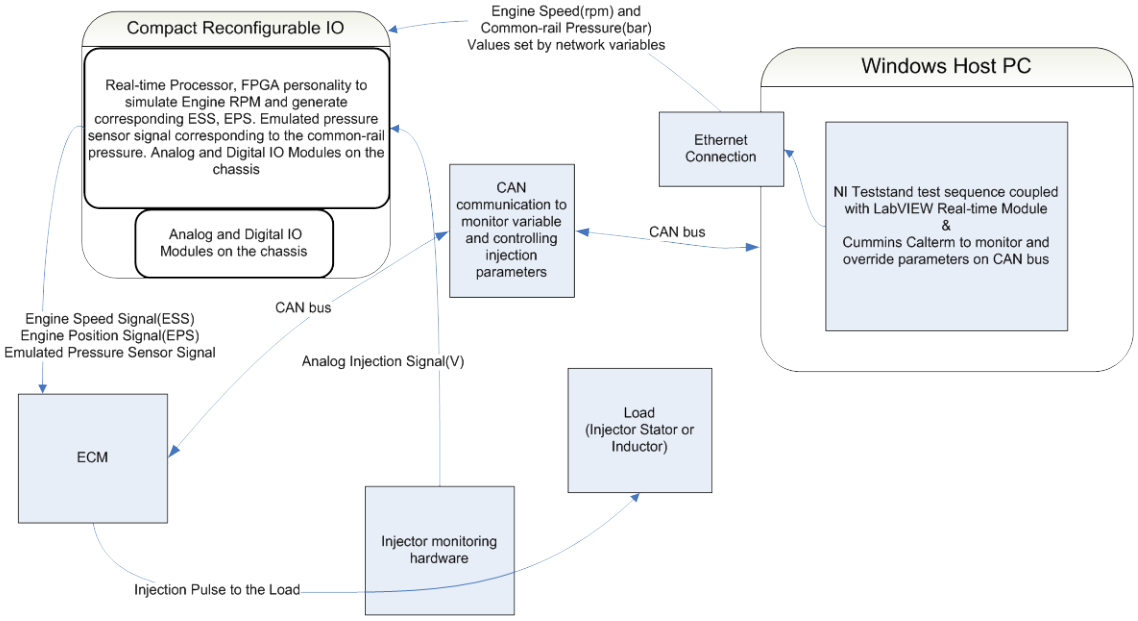

Figure 3.4 Layout of the bench for this research

Figure 3.4 shows the architecture of the closed loop test bench developed to test the proposed measurement system. The host PC works as a supervisory controller that communicates with the cRIO over the ethernet and with the ECM over the CAN bus. The test sequence, that runs on the host PC, goes over different steady state points. The steady state points consist of different engine speed, rail pressure, fueling quantity or injector ontime. It also makes the RT application, that runs on the cRIO, create separate files with individual filenames, at each steady state points. It also makes sure each channel is logged sequentially and that the data is logged separately for each of the injectors. The cRIO generates EPS/ESS signal corresponding to the engine speed commanded from the host PC. It also generates the emulated pressure sensor signal corresponding to the pressure value commanded from the host PC. The ECM generates injector pulses, taking into account the engine speed, rail pressure and the fueling quantity or injector ontime being overridden by the host computer. The electrical injection signal is drained into the

injector stator through the hardware that allows the AI module to probe the voltage value of the electrical signal. The injector stators are replaced by inductor load cells that emulate the injectors. The voltage values were logged and later post processed to study the error and variability.

Different test sequences were developed in different stages of the experimentation. The real-time application contained the FPGA personality that generated the desired EPS/ESS signal, corresponding to the engine speed; The RT application switched over different channels of the analog modules, since the analog module had only one Analog to Digital converter, carrying out the DMA(Direct Memory Access) transfer from the FPGA module to the memory of the RT computer.

2.3 Test Bench

Figure 3.5 shows the injectors and Figure 3.6 shows the inductor load cells. injector stators were used from production injectors. The inductor load cells contain electrical circuitry to emulate the electrical characteristics of the injectors. Figure 3.7 shows the hardware that provided the electrical protection and necessary systems to transform the injector signal to low power DC voltage, for the AI module. It also provided the high power supply to drive the electrical injectors or load cells. The NI cRIO-9014 [7], along with NI 9111 [8] chassis, having AO, AI, DIO cards are shown on the right side of the hardware in Figure 3.7. The NI 9205 [9] analog input module has been a key feature for in this research. The NI 9205 features 32 single-ended or 16 differential analog inputs, 16-bit resolution, and a maximum sampling rate of 250KS/s. Each channel has programmable input ranges of ±200mV, ±1, ±5, and ±10V. To protect against signal transients, the NI 9205 includes up to 60 V of overvoltage protection between input channels and common (COM). In addition, the NI 9205 also includes a channel-to-earth-ground double isolation barrier for safety, noise immunity, and high common-mode voltage range. The 4-slot cRIO-9111 [8] chassis has Xilinx Virtex-5 reconfigurable I/O FPGA core, capable to automatically synthesize custom control and

signal processing circuitry using LabVIEW. The research employed NI 9264 [10] analog output module to generate the pressure signal, in order to emulate the pressure sensor. The ECM requires the pressure signal to calculate the injector on-time (ms) in order to inject certain amount of fuel. The research also utilized NI 9401 [11] 8 channel, 5 V/TTL high speed biderictional digital I/O module to generate the Engine Position Signal(EPS) and Engine Speed Signal(ESS) to feed the ECM with the simulated engine speed. The test setup includes the six voltage dividers to accommodate the voltage provided by the hardware into the NI 9205 module [9]. Other hardware used in the bench were the in-house power supply for the ECM and the electrical hardware, the Tektronix TDS 2024B oscilloscope, PEAK adapter to convert CAN messages and transfer into the computer, the CAN terminators to establish the CAN bus etc.

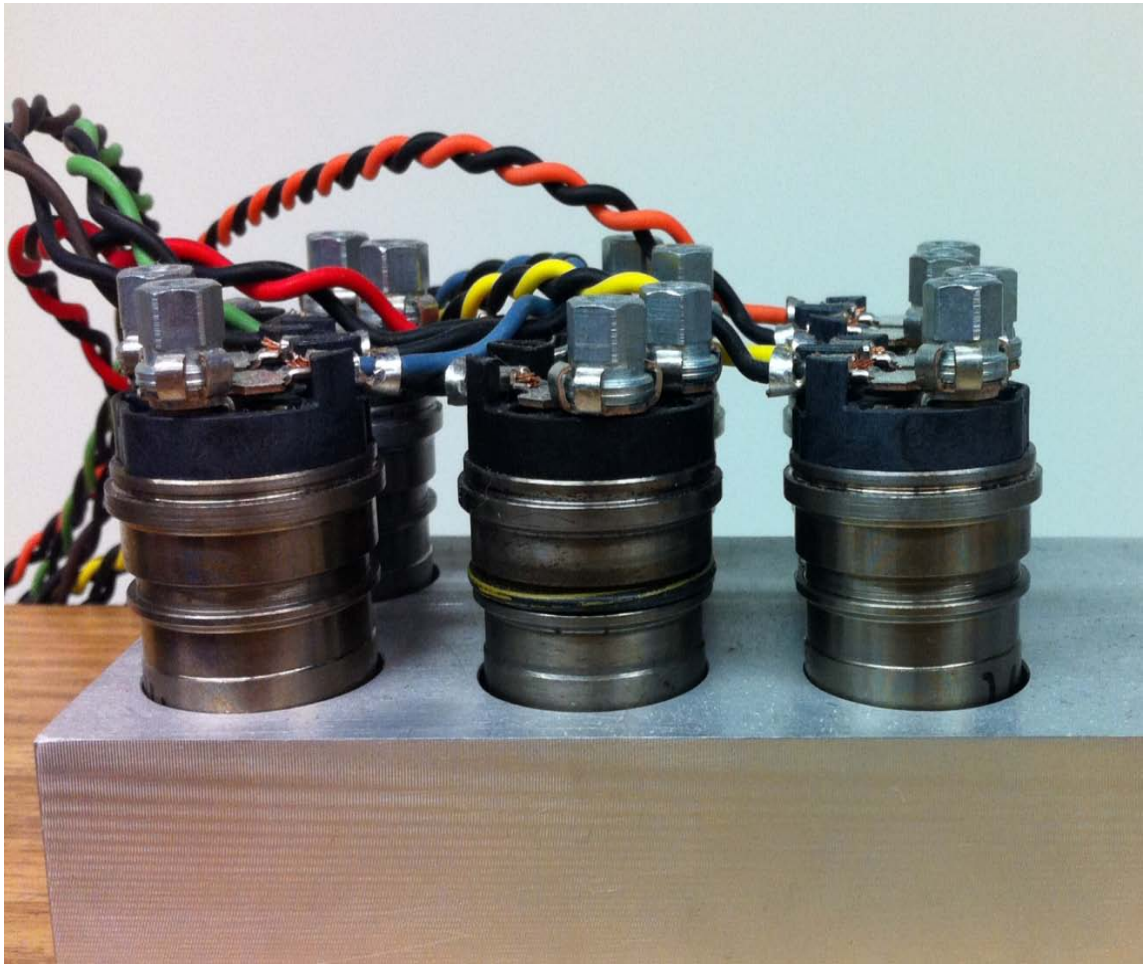

Figure 3.5 Injector stators used as load

Figure 3.6 Inductors that emulates real injectors as load

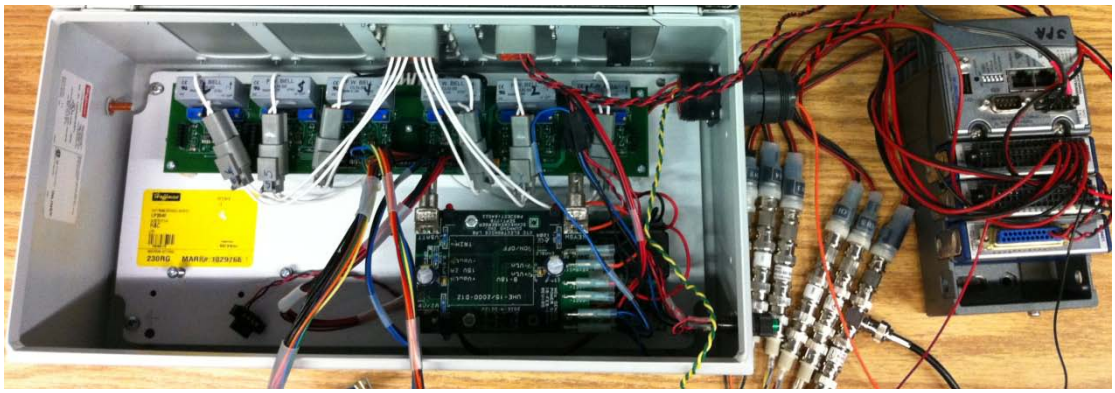

Figure 3.7 Hardware to capture the injection signal

2.4 National Instruments Compact Reconfigurable Input Output(CRIO) System

This research employs a CRIO system offered by National Instruments. It contains an integrated real-time controller and a chassis, with a communication interface with a highly optimized reconfigurable FPGA circuitry that contains slots for different modules. National Instruments facilitates users involved in the development of mechatronic control systems by providing hardware and software solutions in order to accelerate the development and testing of such systems. This supports creating real time applications in LabVIEW, building and deploying the files into the RT system to

implement real time environment for any user defined HIL Bench which falls into the targeted I/O criteria. The CRIO system used in this research is a real-time system for performing fast function prototyping. Following paragraphs explains few specifications of the National Instruments CRIO real time target.

2.4.1 Compact RIO

The cRIO [7] has the ability to allow the user to develop, test, and optimize control functions rapidly and reliably in real time with ethernet and serial interfaces. The NI cRIO-9014 embedded real-time controller features an industrial 400 MHz freescale MPC5200 real-time processor for deterministic, reliable real-time applications. The cRIO-9014 contains 128 MB of DRAM memory and 2 GB of nonvolatile storage. The cRIO embedded controller is designed for extreme ruggedness, reliability, and low power consumption with dual 9 to 35 VDC supply inputs that deliver power to the CompactRIO chassis/modules and a -40 to 70 °C operating temperature range. The cRIO-9014 accepts 9 to 35 VDC power supply inputs on power-up and 6 to 35 VDC power supply inputs during operation, so it can function for long periods of time in remote applications using a battery or solar power.

With the 10/100 Mbits/s ethernet port, one can conduct programmatic communication over the network and built-in Web (HTTP) and file (FTP) servers. For additional storage capability, the cRIO-9014 has a full-speed USB host port to which one can connect external USB-based storage media (flash drives and hard drives) for embedded logging applications requiring additional storage. Also, there is a fault-tolerant file system embedded in the cRIO-9014 that provides increased reliability for data-logging applications.

The cRIO-9014 runs the NI LabVIEW Real-Time Module on the VxWorks real-time operating system (RTOS) for extreme reliability and determinism. With the cRIO-9014 real-time controller, one can use the leading VxWorks RTOS technology to quickly

design, prototype, and deploy a customizable commercially available off-the shelf (COTS) embedded system using LabVIEW graphical programming tools.

2.4.2 Test Sequence on the Host Computer and Real-Time Application on CRIO

The test sequence written on NI TestStand on the host PC communicates with the real-time application over local network with shared variables. At the beginning, it establishes CUTY session, which sets up the communication with the ECM over Controller Area Network (CAN) in order to override calibration parameters, as well as, monitor the values of engine speed, fueling quantity and pressure that is being registered by the ECM. The test sequence was refined through trial and error method to make it more efficient in carrying out the automated tests in less time. Since the FPGA runs in 40MHz, real-time processor runs at 400MHz, the rate of communication between the host PC and the real-time computer is 100Mb/s and the DMA transfer rate reaches up to 20Mb/s. It was found out that the engine speed and pressure values were very consistent in reading the correct values being written over the network, however, some time was required for the network shared variables to take the new values into account. Required time was allowed in the test sequences to allow the sensor values to stabilize at a steady state point and the test sequence was made open loop in terms of engine speed and pressure. The fueling quantity overridden with the calibration parameter over CAN bus proved to require the test sequence to be in closed loop. Therefore, the loop was closed on the filename and fueling quantity in the final test sequence that ran the randomized factor levels in the full factorial DOE. The real-time application created separate Technical Data Management-Streaming (TDMS) files for each of the steady states with different file names. The flowchart of the test sequence running on the host computer is shown in Figure 3.8 that communicates with the network shared variables. The flowchart of the real-time application running on the real-time cRIO is in Figure 3.9. The test sequence was run separately with the injectors and inductors, connected with the hardware that allows the analog module to probe the voltage signal. After the sequence is done, the tdms files created at each steady state points were converted to .mat file to be

post processed in Matlab. Later, code was developed to run on the real-time computer, that reads voltage values from the FIFO, used double threshold to extract the injector ontime. The injector ontime was converted back to the fueling quantity by the reverse fuel-on time table being stored at the real-time computer. This research involved studying the feasibility of using the data acquisition system that uses the voltage signal to interpret into the fueling quantity. Therefore, implementation of delivering the fueling quantity that can ideally be synchronized with the crank angle was left to be done in future.

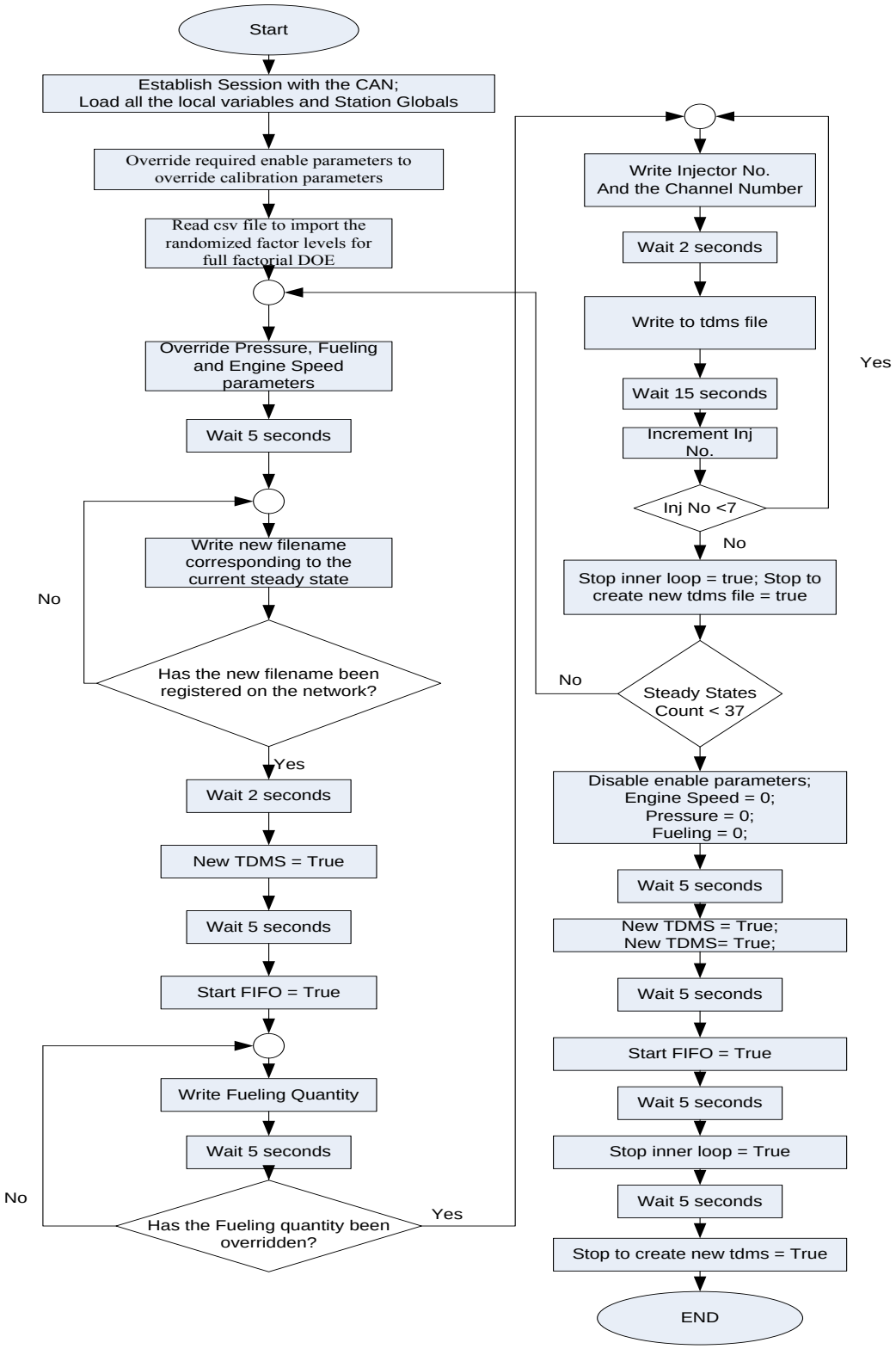

Figure 3.8 Flowchart of the test sequence on the host computer with NI Teststand

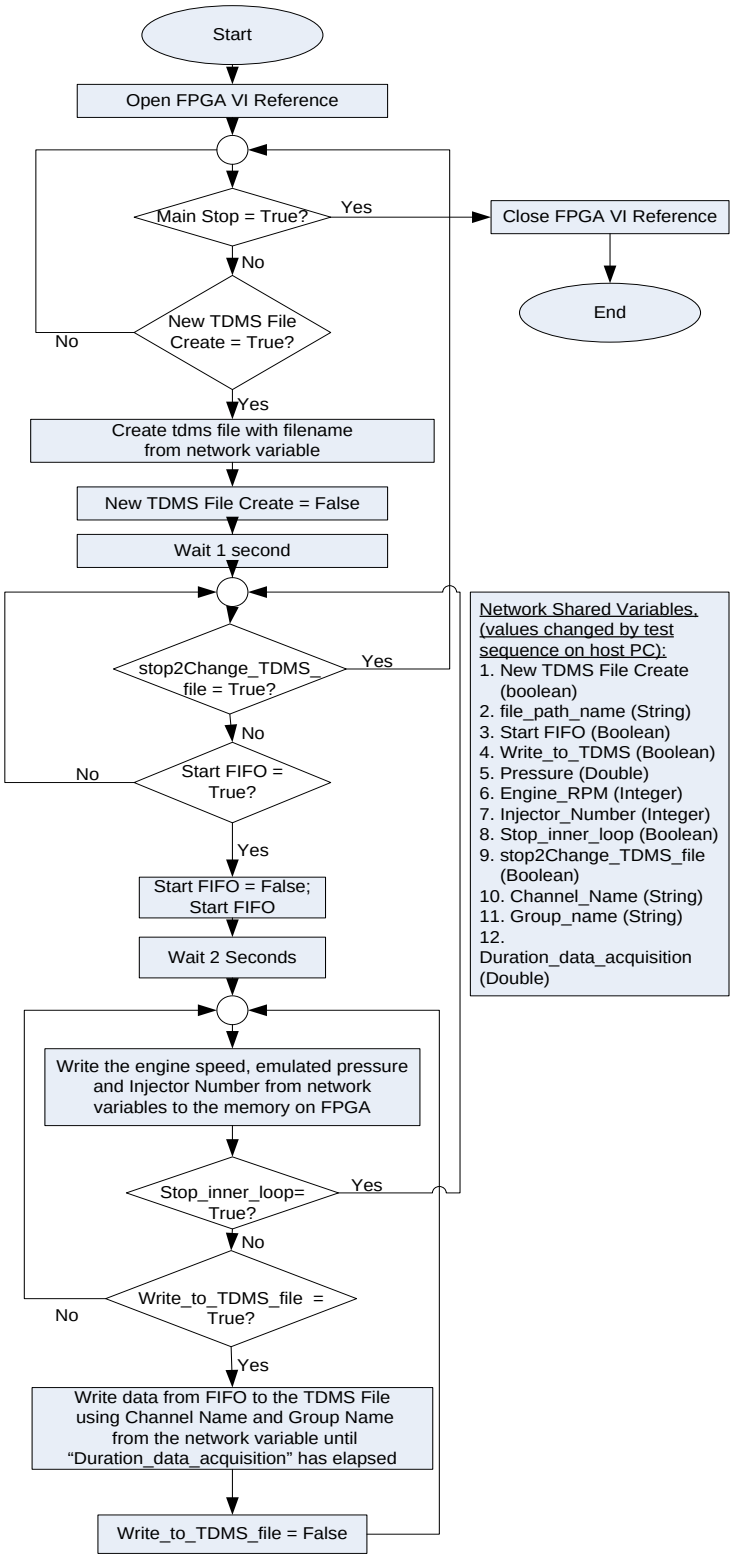

Figure 3.9 Flow Chart of the code running in real time on cRIO

2.5 Experimental Procedure

The experimentation was carried out on the experimental bench to find the most cost effective, efficient, recalibrate-able and reproducible solution to the injector monitoring problem with the following variable parameters under consideration:

- Fuel quantity or injector on-time (ms)
- Engine speed
- Common-rail pressure
- Two different loads, i.e. injectors or cost saving inductors to simulate injectors
- Six different injectors or inductors
- Different thresholds

In order to implement the injector monitoring system in the HIL system, the system is required to maintain good accuracy in capturing the correct amount of fuel quantity over large range of fueling, engine speed, common-rail pressure with as little variation as possible. The research also investigates if the accuracy varies with injector or inductor. Since the system, if satisfies requirements, is going to be implemented in large number of hardware-in-the-loop benches, the cost of implementation is an important factor to consider as well.

The research begins with varying all the variables, consecutively ruling out some of the variations, if found to have insignificant influence over the accuracy of the system. The data acquisition hardware available from NI had limitation in sampling rate. Therefore, initially only one NI-9205 module with 20.8kHz sampling rate at each channel was considered to be used for all six channels.

To identify the start of injection and the end of injection, different thresholds were considered, narrowing down to the most effective approach. Initially, the end of injection was identified using the slope of injection pulse, which was not very successful, due to the noise involved in the signal captured. Therefore, thresholds were used to identify the SOI and EOI, having only one threshold for both ends or two thresholds. The initial

experiments show that, the influence of varying common-rail pressure is comparatively insignificant. Therefore, the tests were carried out at varying engine speeds and fueling quantities with different threshold approaches on both kinds of loads. The sampling rate turned out to be the most significant factor in the accuracy of the system. Since the injector on-time remains the same with the constant fueling quantity over varying engine speed, it was expected to have same accuracy. However, the experimental results show that, the accuracy varies over different engine speed.

Initially, tests showed that the accuracy of the system is not significantly dependent on common-rail pressure, therefore, tests were run at 1200bar common-rail pressure over different engine speeds and fueling quantities for both injector stators and the inductors, six of them each. The injection pulses were logged in the form of discrete voltage values with 20.8khz sampling rate at each injector channels with a precision of 1V, which was later increased to 0.0156V precision value. The injection voltage values were logged in .tdms format. National Instrument's data analysis software DIAdem script was used to convert the .tdms files to .mat files, in order to post process the data on Matlab. The fueling "ontime" was extracted using various single thresholds or double thresholds in MATLAB. Single threshold approach uses same threshold value for both SOI and EOI. The SOI threshold is the value that determines when the injection has started, i.e. as soon as the voltage value goes above the SOI threshold, the injection is considered to have started. Similarly, the EOI threshold is the value that determines when the injection has ended, i.e. as soon as the voltage value goes below the EOI threshold, the injection is considered to have ended. In the first phase of the experiment, the double threshold approach considered EOI at the point where the voltage value starts to drop from a steady value, i.e. instead of using a threshold to identify the EOI, the code considered five consecutive data points and if the voltage value kept on falling through five points, the third point was considered the EOI point. The test sequence goes over different values of engine speeds and fueling quantities to be injected. The extracted pulse lengths are measured in milliseconds. The mean of all the pulselengths are calculated for each injector channels at each state, in both cases of injectors and

inductors. The expected fueling "ontime" is the value overridden on the ECM. Therefore, the error in the fueling quantity was calculated at each of the states on the mean values using the following equation .

$$error\ (\%) = \frac{ontime_{mean\ ontime\ in\ a\ certain\ state} - ontime_{expected\ ontime(overridden\ value)}}{ontime_{expected\ ontime(overridden\ value)}} \times 100$$

2.6 Experimental Results

Due to confidentiality agreement with Cummins Inc. original fuel-ontime table cannot be published in this paper, therefore, a simplified fuel-ontime table is shown in Table 3.1 that assumes linear relations between fueling quantity and injector ontime, as well as, common-rail pressure and injector ontime.

Table 3.1 Simplified Fuel-Ontime Table with sample ontime (ms) at X=Fueling quantity (mg/stk) and Y=Common-rail Pressure (bar) that shows the trend

X/Y	0	300	400	500	600	700	800	900	1000	1100	1200	1300	1400	1500	1600.25	1800.25
0	0	0	0	0	0	0	0	0	0	0	0	0	0	0	0	0
0.88	16	15	14	13	12	11	10	9	8	7	6	5	4	3	2	1
1.69	17	16	15	14	13	12	11	10	9	8	7	6	5	4	3	2
3.5	18	17	16	15	14	13	12	11	10	9	8	7	6	5	4	3
5.5	19	18	17	16	15	14	13	12	11	10	9	8	7	6	5	4
9	20	19	18	17	16	15	14	13	12	11	10	9	8	7	6	5
16	21	20	19	18	17	16	15	14	13	12	11	10	9	8	7	6
25	22	21	20	19	18	17	16	15	14	13	12	11	10	9	8	7
33	23	22	21	20	19	18	17	16	15	14	13	12	11	10	9	8
38	24	23	22	21	20	19	18	17	16	15	14	13	12	11	10	9
45	25	24	23	22	21	20	19	18	17	16	15	14	13	12	11	10
51	26	25	24	23	22	21	20	19	18	17	16	15	14	13	12	11
68	27	26	25	24	23	22	21	20	19	18	17	16	15	14	13	12
86	28	27	26	25	24	23	22	21	20	19	18	17	16	15	14	13
120.44	29	28	27	26	25	24	23	22	21	20	19	18	17	16	15	14
160	30	29	28	27	26	25	24	23	22	21	20	19	18	17	16	15

2.6.1 Inductors as Load, Single Module with Lower Precision

Inductor load cells were used as load on the bench. The common-rail pressure was held constant at 1200bar and injector pulses were logged for 5 seconds at each state. The precision of analog voltage was 1V. The error is found to be lowest with single threshold at 2V Figure 3.10 and double threshold Figure 3.11. Remaining plots with the error percentages are shown in Figure A.1, Figure A.2, Figure A.3 in the Appendix.

It is observed that, if the inductors are used as a load, the injector pulse cannot be captured reliably. The shape of the pulse that are obtained were distorted and results in high amount of error. The error is pronounced at lower fueling quantity, which leads to the conclusion that, the sampling rate of 20.8khz (each channel) with a precision of 1V is not adequate to capture the fueling quantity with reasonable accuracy. The minimum fueling amount of 25mg/stk shows about 8% to 9% error when single threshold at 2V is used, the double threshold approach shows higher percentage error, since the pulses captured are not well defined when inductors are used. Therefore, if this amount of error is acceptable at higher fueling values for certain HIL application, it is cheaper to use the inductors as load and at the same time, single module is adequate to simultaneously log all six channels.

The second parameter to evaluate the performance of the system is the standard deviation in captured on-time. Single threshold at 2V and double threshold gives least variability shown in Figure 3.12 and Figure 3.13. Remaining experimental results are shown in Figure A.4, Figure A.5, Figure A.6 on the Appendix. Following figures plot the standard deviations of the pulse length, in terms of milliseconds of ontime, captured from pulse to pulse at each state on each injector. It is observed that, the variation does not follow a certain pattern, therefore, the fidelity of the data captured with this system is very low, in order to be used in HIL application.

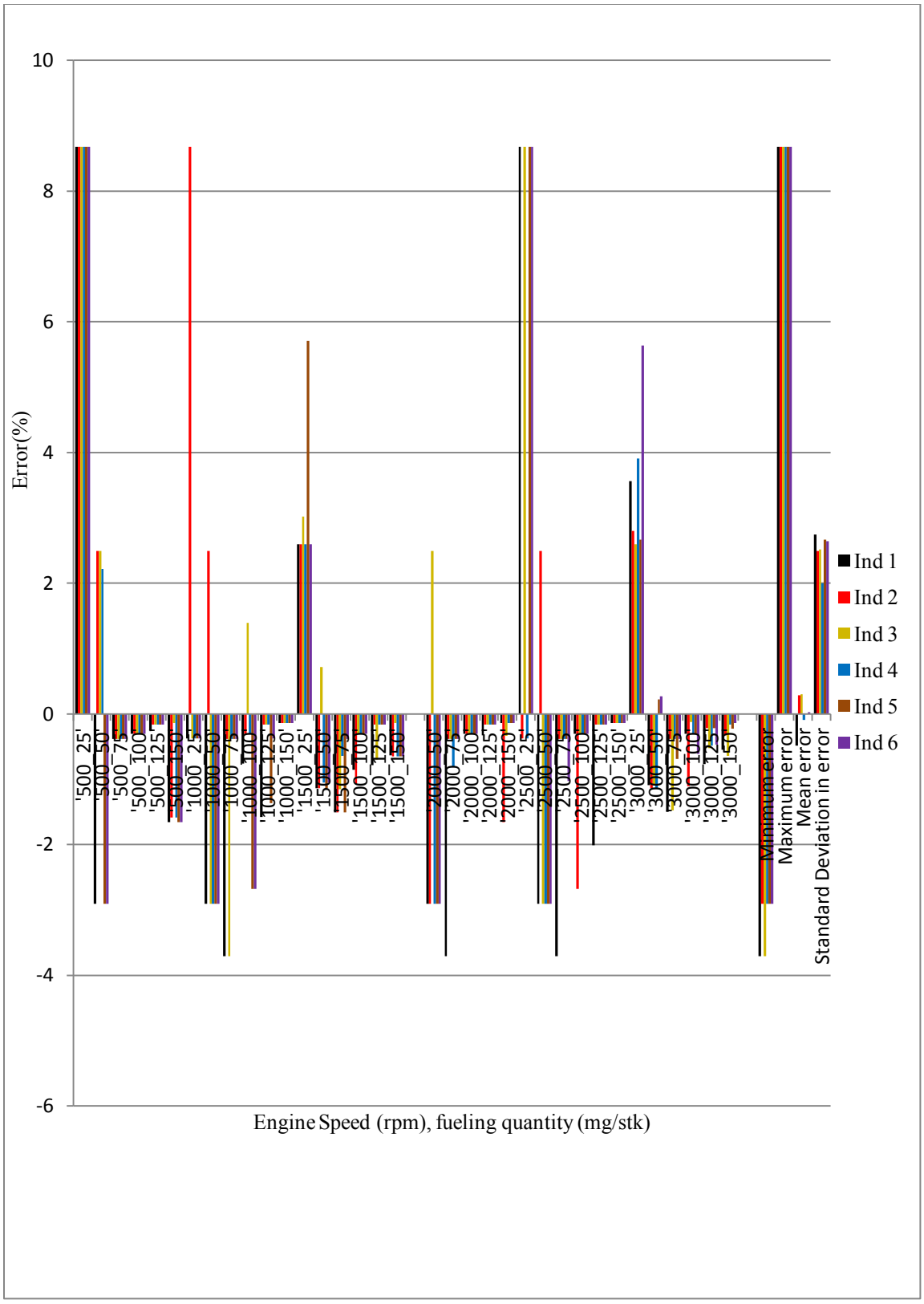

Figure 3.10 Error percentage with single threshold at 2V(Inductor)

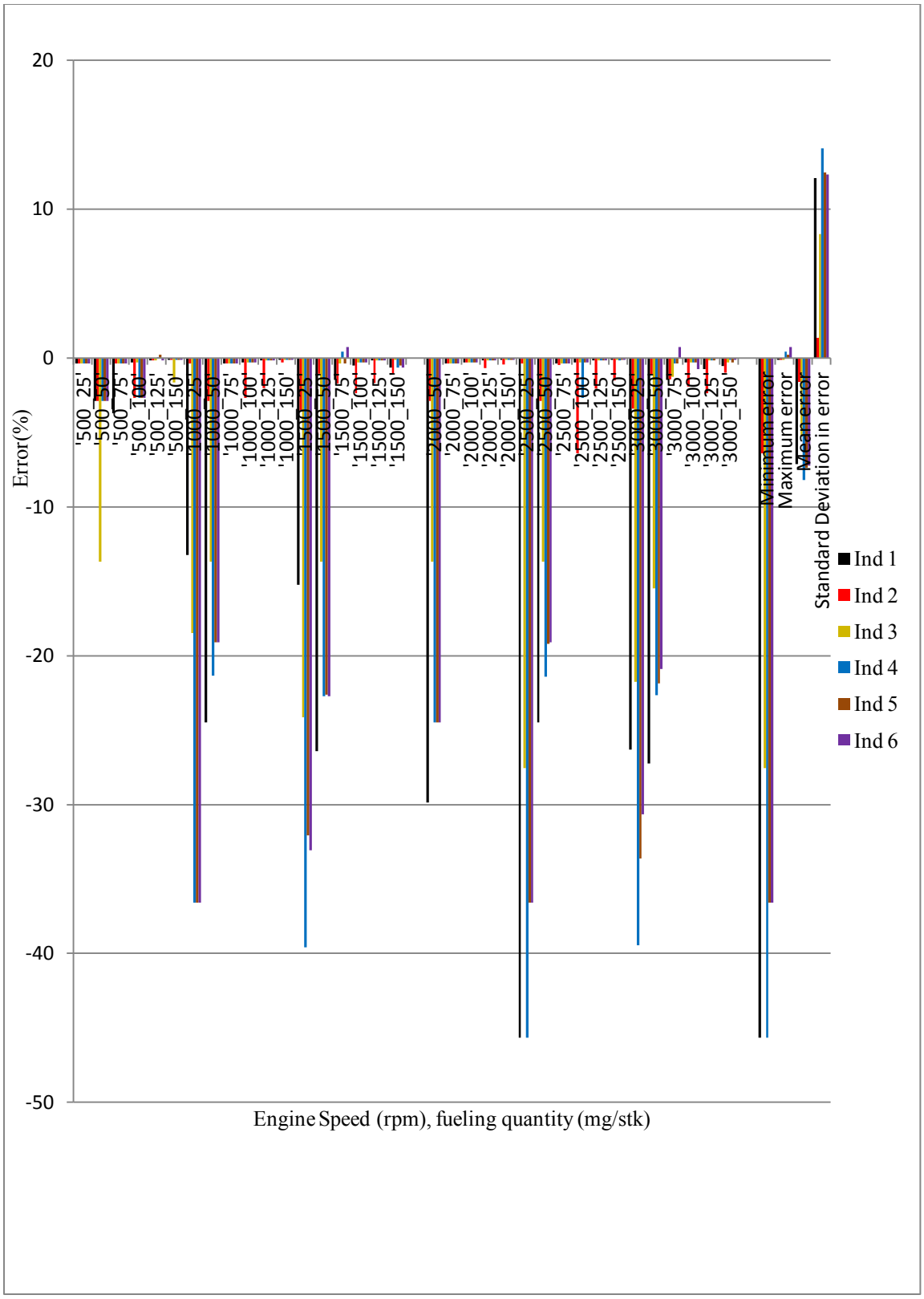

Figure 3.11 Error percentage with double threshold (Inductor)

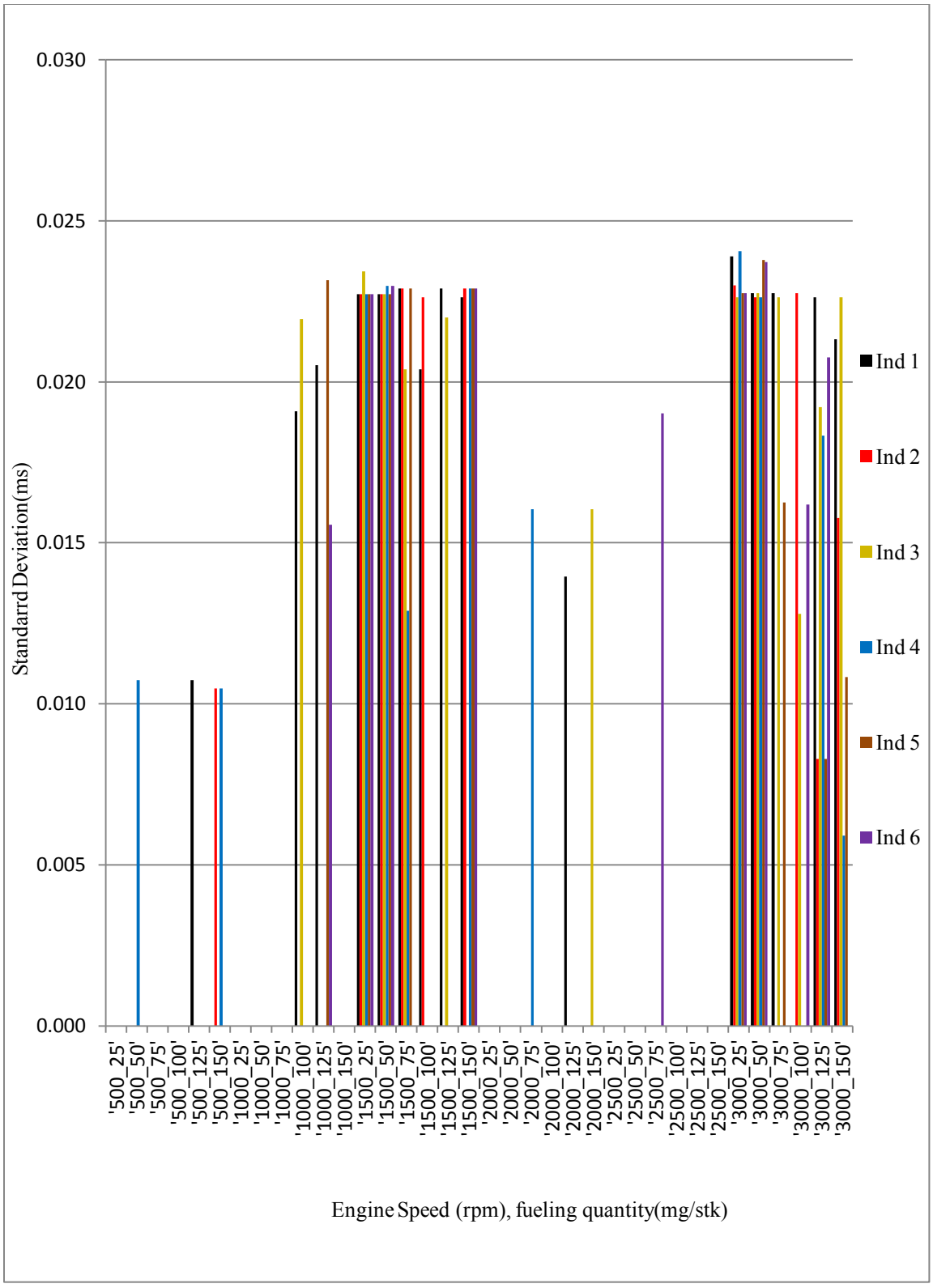

Figure 3.12 Single threshold at 2V(Inductor) – Standard Deviation (Ontime)

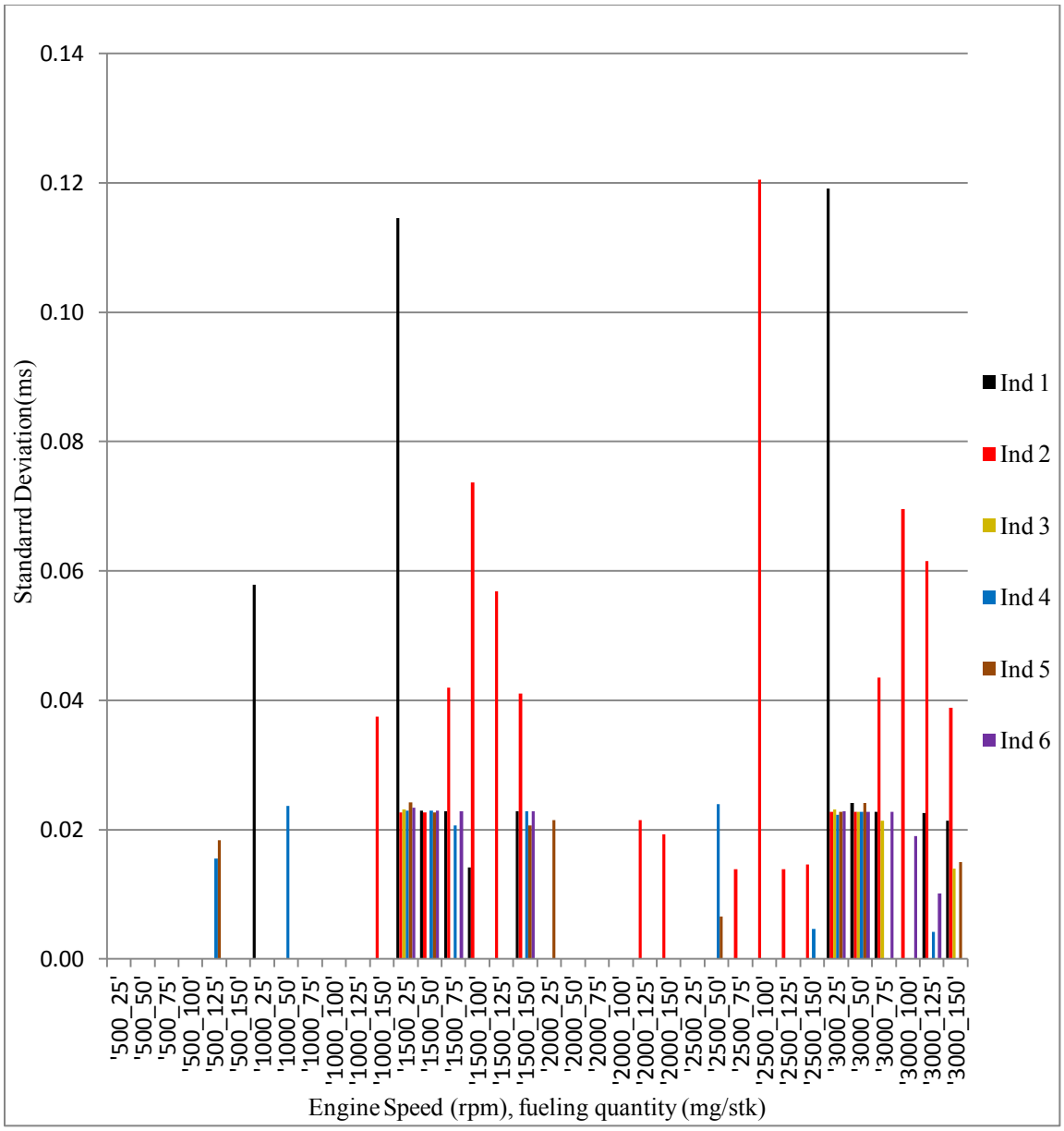

Figure 3.13 Double threshold (Inductor) – Standard Deviation (Ontime)

2.6.2 Injectors as Load, Single Module with Lower Precision

Injector stators were used in the following experimentation as load. The pulses captured were well defined when injectors were used that resulted in better accuracy. In case of double threshold approach, EOI was considered at the point where the voltage starts to drop. Fueling quantity values varied from 25mg/stk to 150 mg/stk.

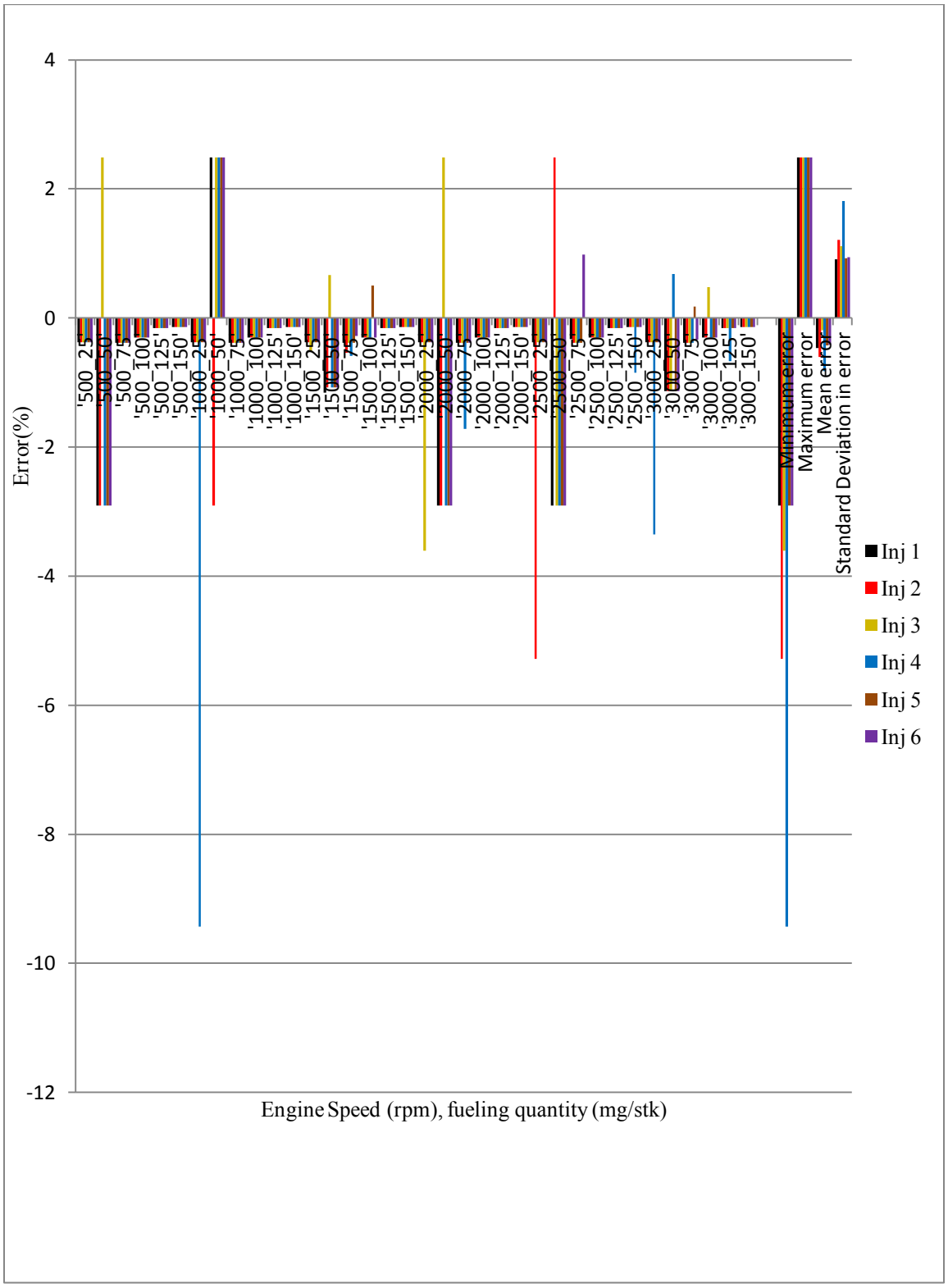

Figure 3.14 Error percentage with single threshold at 2V (Injector)

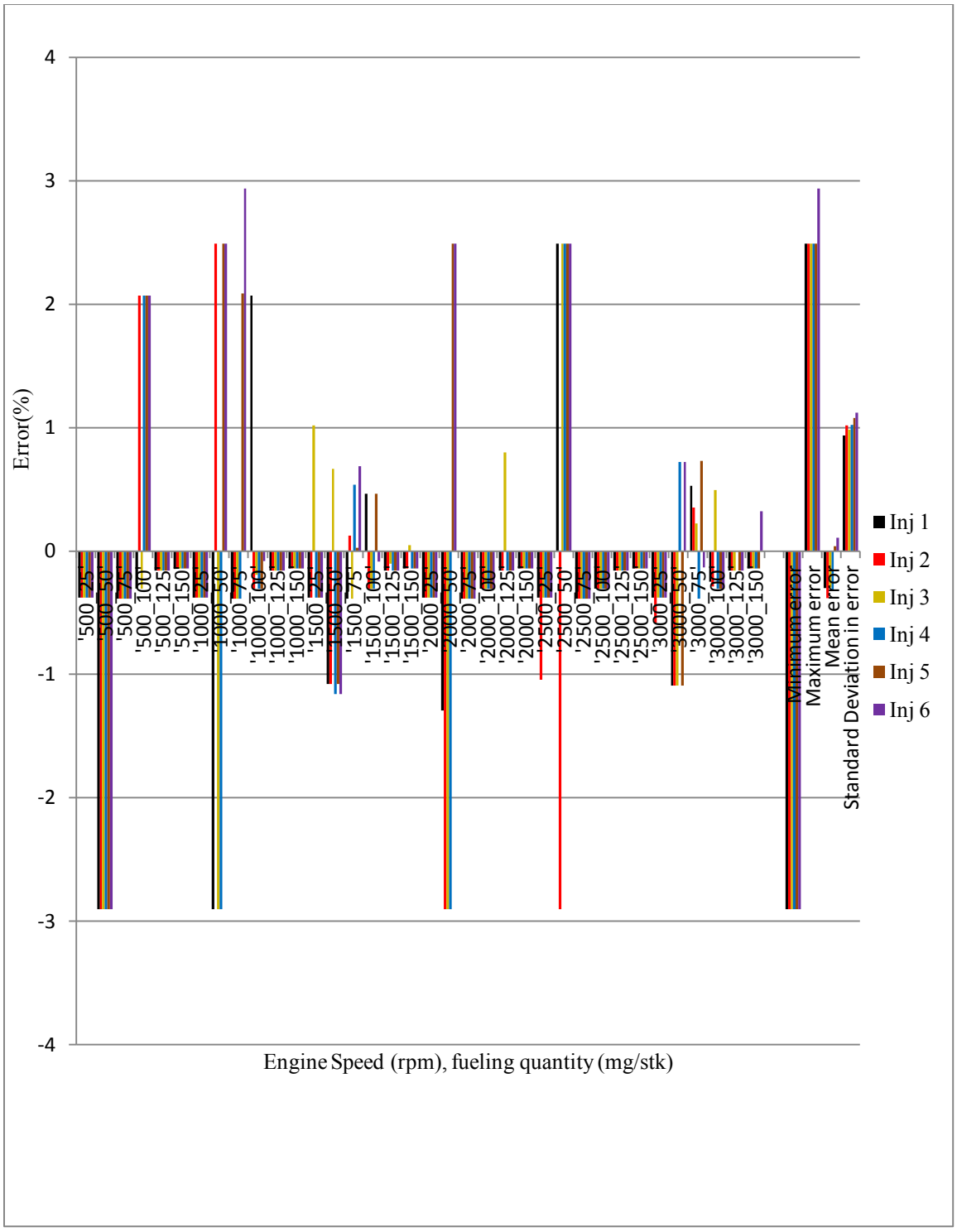

Figure 3.15 Error percentage with double threshold (Injector)

With single threshold at 2V, ±3% error was observed. Unpredictable high error with injector 4 was observed as shown in Figure 3.14. Double threshold showed better

result in terms of error percentage, but the error prevails at higher values of fueling quantities as well, shown in Figure 3.15.

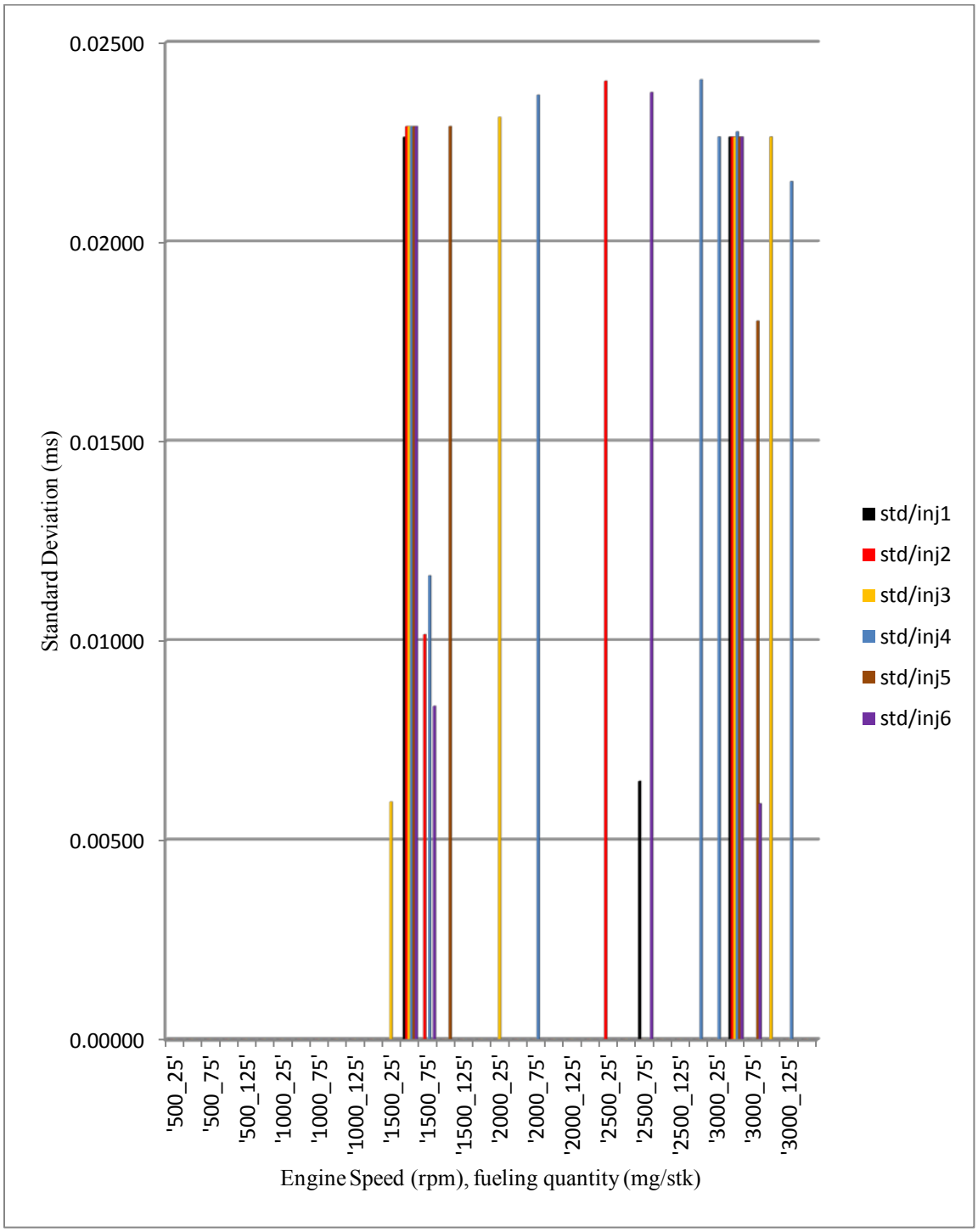

Figure 3.16 Single threshold at 2V (Injector) – Standard Deviation (Ontime)

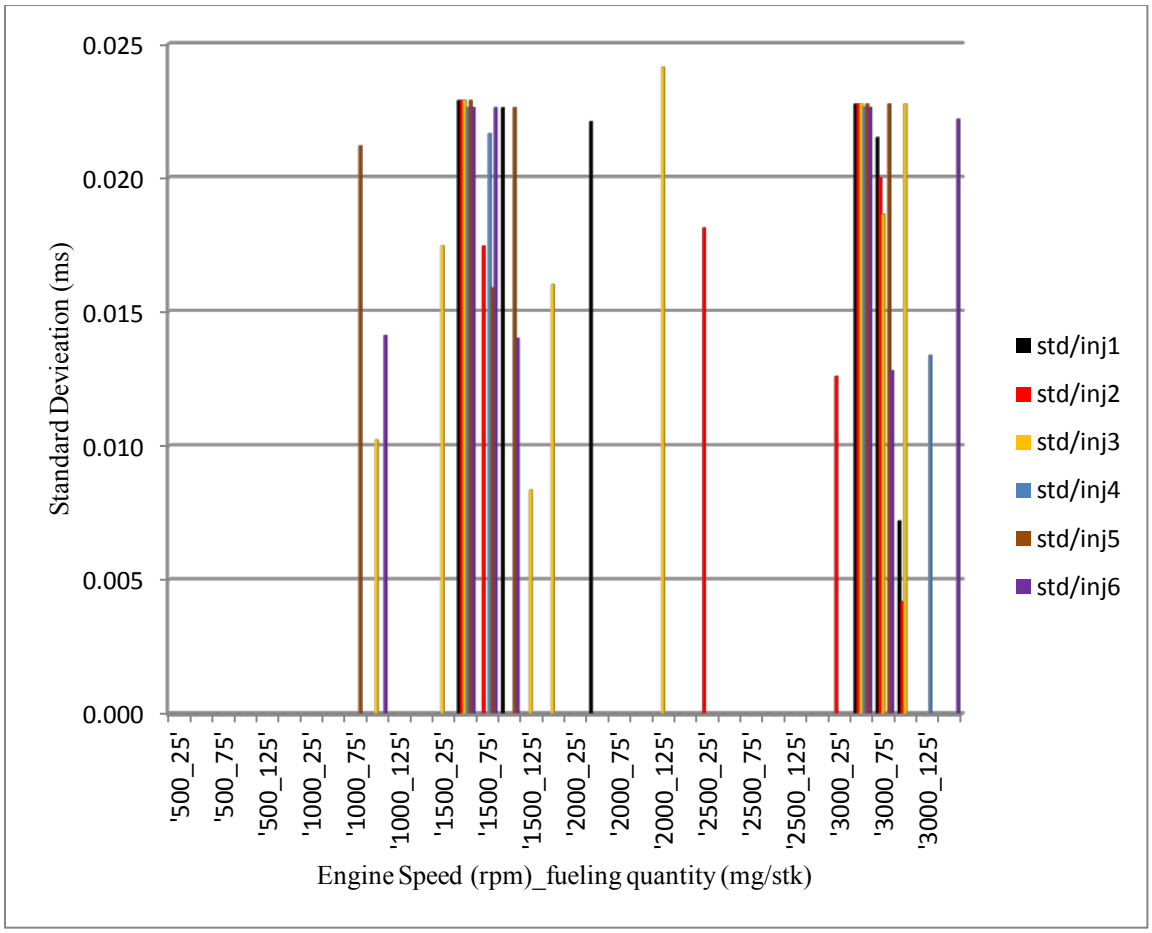

Figure 3.17 Double threshold (Injector) – Standard Deviation (Ontime)

Although the captured pulses show better accuracy at the lowest fueling quantity of 25mg/stk, within ±3% when double threshold approach were used, the error is not consistent, which will render it unsuitable to be used in HIL bench. Moreover, in idle speed condition, the fueling quantity injected is less than 25mg/stk, in which case, it will have more error. Therefore, higher sampling rate with higher precision was tried in the later stages of the experimentation. The pulse to pulse "ontime" variation is plotted in Figure 3.16, Figure 3.17 and Figure A.12.

Double threshold and single threshold at 2V showed less variation from pulse to pulse, however, the variation is pronounced at 1500rpm and 3000rpm engine speeds. The mean of percentage errors at each states were calculated and plotted to compare the performance of the system with injectors or the inductors used as loads. Following plots

shows the comparison with different threshold approaches. Figure 3.18, Figure 3.19, Figure 3.20 and Figure A.13 in the appendix show that the error with inductors is lot more than the injectors. They signify the fact that, if cheaper solution, i.e. inductors are used as the loads instead of using six production injectors for each bench, single threshold at 2V is the best option. However, injectors show better results in double threshold approach. Figure 3.21, Figure 3.22, Figure 3.23, Figure 3.24 shows the maximum and minimum error occurring at each state. These experimental results pave the way for further experimentation, to investigate the performance of the system with higher precision and higher sampling rate. These plots imparts the knowledge, how much error can be expected, should we implement it. However, the error percent are unacceptable for the HIL application, since the HIL application requires higher accuracy at a fueling quantity as low as 10 mg/stk at a lower pressure than 1200bar, which would certainly lead to much more error.

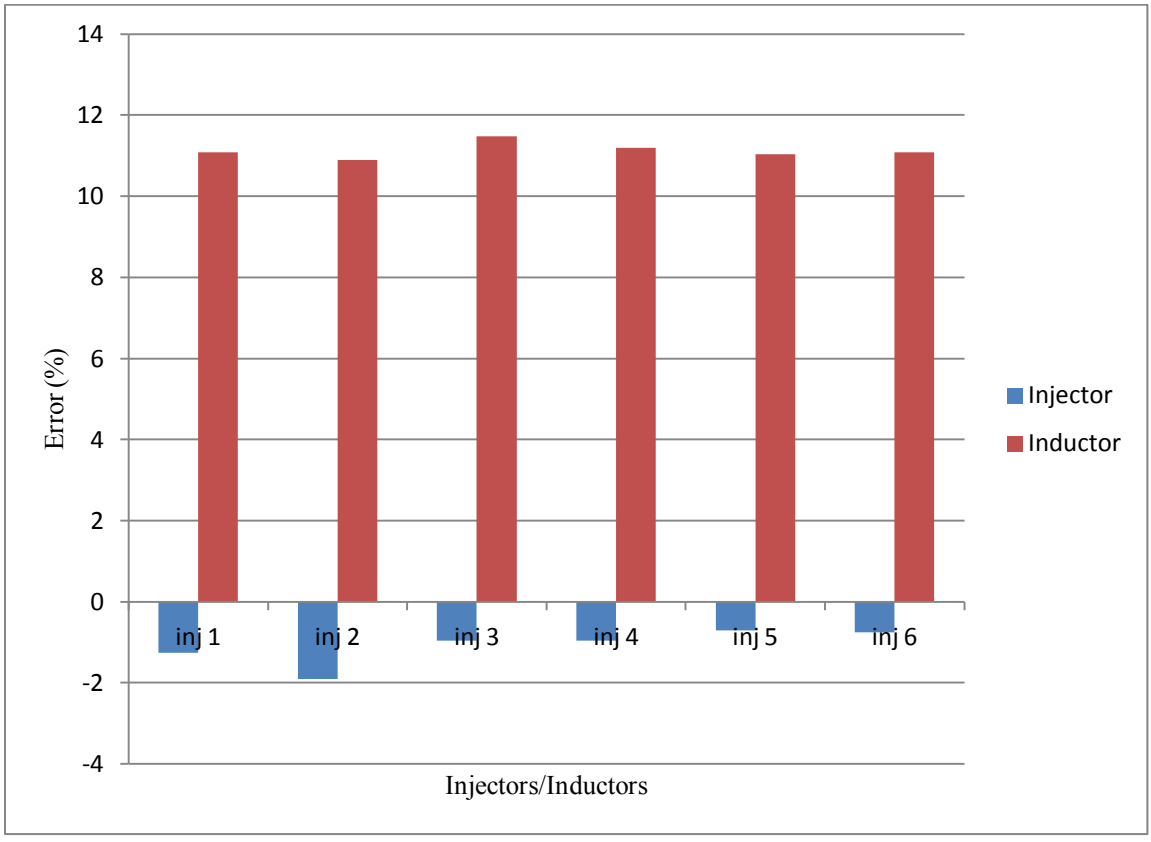

Figure 3.18 Mean error percent using threshold at zero volt

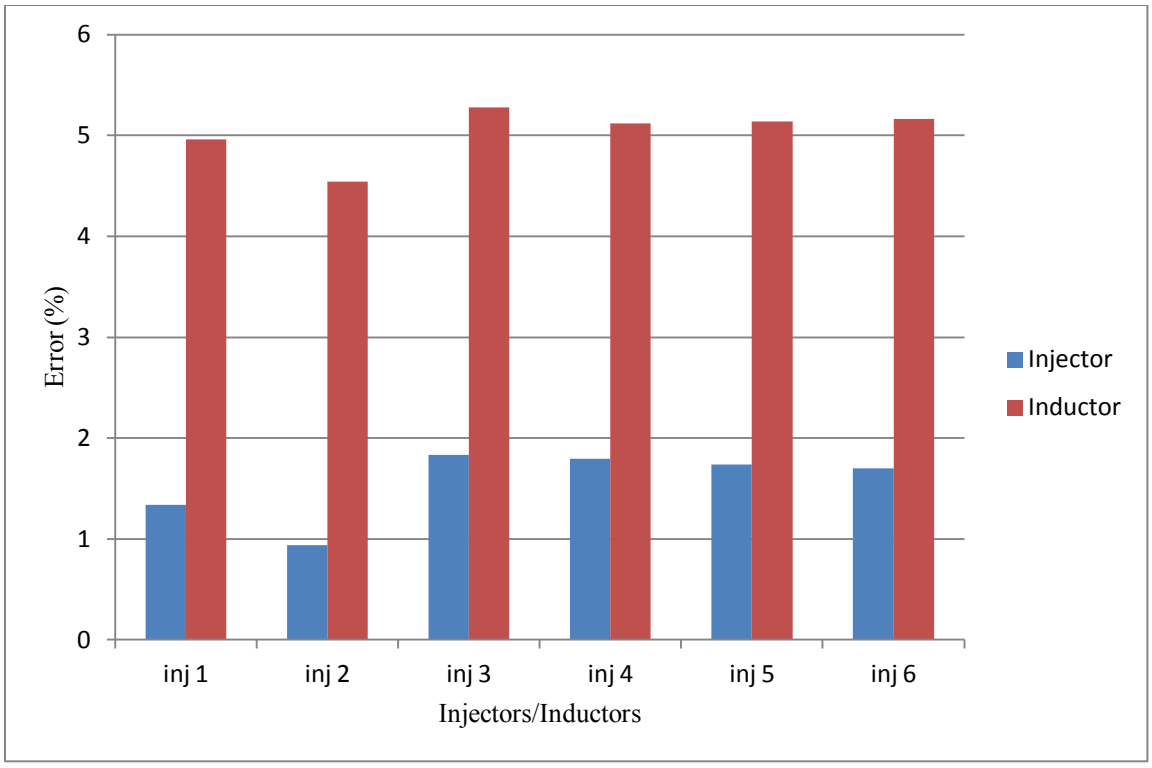

Figure 3.19 Mean error percent using threshold at 1V

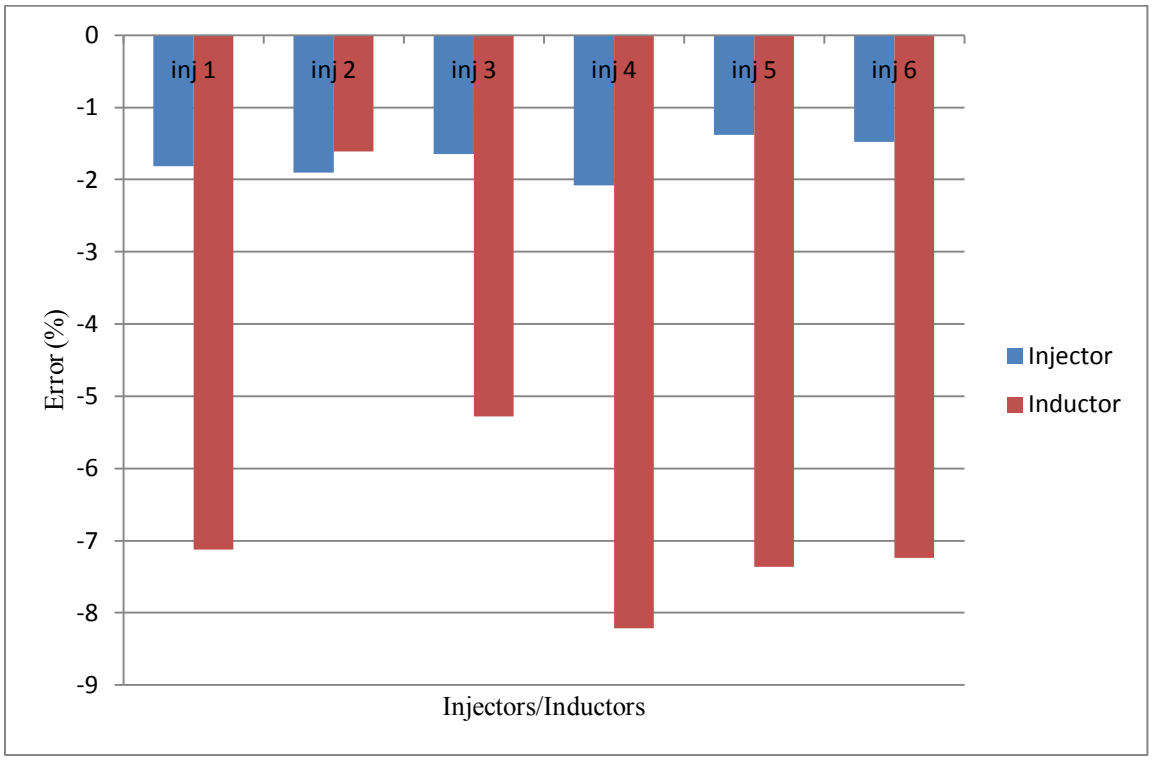

Figure 3.20 Mean error percent using double threshold

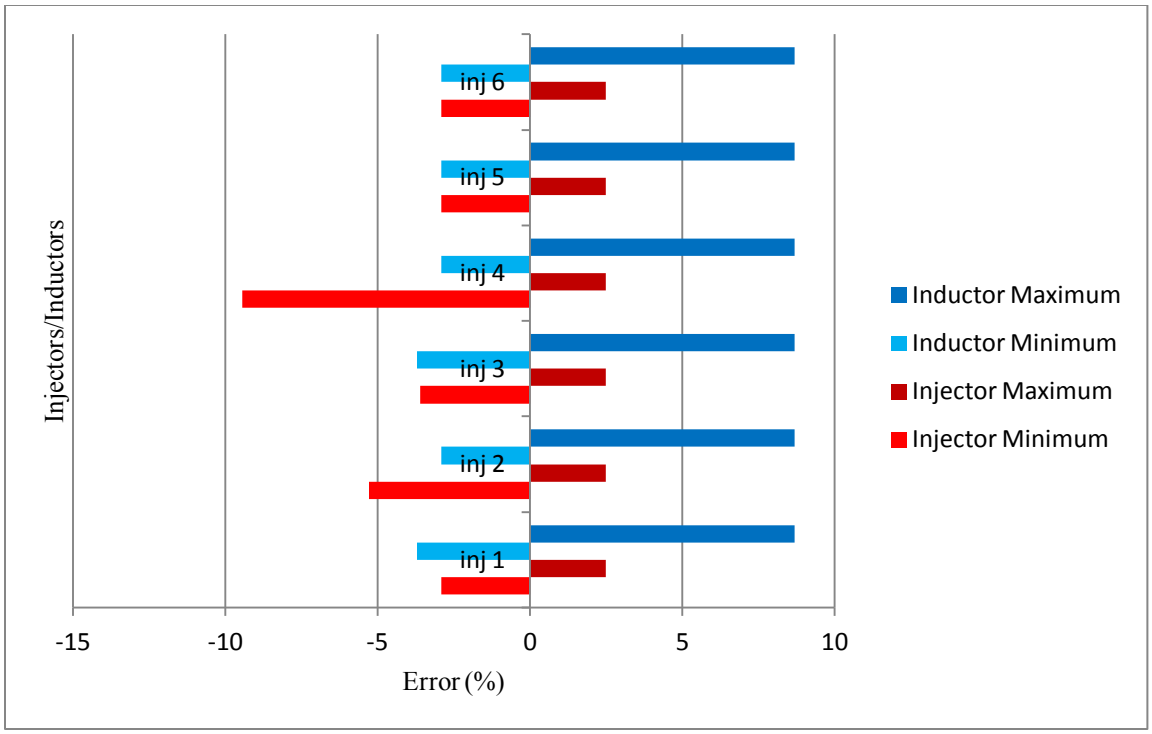

Figure 3.21 Range of error percent using Threshold at 0V

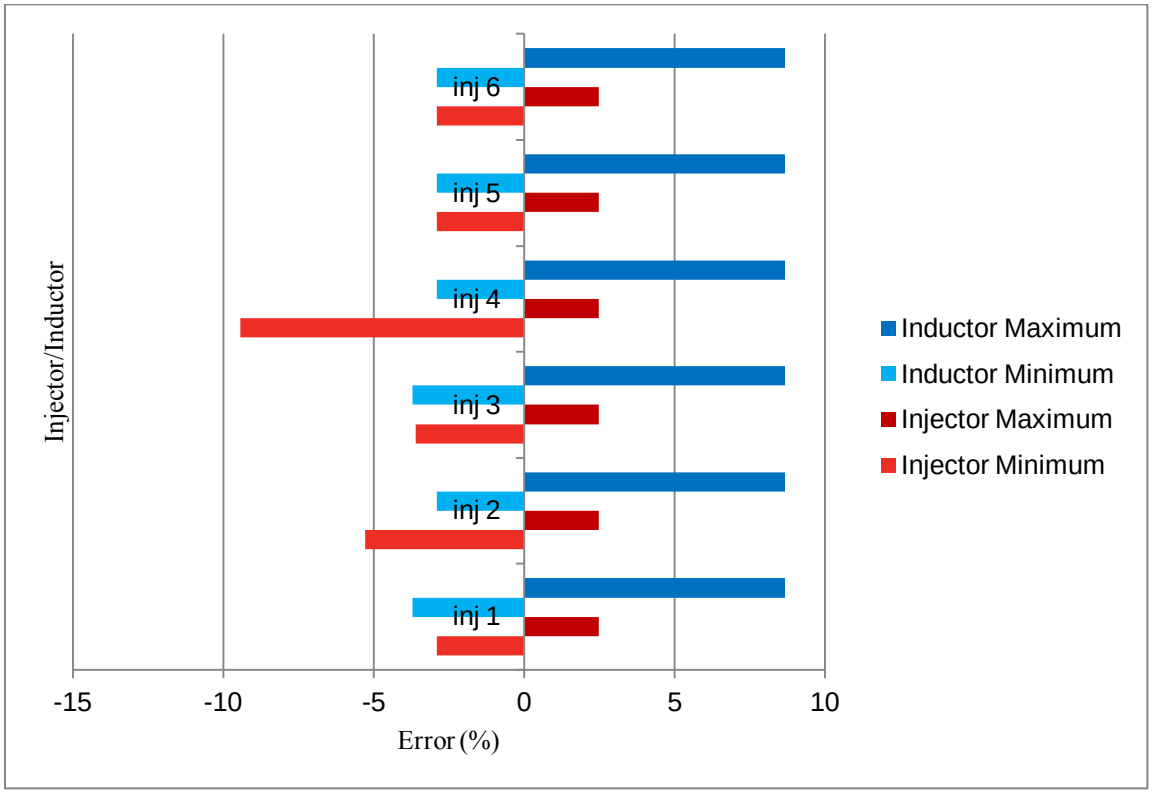

Figure 3.22 Range of error percent using Threshold at 1V

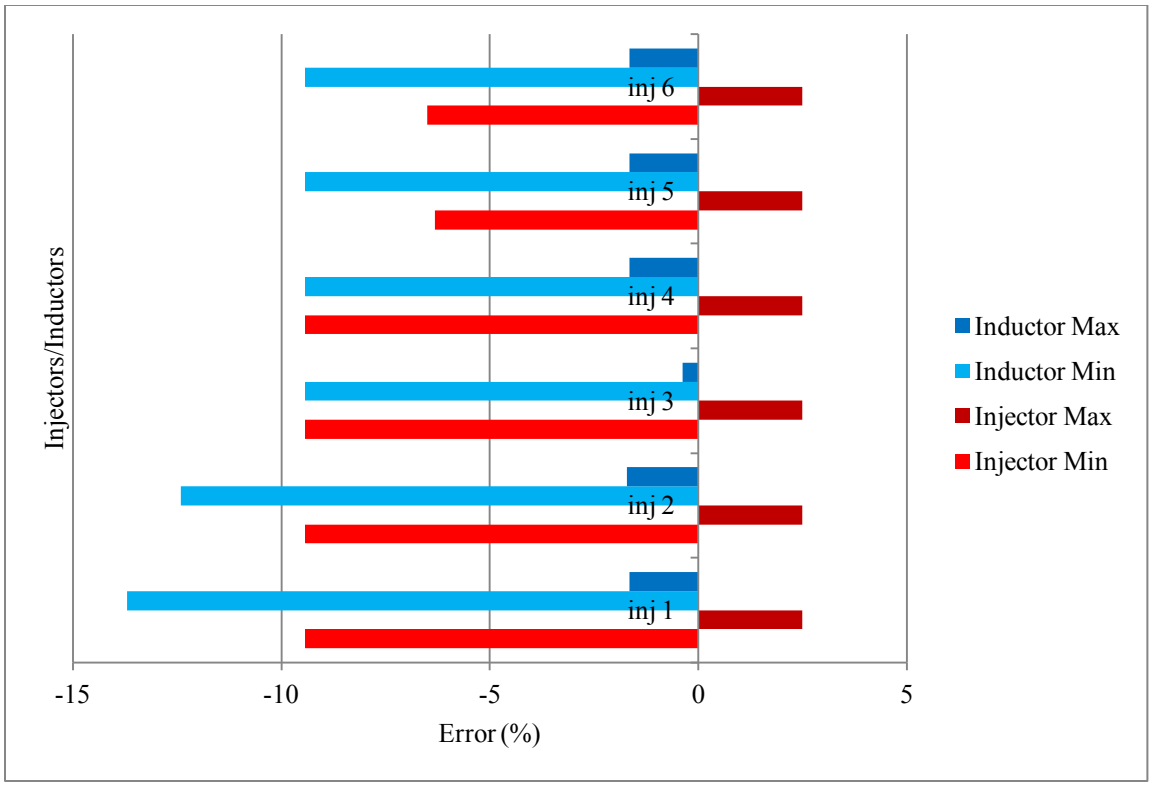

Figure 3.23 Range of error percent using Threshold at 3V

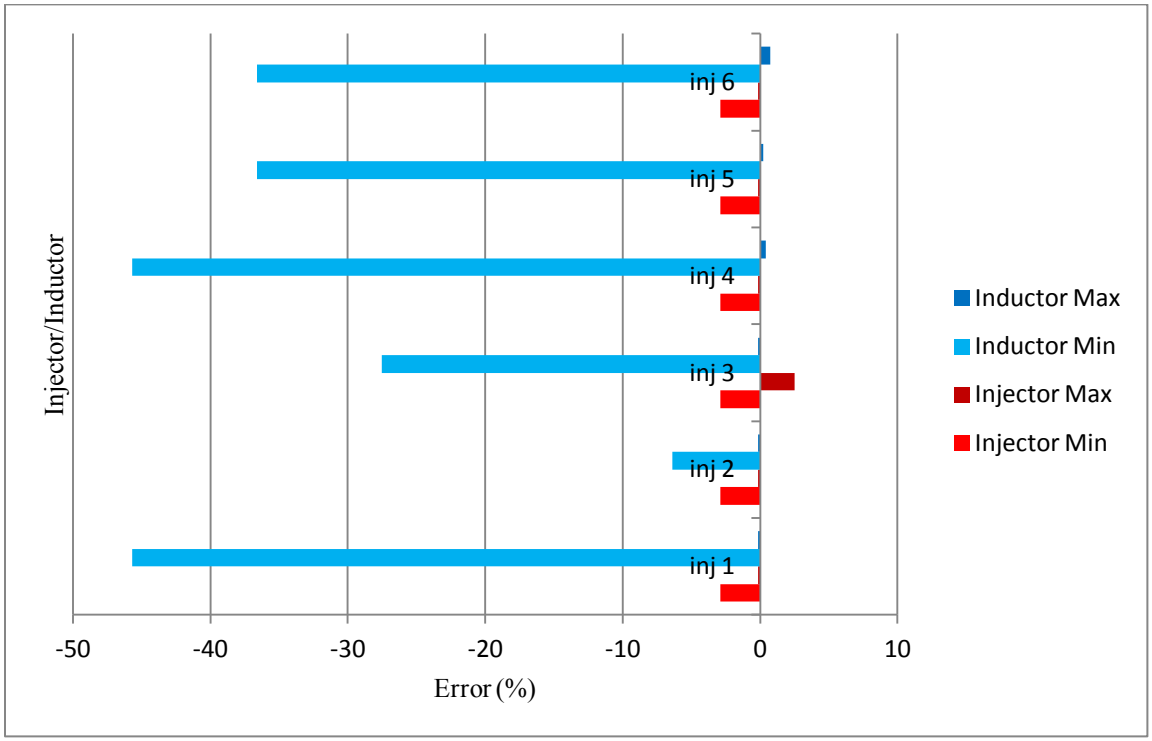

Figure 3.24 Range of error percent using double threshold

2.6.3 Injectors as Load, Two Modules with Lower Precision

The sampling rate previously used was not adequate to capture low fueling quantity. Therefore, two analog modules were used, that provided twice the sampling rate of 41.6kHz or data points at every 24µs instead of 48µs intervals. Still the data were logged at 1V precision. Since the previous plots show very little effect of engine speed, rather it fails to capture low fueling quantity, next test sequences go over different common-rail pressures and different fueling quantities. In order to inject a certain amount of fuel, the increase in engine speed only increases the number of injector pulses over a certain period of time. It does not change the injector ontime (ms). However, the increase in common-rail pressure decreases the injector ontime (ms) significantly, the trend is shown in Table 3.1. Double threshold approach has been chosen and the pulse lengths have been extracted by the real-time application running on the real-time processor on the Compact RIO.

Table 3.2 Common-rail pressure and fueling quantities in the test sequence

Common-rail pressure(bar)	Fueling quantities (mg/stk)
300	0.88
400	1.69
500	3.5
600	5.5
700	9
800	16
900	25
1000	33
1100	38
1200	45
1300	51
1400	68
1500	86
1600	120
1800	160

The double threshold identified the end of EOI with the previously used method, i.e., if five consecutive data points show decreasing voltage, it chooses the third data point as the EOI. The test sequence goes over the pressure and fueling quantity combinations listed in Table 3.2.

The resulting error in fueling quantity, sensed by the RT, was observed to be less than the previous case with lower sampling rate.

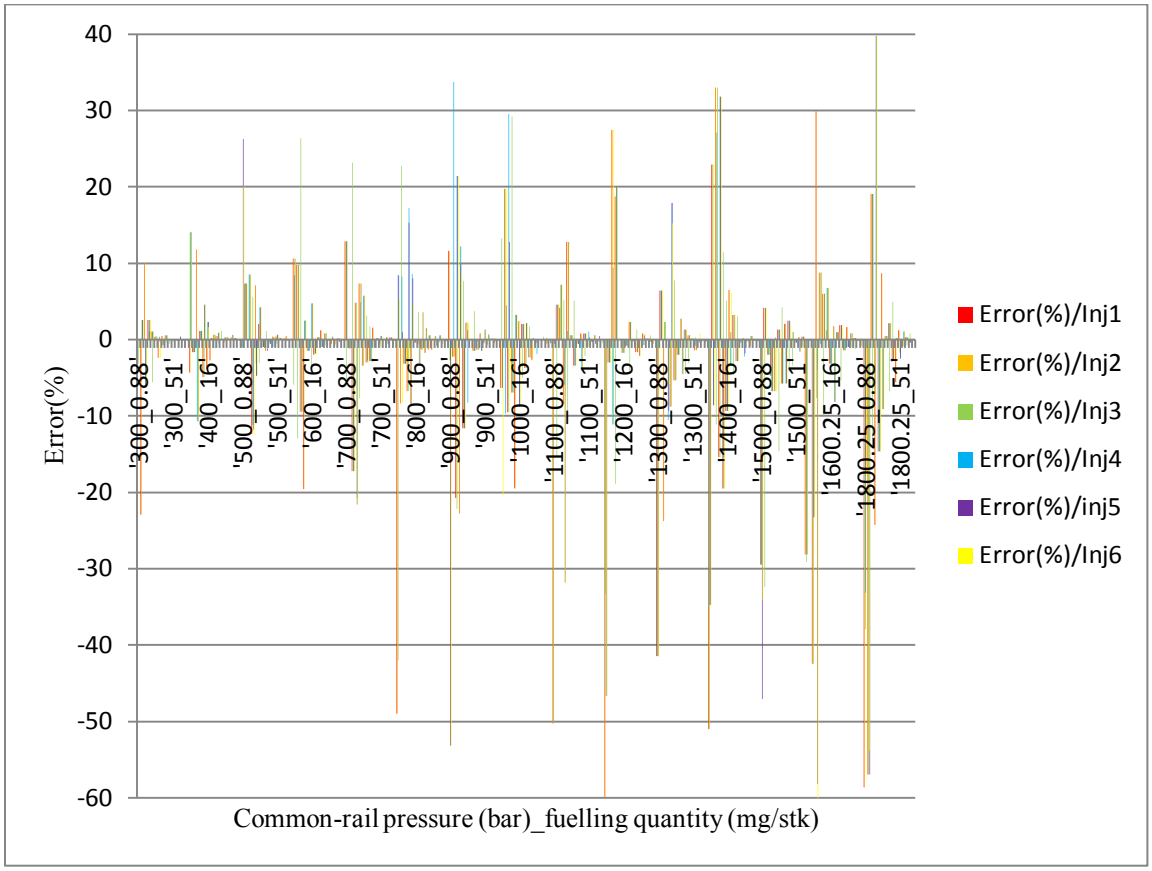

Figure 3.25 Error percent with injectors at 500rpm

The plots in Figure 3.25 and Figure 3.26 show that, the percentage error increases as the common-rail pressure goes higher, because of the fact that, the injector “ontime” decreases as the common-rail pressure increases, for the same amount of fueling quantity. The result signifies that, the accuracy is directly related to injector “ontime” and almost independent of common-rail pressure or engine speed. The inductors show much higher error than the injectors.

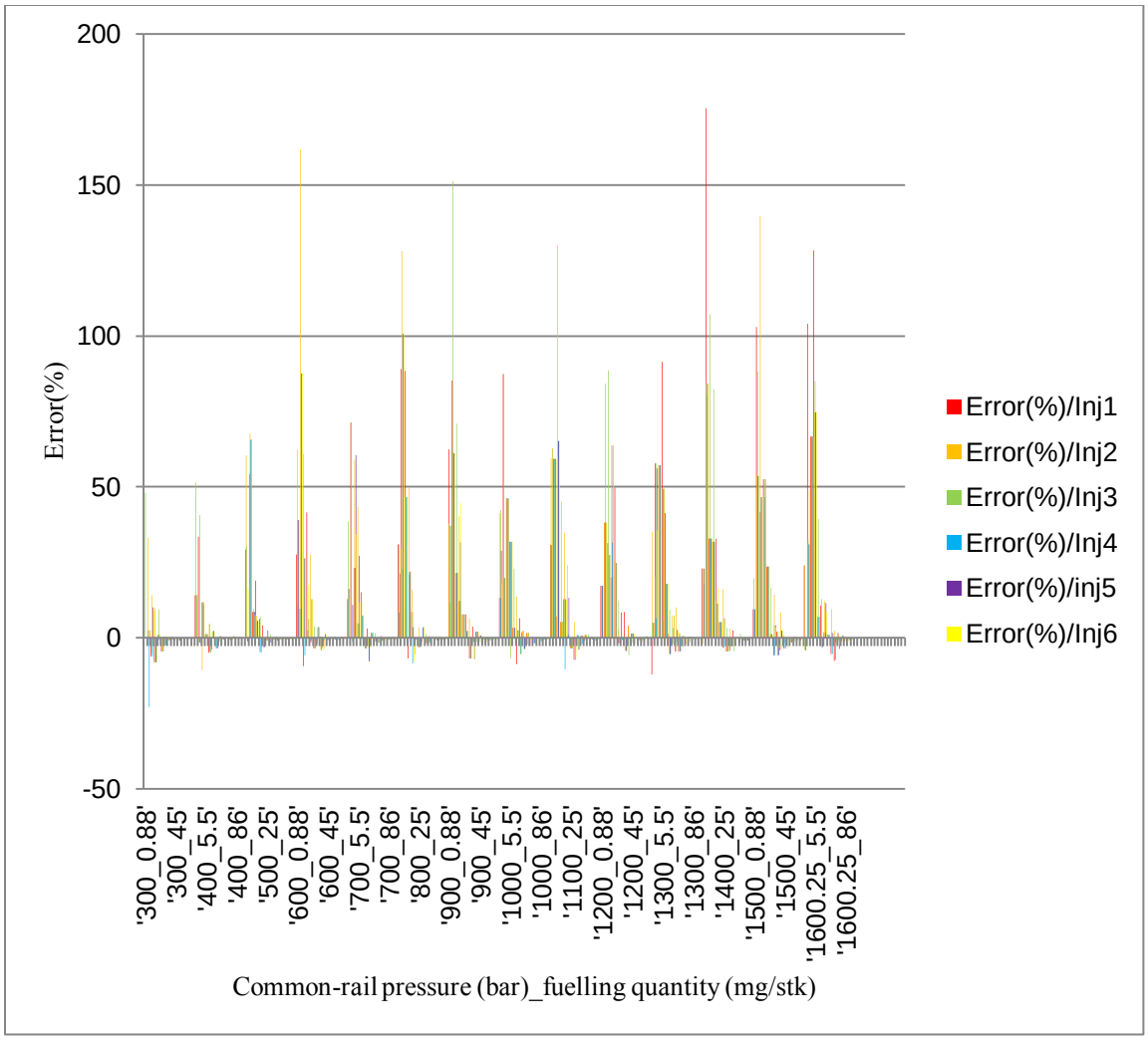

Figure 3.26 Error percent with inductors at 500rpm

To compare the result with two sampling rates, the percentage error with injectors at 500rpm and 1200bar common-rail pressure is shown in Figure 3.27 and Figure 3.28. If percentage error of lower than 2% is acceptable at an “ontime” corresponding to fueling quantity as low as 9mg/stk at 1200bar and 500rpm, two module can be used to simultaneously log all six channels. Two modules will allow simultaneous logging of all pulses at 41.6kHz of all the injectors which will facilitate real-time data delivery in the closed loop HIL test. However, as the common-rail pressure increases to more than 1200bar, the ontime will be decrease, that will result in higher error. Therefore, further improvement is necessary, which can only be manifested by higher precision and higher sampling rate.

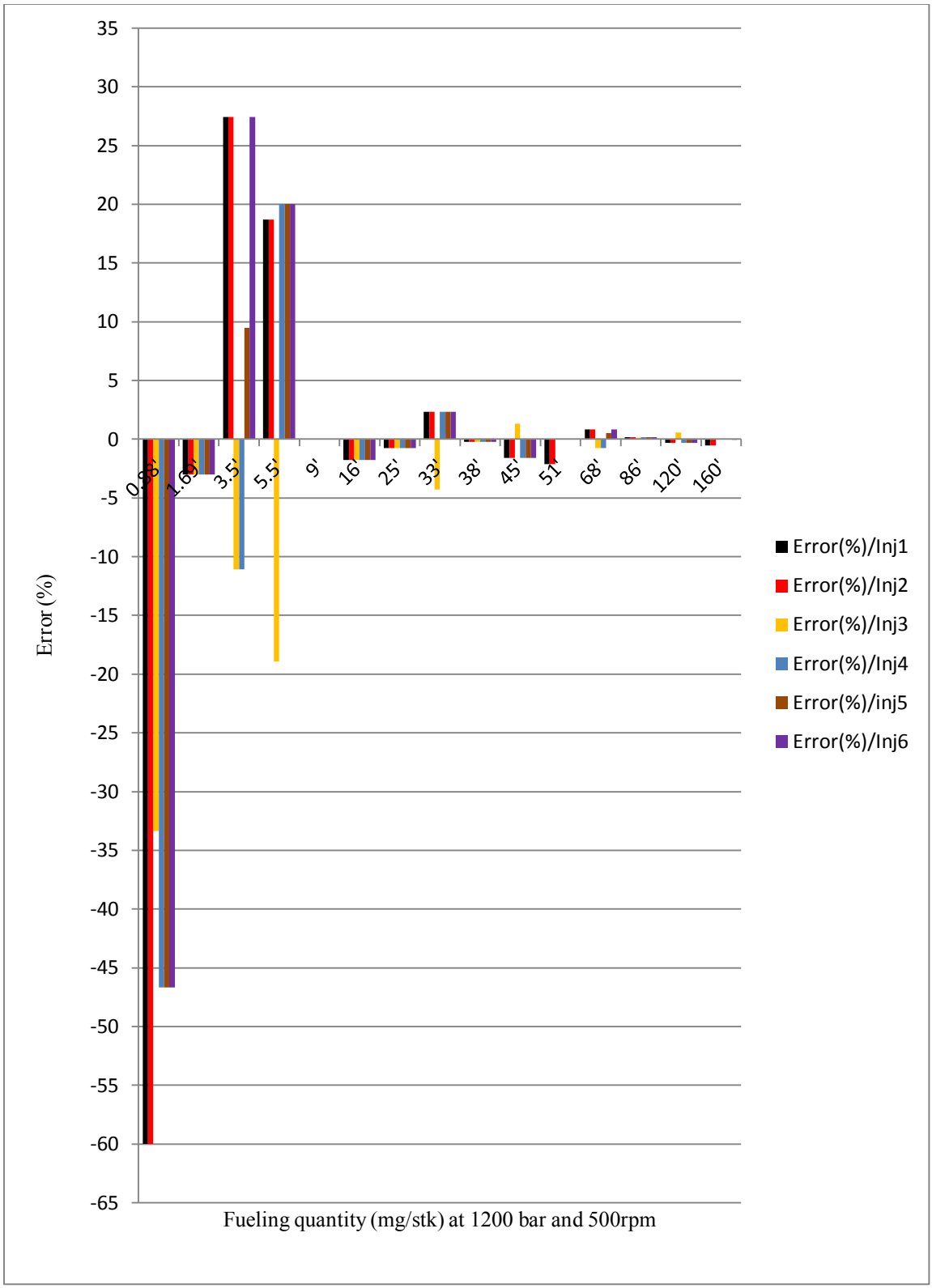

Figure 3.27 Error percent with double threshold with injectors at 500rpm and 1200bar 41.6kHz

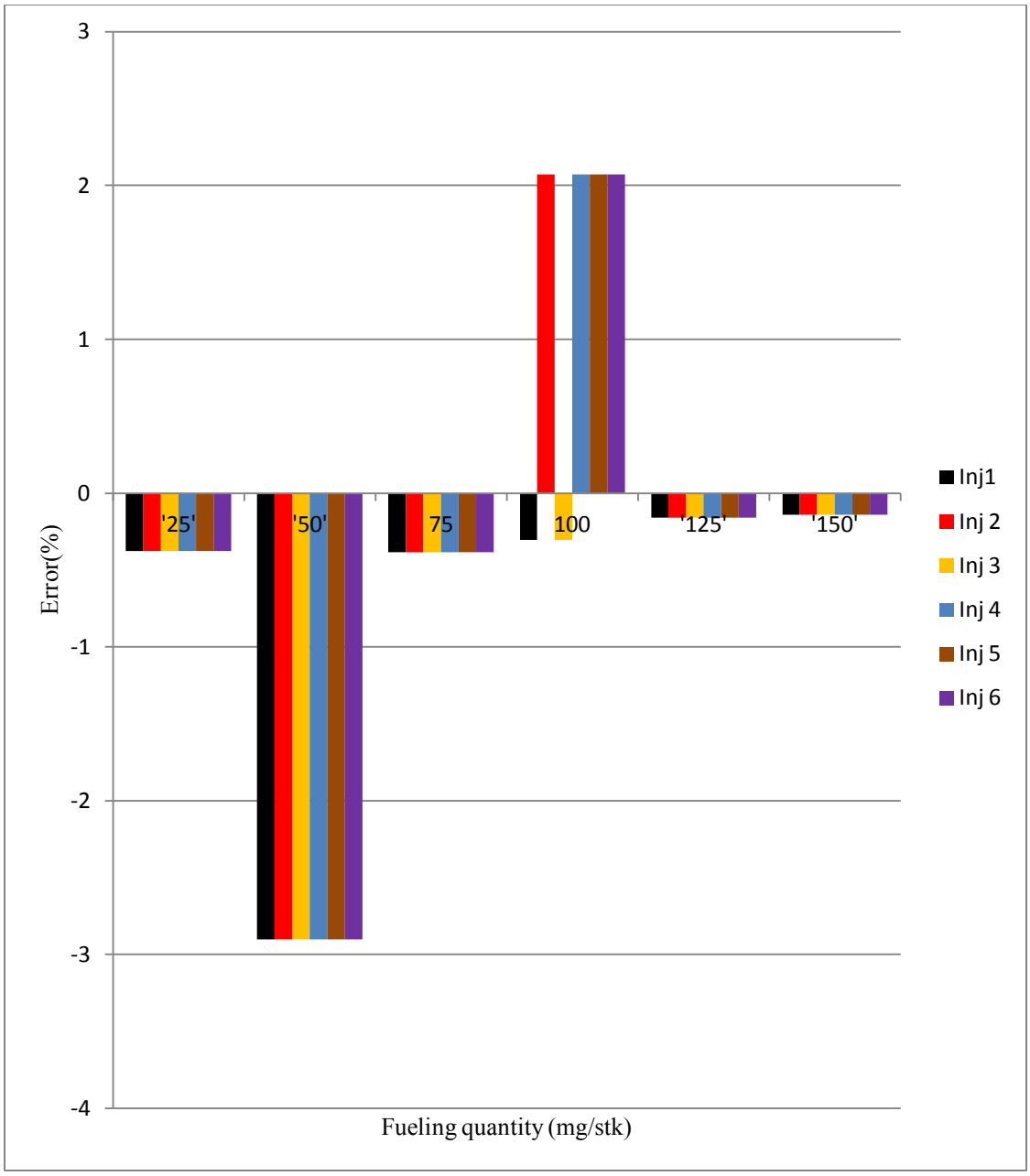

Figure 3.28 Error percent with double threshold (Injector) at 500rpm and 1200bar with lower sampling rate of 20.8kHz

In order to compare the performance with inductor load cells, Figure 3.29 and Figure 3.30 further establishes the inferior accuracy if the inductors are used. Figure 3.29 shows that, around 25% error take place at 9mg/stk at 1200bar and 500rpm even at higher sampling rate of 41.6kHz, while Figure 3.30 shows the data previously collected with lower 20.8kHz sampling rate.

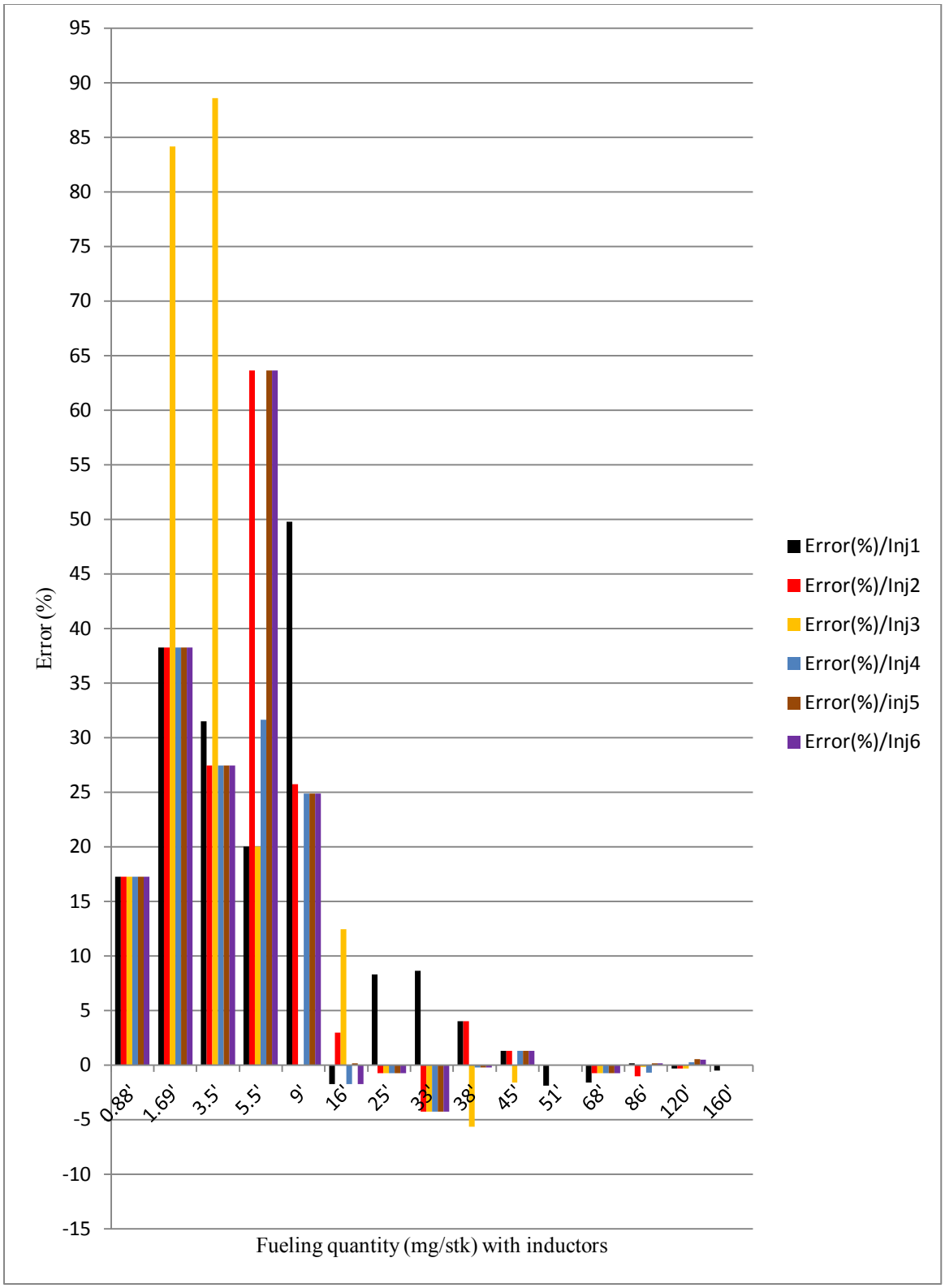

Figure 3.29 Error percent with inductors at double threshold at 500rpm and 1200 bar at 41.6kHz sampling rate

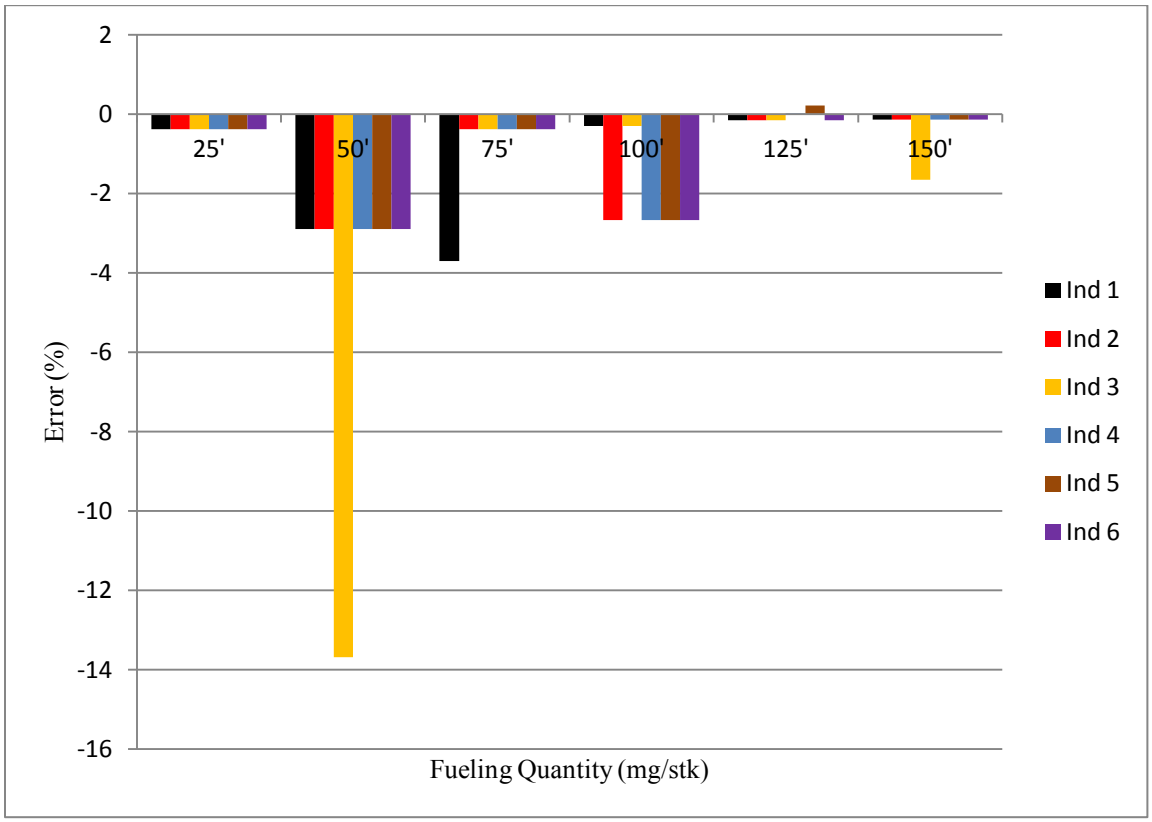

Figure 3.30 Error percent with inductors at 500rpm and 1200bar with lower sampling rate of 20.8kHz

In order to find out how much variation exists in pulse to pulse ontime, i.e. shot to shot variability, standard deviation has been plotted in Figure 3.31, with the injectors at 500rpm and varying common-rail pressure. The plot shows the increasing variation in injector on times with the increase in common-rail pressure. The plot also signifies that, injector 2 has been performing with the highest amount of variation, this observation signifies that the injectors has variation from part to part as well. Therefore, the injectors need to be tested before being used in a HIL bench. Figure A.14 in the appendix shows the result with similar operating points, i.e. standard deviation with 1500rpm engine speed. Figure 3.32 shows the magnified view of the standard deviations at similar operating conditions as previous results, i.e. 1200bar common-rail pressure, 500rpm engine speed and varying fueling quantities. The plot shows the high amount of variation in injector 2. Otherwise, the variation is very low, as far as, other injectors are concerned.

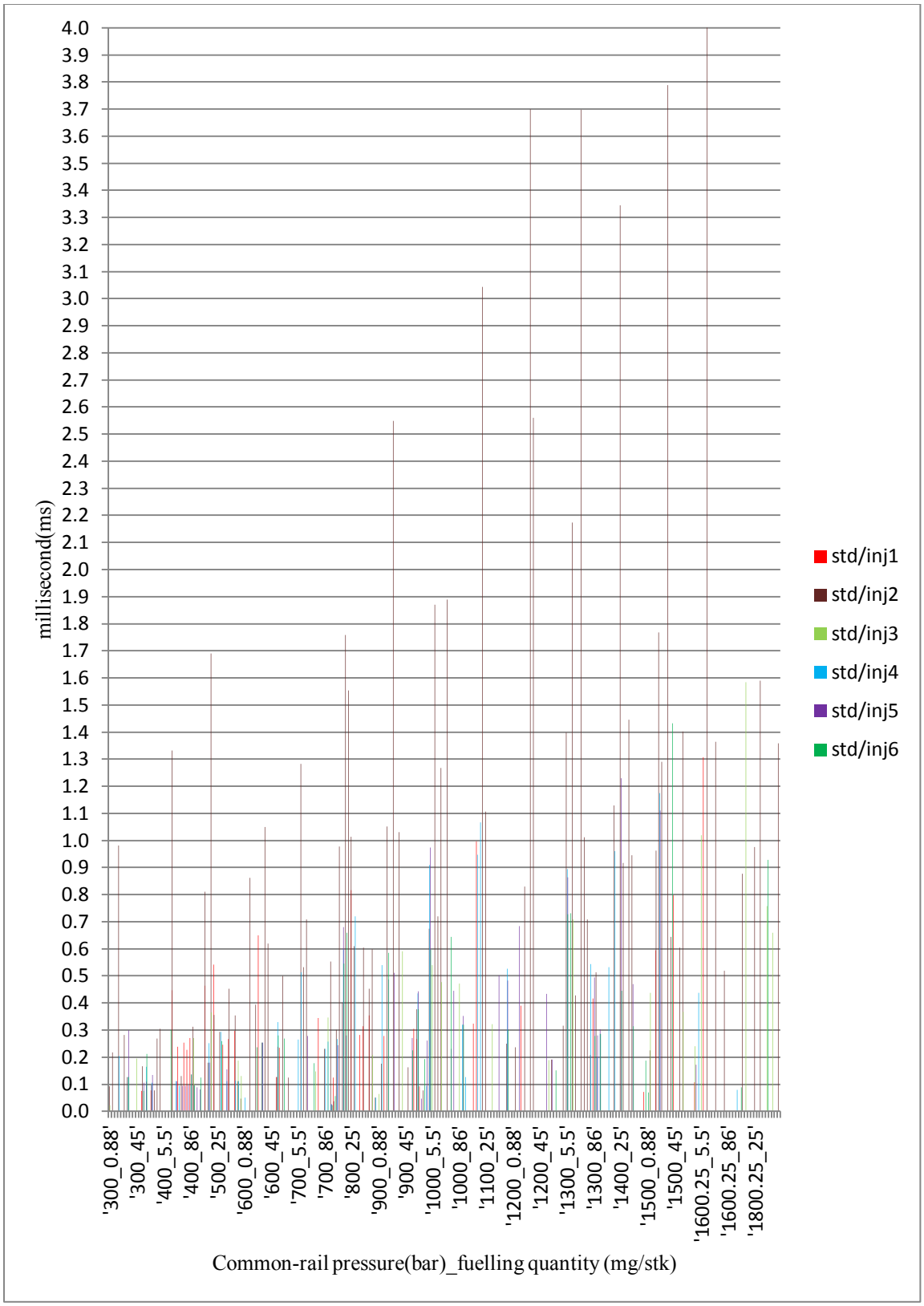

Figure 3.31 Standard deviation 500rpm with injector (two module)

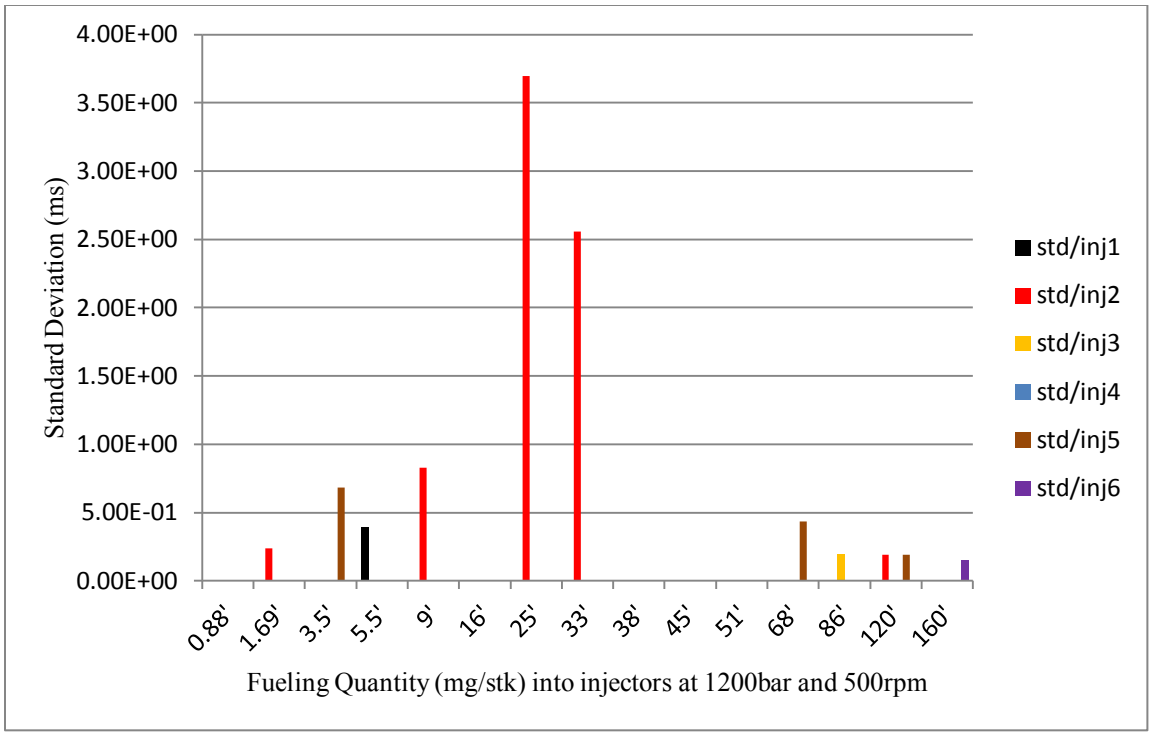

Figure 3.32 Standard deviation in injector pulse to pulse ontimes with 1200bar common-rail pressure and 500rpm engine speed at various fueling quantities

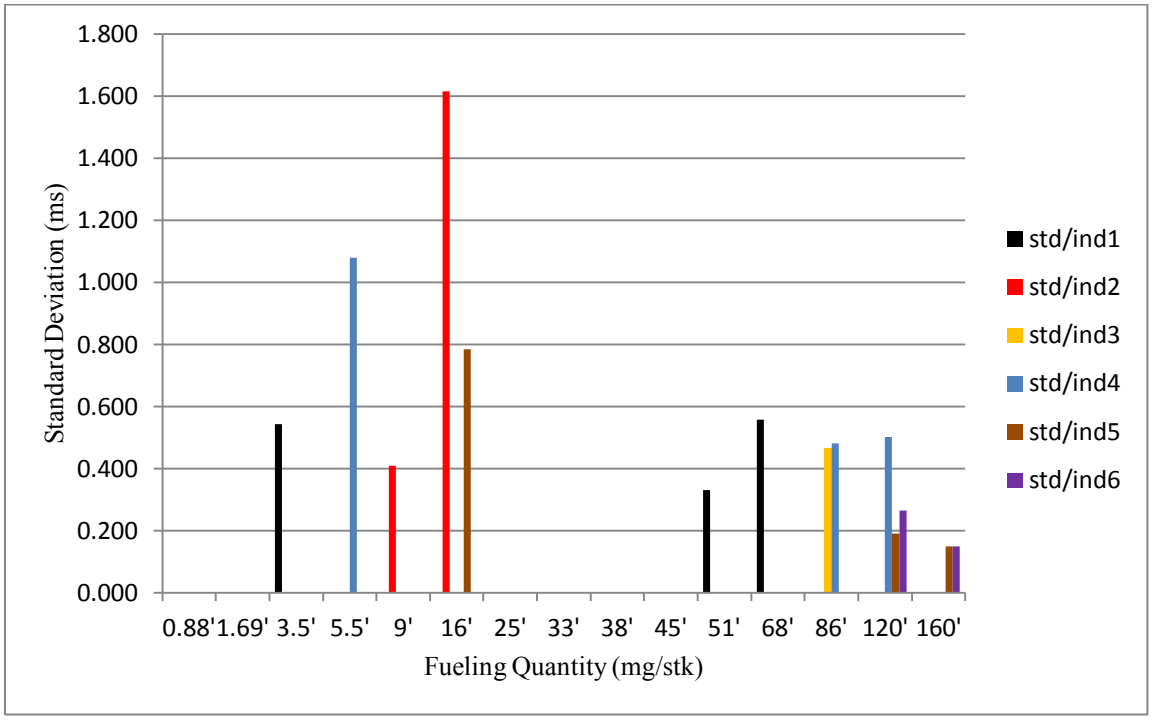

Figure 3.33 Standard deviation in inductor pulse to pulse ontimes with 1200bar common-rail pressure and 500rpm engine speed at various fueling quantities

With the increase of engine speed, the pulse to pulse variation was observed to increase as shown in the Figure A.14 in the Appendix. Figure 3.33 shows the variability with inductors at a similar condition as with injectors in Figure 3.32. Analysis needs to be carried out to find out if the engine model is sensitive to this amount of variation in error percent. Thus, from above experimental result, it can be concluded that, the precision and sampling rate needs to be increased if the variability in ontime of around 0.5ms standard deviation is not acceptable, assuming that the injector 2 will be discarded. Therefore, further investigation was carried out with the sampling rate increased to 125kHz or data points at each 8μs interval with precision of 0.0156V. In order to implement this sampling rate, all six injector channels cannot be logged simultaneously with one module. Therefore, either six analog input modules are needed for simultaneous logging of injector pulses or a windowing scheme is needed, in order to capture injector voltage of different injectors synchronized with crank angles.

2.6.3.1 Injectors as Load, One Module for each Injector, with Higher Precision

With the increased precision of 0.0156V in captured injector voltages, the DMA FIFO transfer needed to transfer 10 bits fixed point number for each data point. In the following experiments, the injector pulses were logged at a higher sampling rate of 125kHz, i.e. every 8μs interval. The double threshold approach is implemented with two thresholds, instead of capturing the point where the voltage value starts to drop from a steady value. The SOI is selected at 0.1V instead of 0V, to avoid the noise. Different voltage values are selected for the EOI threshold and the result is shown with a histogram. In order to evaluate the pulse to pulse variability, as well as, the accuracy in the value of fueling quantity captured, the fueling “ontime” is overridden on the ECM to inject fuel for a particular “ontime”. The test sequence holds the engine speed at 500rpm and common-rail pressure at 1200bar. The chosen fueling “ontime” is based on the previous results, lower values of “ontime” that cover the region of higher common-rail pressure and medium fueling quantity or at a lower common-rail pressure and low fueling quantity, the region on the fuel ontime table that is of importance for closed loop testing.

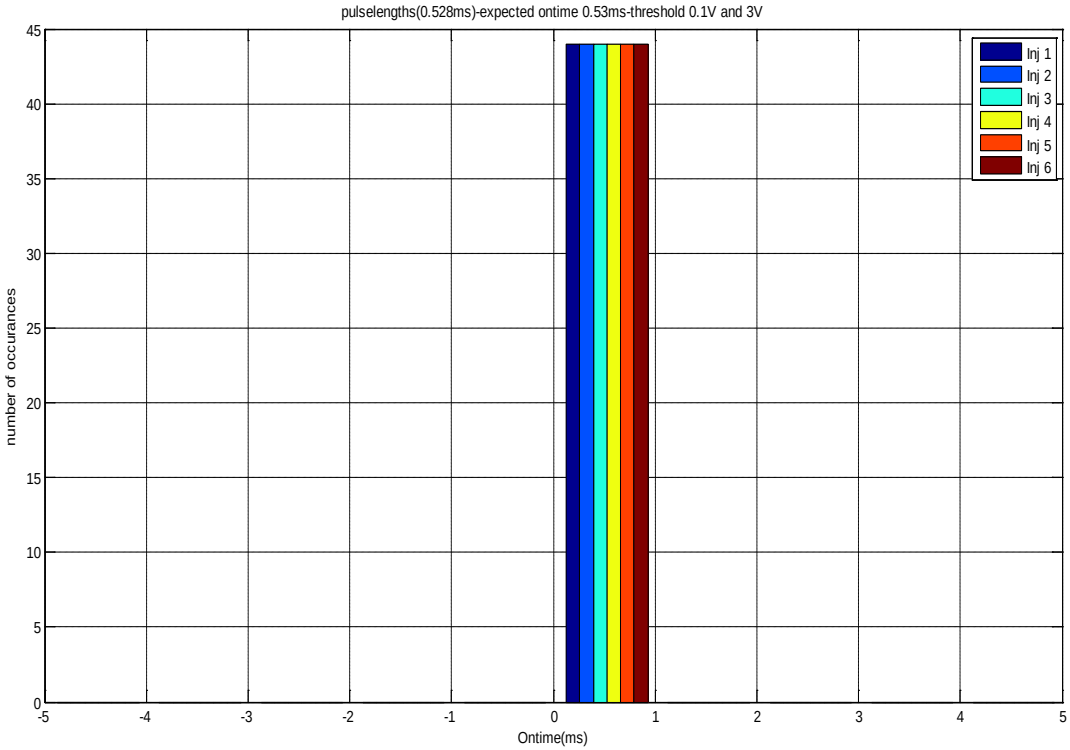

Figure 3.34 Histogram – pulselengths extracted as 0.528ms ontime (0.1V and 3V)

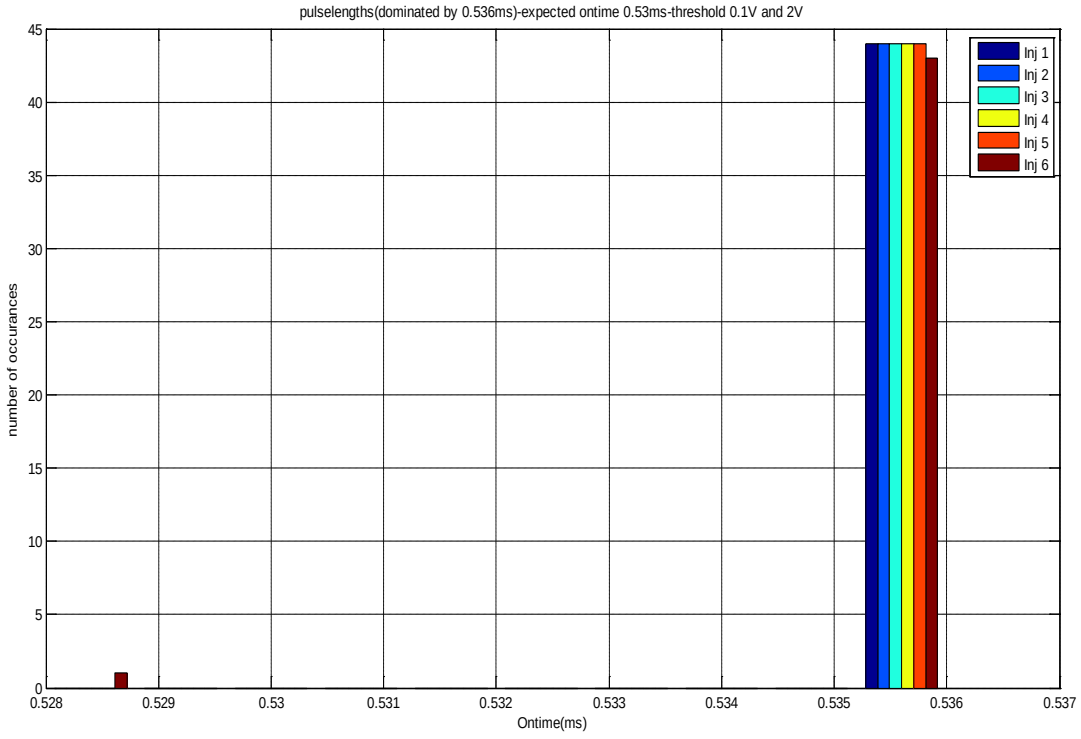

Figure 3.35 Pulselengths captured as 0.536ms (0.1V and 2V)

The way data have been presented has been changed, since the error is expected to have decreased to a great extent. Figure 3.34 and Figure 3.35 shows the histograms of pulses, with overridden “ontime” of 0.53ms. 45 pulses are extracted and the double threshold captures the “ontime” better, compared to previous sampling rate and precision.

The plots show that, the double threshold at 0.1V-2V captures the ontime as 0.536ms and 0.1V-3V captures the fueling ontime as 0.528ms with very little variability. Since the resolution of the captured ontime is 0.008ms, the system cannot capture exactly 0.53ms, however, the result is significantly better than the previous results. The results with thresholds at different other values, both in single and double threshold cases are documented in Figure A.15, Figure A.16, Figure A.17, Figure 6.18, Figure A.19, Figure A.20, Figure A.21, Figure A.22 in the appendix. The same experiments are carried out at 0.0189ms ontime and the resulting plots are in Figure 3.36 and Figure 3.37. These plots signifies that, the system with higher precision and sampling rate manages to capture the ontime as small as 0.189ms with very good accuracy and variability, varying by only ±1 time step of 0.008ms. Remaining figures with different thresholds have been documented in Figure A.23, Figure A.24, Figure A.25, Figure A.26, Figure A.27, Figure A.28, Figure A.29, Figure A.30 and Figure A.31 in the appendix.

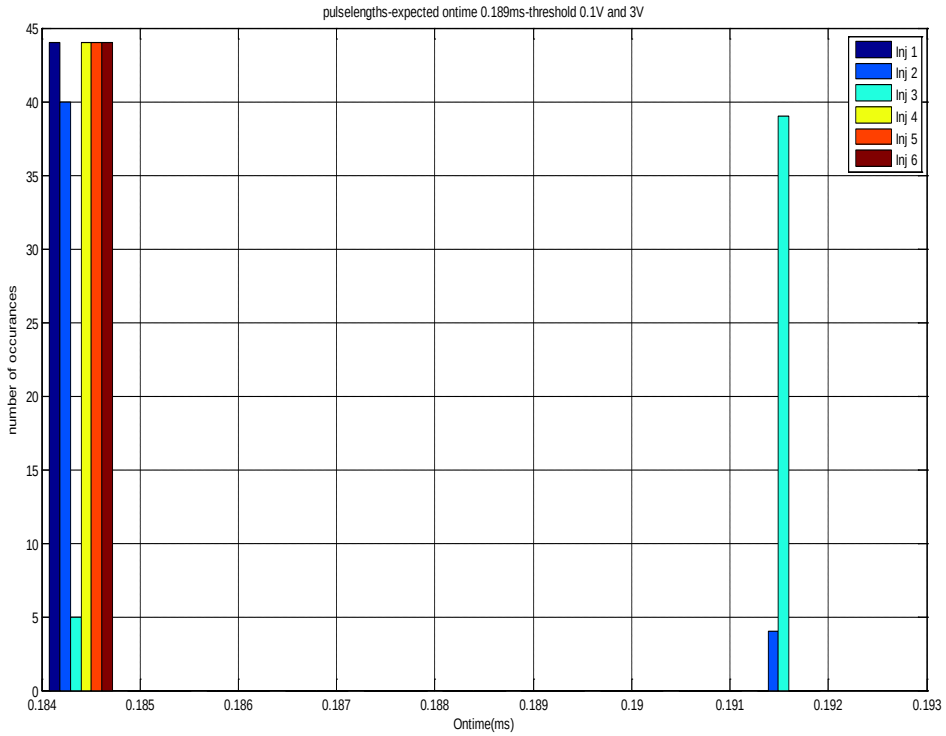

Figure 3.36 Histogram of captured ontime (ms) with threshold at 0.1V and 3V

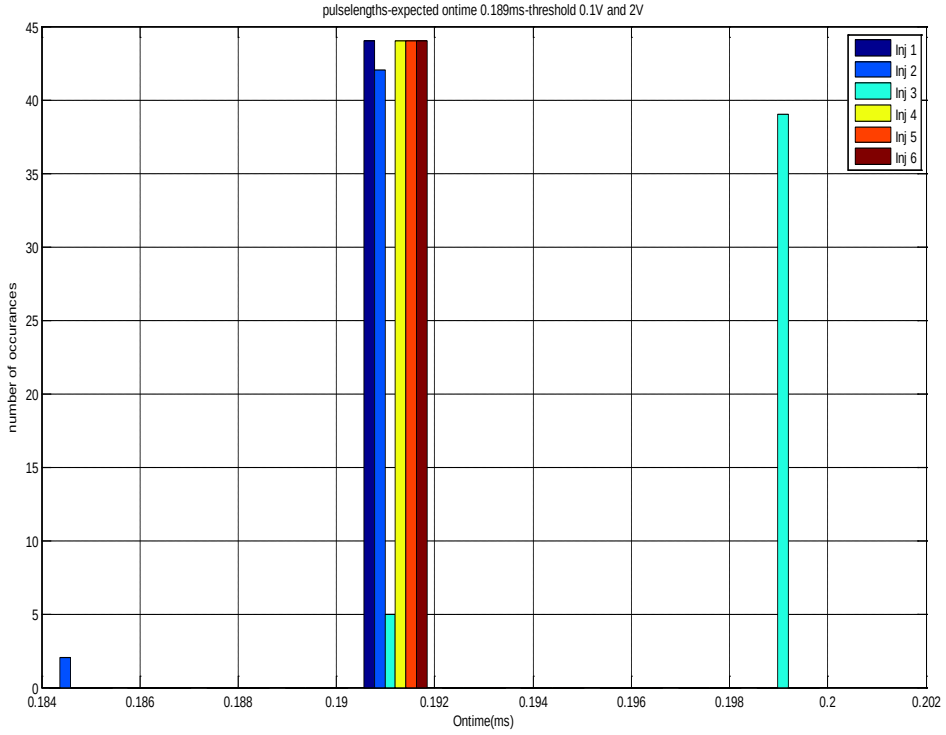

Figure 3.37 Histogram of captured ontime (ms) with threshold at 0.1V and 2V

The above plots show that, the 125kHz sampling rate manages to capture low "ontime", as low as, 0.189ms very well, when double threshold 0.1V and 3V is used. The "ontime" captured sometimes vary by only one data point of 8µs. The pulse to pulse variability was observed to be very low as well.

2.6.3.2 Inductors as Load, One Module for each Injector, with Higher Precision (500 rpm)

If the inductors are used as load, it fails to capture the "ontime" well. Figure 3.38 and Figure 3.39 show that, the inductors do not perform as good as the injectors. However, the inductors perform reasonably well with about ±7 time steps of 0.008ms distortion. The inductor performance deteriorates with other thresholds, as documented in Figure A.33, Figure A.34, Figure A.35, Figure A.36, Figure A.37, Figure A.38, Figure A.39, Figure A.40 in the appendix.

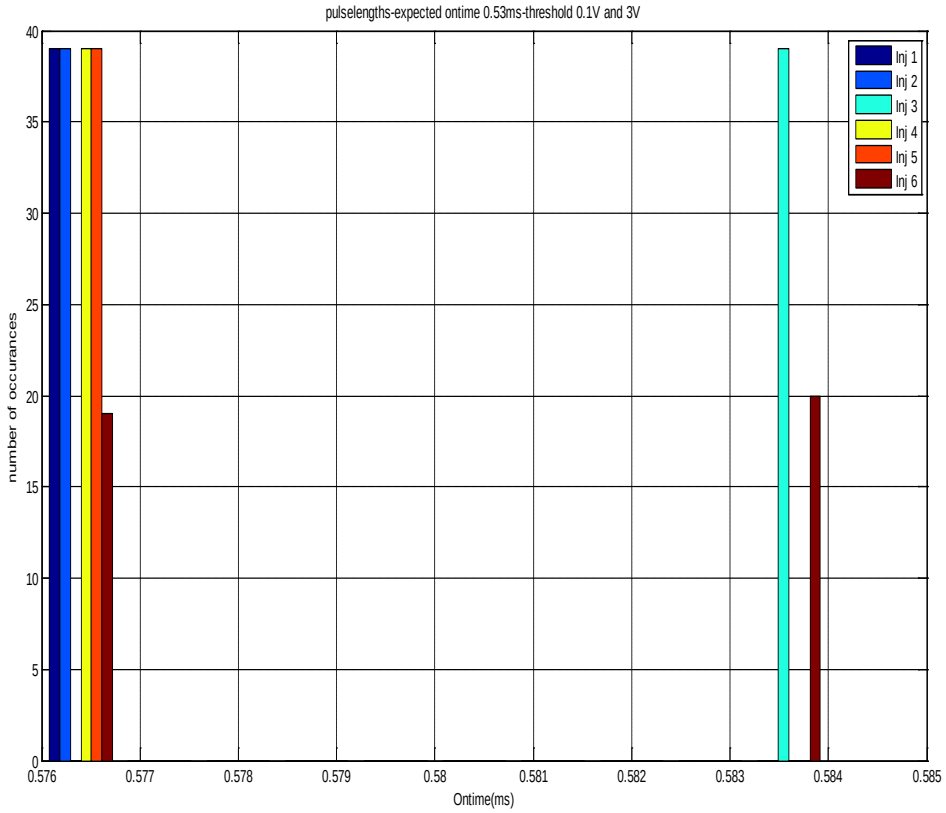

Figure 3.38 Histogram of captured ontime (ms) with threshold at 0.1V and 3V

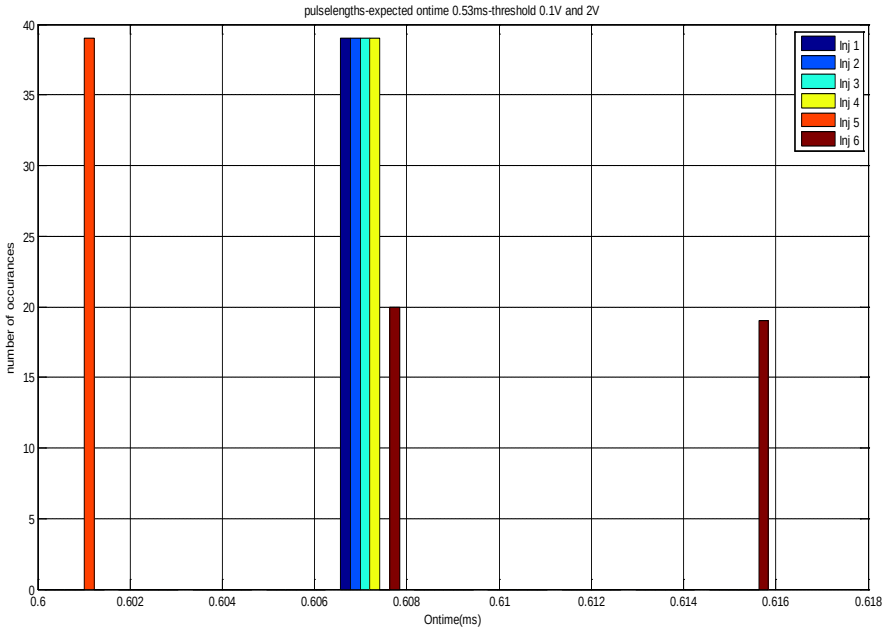

Figure 3.39 Histogram of captured ontime (ms) with threshold at 0.1V and 2V

2.6.3.3 Inductors as Load, One Module for Each Injector, with Higher Precision at 1500 rpm

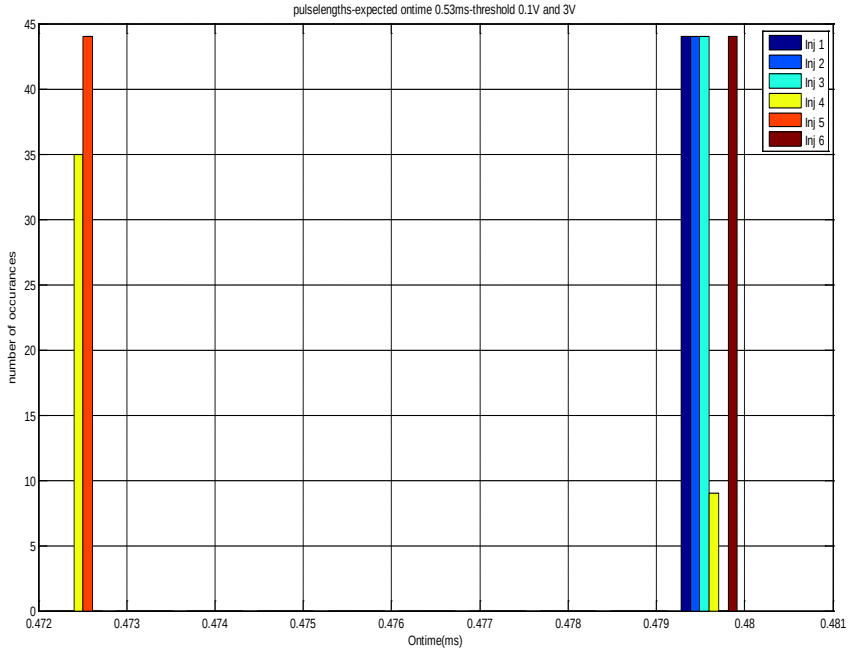

Figure 3.40 Histogram of captured ontime (ms) with threshold at 0.1V and 3V at 1500rpm (Inductors)

The performance of inductors at higher engine speed is shown in Figure 3.40. The inductors perform reasonably well within about ±7 time steps of 0.008ms distortion. However, the error is negative, i.e. the sensed ontime is lower than 0.53ms. With lower engine speed, the error was observed to be positive. This observation shows that the error varies over a wider range with varying engine speed.

2.6.3.4 Injectors as Load, One Module for Each Injector, with Higher Precision at 1500 rpm

Figure 3.41 and Figure 3.42 shows the performance of injectors at higher engine speed of 1500rpm. The plots show that, the accuracy remains very well and does not vary over different engine speed. Figure 3.41 shows injectors capturing very low fuel quantity of 0.0189mg/stk and the performance is as remarkable at low engine speed.

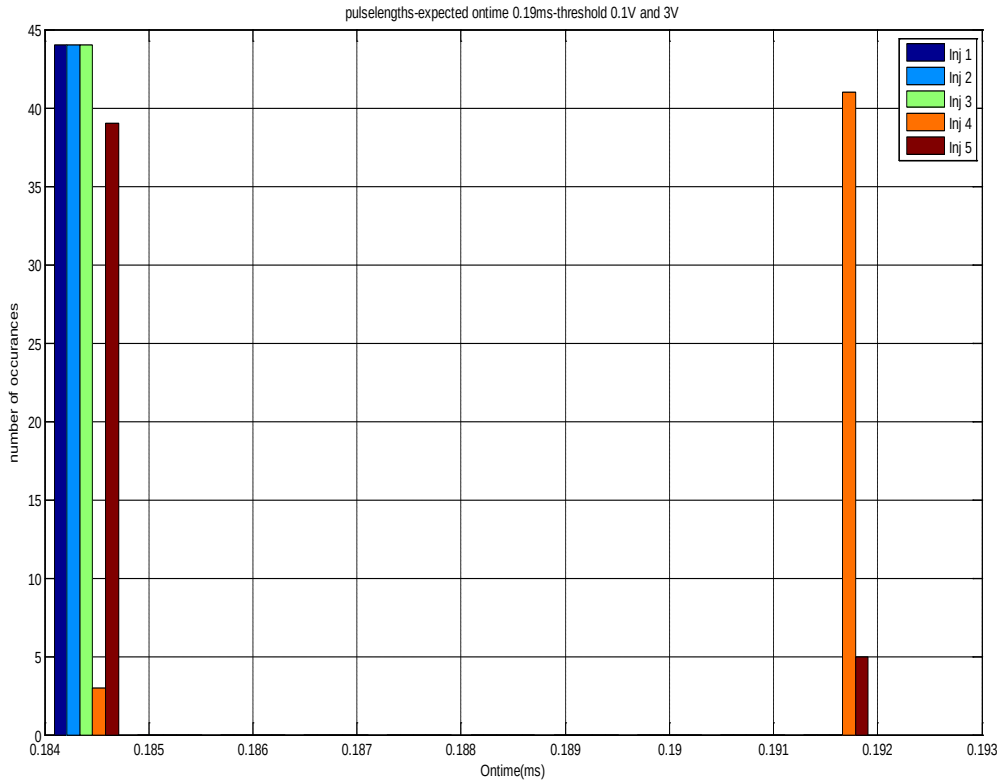

Figure 3.41 Histogram of captured ontime (ms) with injectors with threshold at 0.1V and 3V at 1500rpm

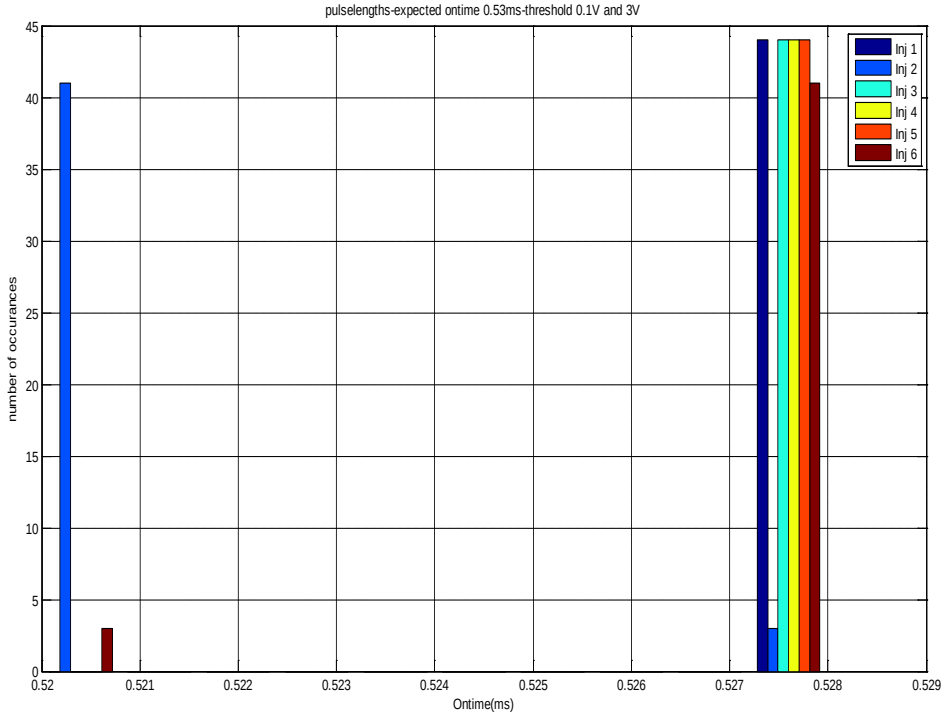

Figure 3.42 Histogram of captured ontime (ms) with injectors with threshold at 0.1V and 3V at 1500rpm

2.7 Design of Experiment and Mixed Model ANOVA

It is evident from the previous experimental result that, using the highest sampling rate available with double threshold provide the best estimate of the calculated fueling quantity by the ECM, however, there is variability involved in the process. In order to implement this system in the HIL bench, it is critical to know the variability involved, and the factors that contribute to the variability in order to have confidence in the system, as well as, a correction model can be sought in future to make the system as accurate as possible over the entire operating range. Three fixed factors have been identified, i.e. engine speed, common-rail pressure and fueling quantity at various levels in Table 3.3. Fifty replicates, i.e. pulses were collected over randomized sequence of factor levels were collected using double threshold with SOI at 0.5V and EOI at 2V, with six injectors, as well as, six inductors. Statistical analysis of error and variability with full factorial DOE, considering the fixed factors, as well as, the random factors, was carried out.

Table 3.3 DOE fixed-factors and their levels

Factors	Levels			
Engine Speed (rpm)	750	1500	2250	
Pressure (bar)	600	1200	1800	
Fueling quantity (mg/stk)	10	50	100	150

The six injectors/inductors also showed variation in performance, however, the six injectors/inductors have been considered random factors, since they are expected to be identical and only the variability involved in the production process of the injectors contribute to the variability in them.

A full factorial DOE was carried out with randomized run order of the fixed factors both on injectors and inductors, having the error percentage in the estimation of the fueling quantity being the response variable. The DOE result with 95% confidence interval showed that, all the fixed factors and interactions were contributing to the rejection of the null hypothesis. Null hypothesis claims that, the data collected over all the levels of all the factors represent the natural variability of only one process. The mathematical model of this experiment that uses three way analysis of variance (ANOVA) and design is,

$$E = \mu + S_i + P_j + F_k + SP_{ij} + SF_{ik} + PF_{jk} + SPF_{ijk} + \varepsilon_{m(ijk)} \text{.....(i)}$$

Where, S = engine speed, P = common-rail pressure, F = fueling quantity, i, j, k are 1 through 50 and m=1, 2, 3, 4.

2.7.1 Design of Experiment and Mixed Model ANOVA with Injectors

The fourth injector has been chosen to represent the similar results obtained for all six injectors in the DOE. The residual plot in Figure 3.43 shows that the error percentage in fueling quantity monitoring is normally distributed and the ANOVA result is shown in

Table 3.4. It is important to have the residual being normally distributed, since ANOVA requires the residual to be normally distributed. One of the four residual plots shown in Figure 3.43 shows that the residuals are randomly scattered in the scatter plot. The histogram shows that the mean of the residuals are close to zero error. However, ANOVA is not about the fact, if the error is closer to zero, it indicates if the data means at various values of factors are significantly different. The P value indicates the probability of making type I error, i.e. being wrong to reject null hypothesis if the data adheres to the null hypothesis in reality.

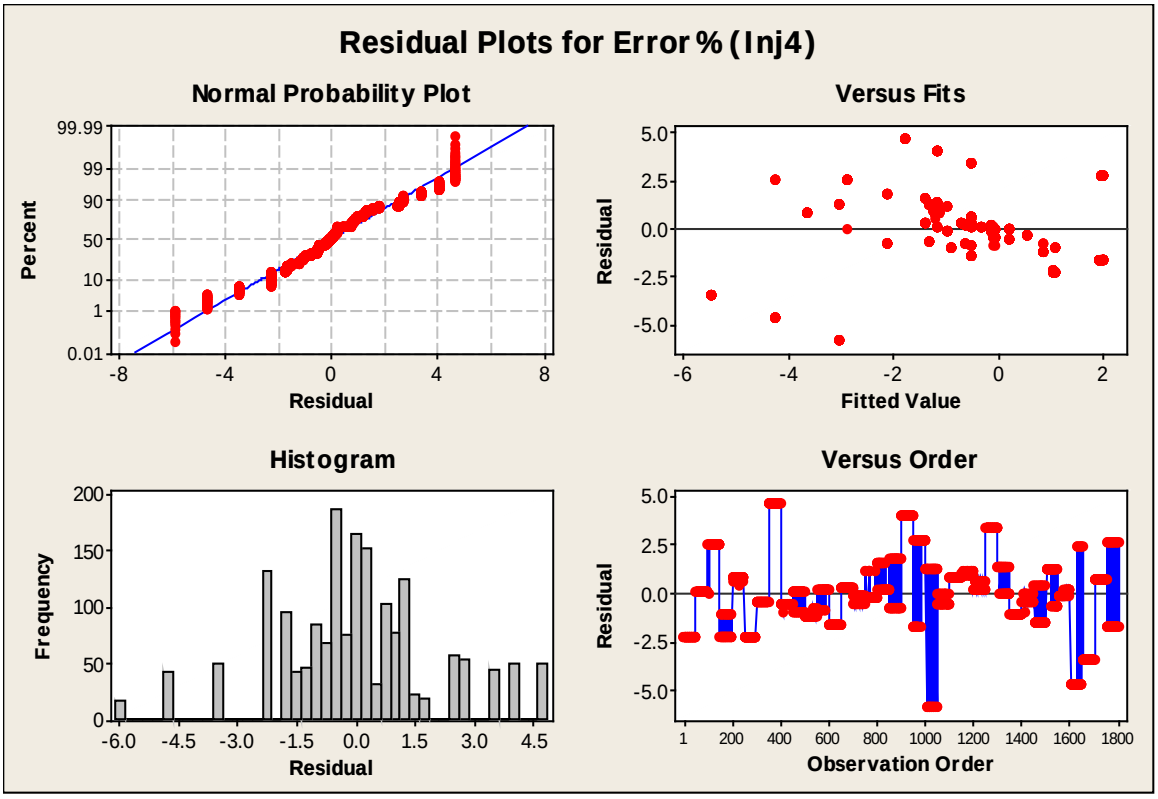

Figure 3.43 Three-way ANOVA DOE for Injector 4

The P values in Table 3.4 indicate that all the factors and their interactions reject the null hypothesis of ANOVA, since the analysis is carried out with 95% confidence interval and the probability of being wrong is zero percent, if the null hypothesis is rejected. This result led to further investigation of the variability in standard deviation. In order to find out if an effort towards finding a model that will estimate the error at

various values in factors based on the mean values is going to be effective, because, if the variability in the data is too high, the proposed system will deem unsuitable for the HIL application.

Table 3.4 ANOVA for error percentage in monitoring of fueling quantity

Source of Variation	Degrees of Freedom (df)	Sum of Squares (SS)	Mean Square (MS)	F	P
S	2	88.34	44.17	50.47	0
P	2	2393.89	1196.95	1367.57	0
F	3	346.1	115.37	131.81	0
S*P	4	196.28	49.07	56.07	0
S*F	6	258.74	43.12	49.27	0
P*F	6	6503.92	1083.99	1238.51	0
S*P*F	12	556.89	46.41	53.02	0
Error	1754	1535.16	0.88		0
Totals	1789				0
S	0.93554				
R-Sq	87.08%				
R-Sq(Adj)	86.83%				

Where, S = engine speed, P = common-rail pressure, F = fueling quantity, *P values less than 0.05, therefore, null hypothesis has been rejected.

The mean error percentage at each level of the three factors shown in Figure 3.44 indicates that, the mean is varying within -2.4% to 0.15% error.

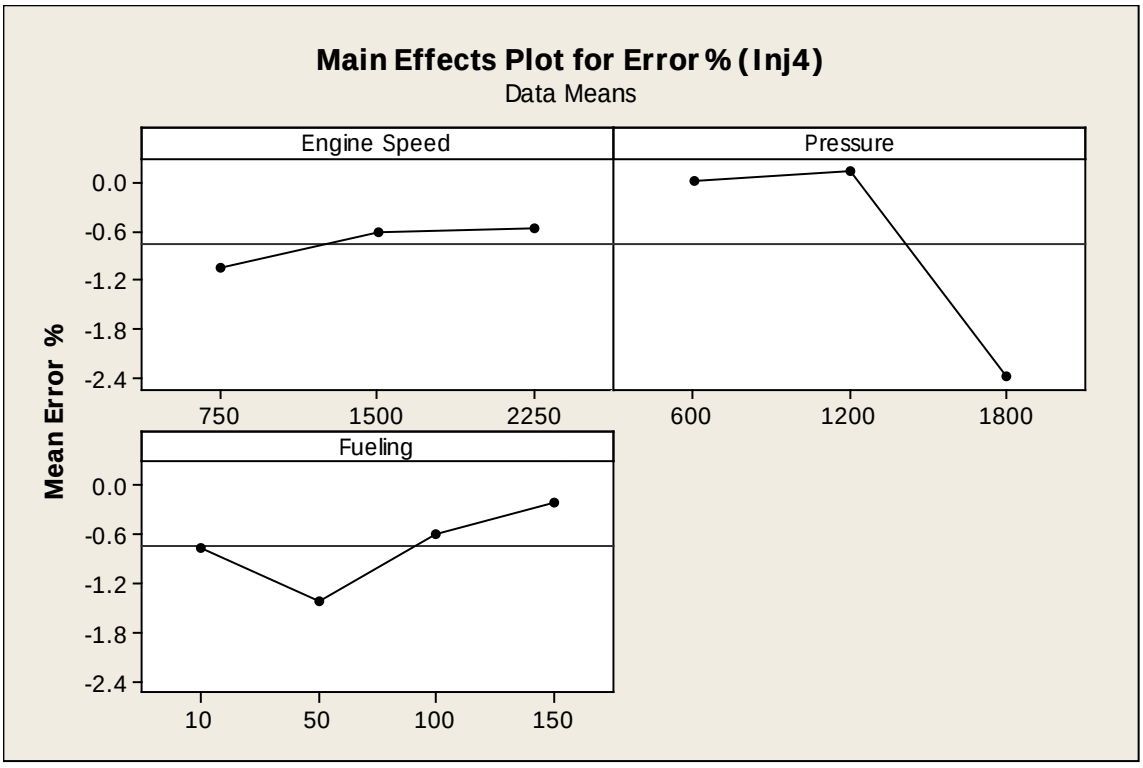

Figure 3.44 Main effect plots on the mean of error percentage with injectors

The interaction effect of engine speed and pressure on mean error percent is shown in Figure 3.45. It shows that the effect of pressure is higher than the engine speed.

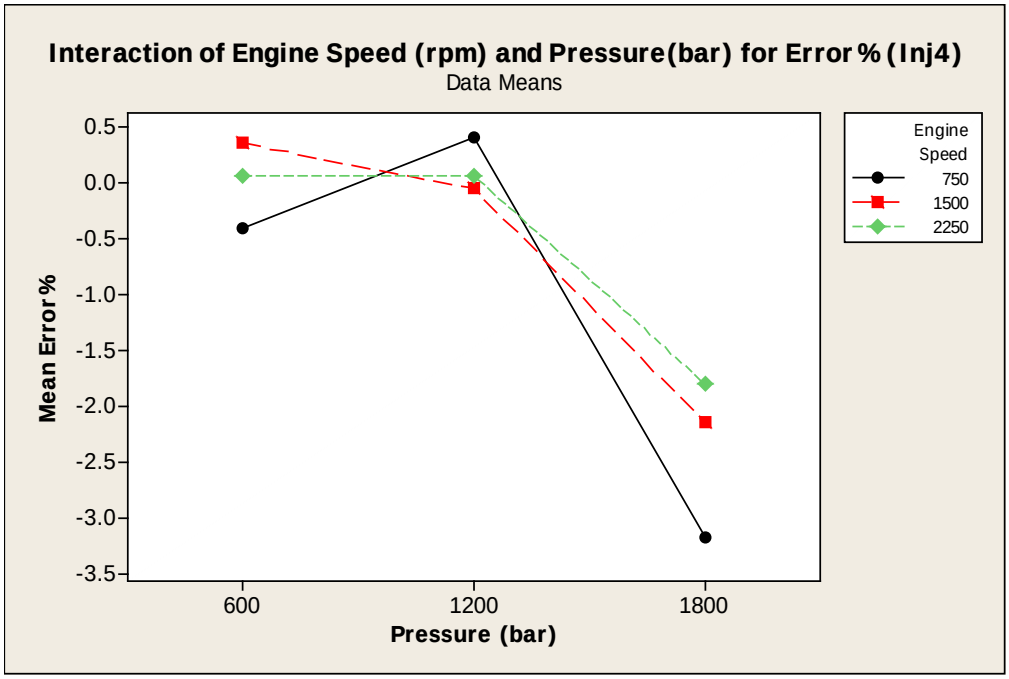

Figure 3.45 Interaction of pressure and engine speed on error percent with injectors

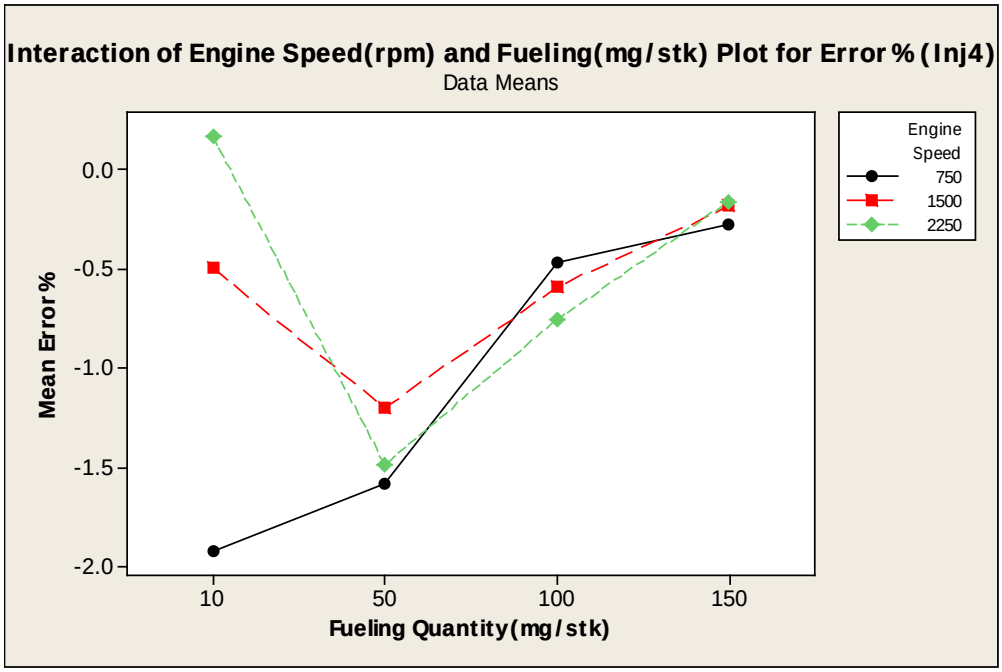

Figure 3.46 Interaction of fueling and engine speed on error percentage with injectors

Figure 3.46 shows that, the error varies over different engine speeds at lower fueling quantity, while at higher fueling values, the effect of varying engine speeds

diminishes to dominate. Figure 3.47 shows that the error is higher at lower fueling quantity. The effect of pressure on mean error percent is lower compared to the effect of fueling quantity, but the effect was observed to be higher compared to engine speed. The error percent at various pressure values are close at higher fueling quantity, but the error deviates from zero at higher pressure irrespective of engine speed.

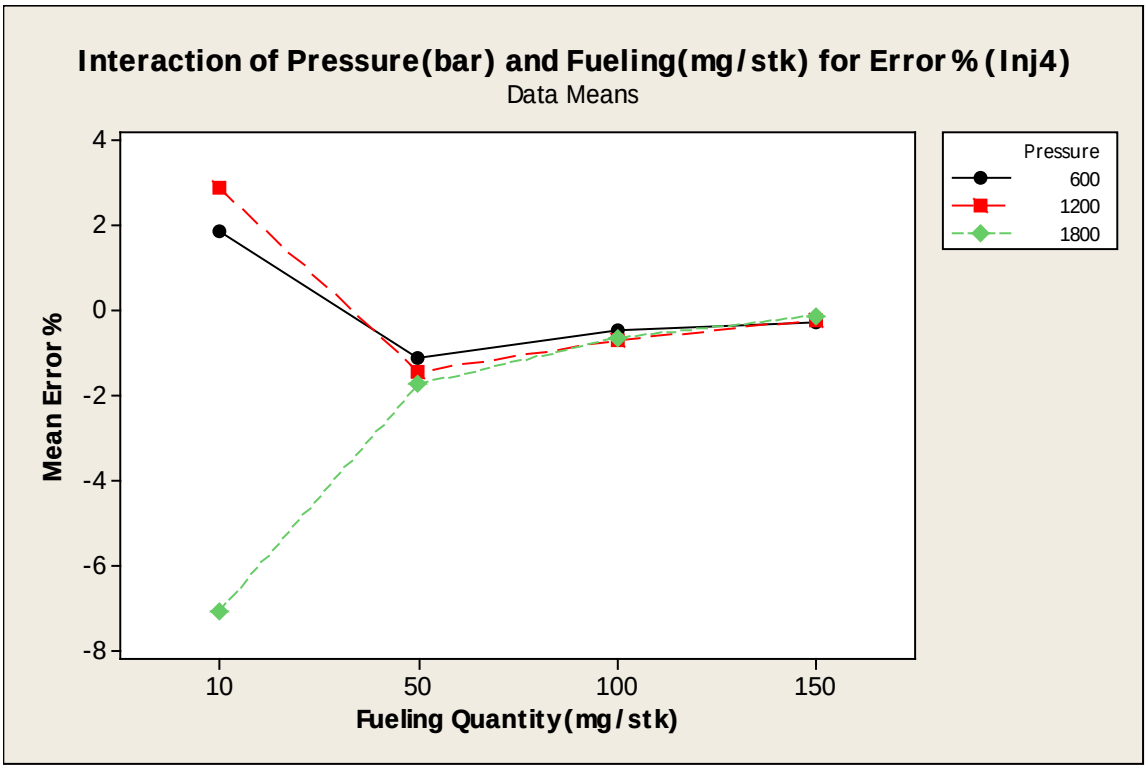

Figure 3.47 Interaction of fueling and pressure on error percentage with injectors

Results above shows promise that, error can be modeled and corrected only if the variability, i.e. the standard deviations at each of the factor levels are not too high. Therefore, standard deviations of error at each factor levels were calculated for 50 replicates, i.e. pulses in

Table 3.5. The standard deviations at thirty six states were considered as the dependent variable in the study of variability of standard deviation. The ANOVA was carried out on the standard deviation values.

Table 3.5 Standard deviations of error among 50 pulses using injectors

Eng Speed (rpm)	Pressure (bar)	Fueling (mg/stk)	Inj 1	Inj 2	Inj 3	Inj 4	Inj 5	Inj 6
750	600	10	0.0001	0.001	2.201247	0.0001	2.112718	0.0001
750	600	50	0.0001	0.001	0.590279	0.0001	0.642928	0.0001
750	600	100	0.241061	0.248703	0.184557	0.241061	0.09478	0.177317
750	600	150	0.045061	0.068985	0.045061	0.032193	0.04599	0.084301
750	1200	10	0.0001	0.001	0.0001	0.0001	0.0001	2.964272
750	1200	50	0.271865	0.673812	0.970947	0.871908	0.0001	0.0001
750	1200	100	0.0001	0.001	0.200275	0.0001	0.242717	0.0001
750	1200	150	0.079901	0.001	0.0001	0.156942	0.0001	0.0001
750	1800	10	0.0001	0.001	0.0001	0.0001	3.502245	3.365801
750	1800	50	0.0001	0.955685	0.0001	0.0001	0.0001	0.0001
750	1800	100	0.526221	0.676026	0.445099	0.6799	0.001	0.001
750	1800	150	0.001	0.001	0.107971	0.123341	0.215367	0.06365
1500	600	10	0.001	0.001	1.635045	1.956287	1.547545	0.873968
1500	600	50	0.001	0.24595	0.563541	0.001	0.001	0.172165
1500	600	100	0.067714	0.067714	0.217168	0.067714	0.178632	0.209492
1500	600	150	0.056138	0.04599	0.112652	0.087743	0.114144	0.07979
1500	1200	10	3.835748	2.815088	0.001	0.001	0.001	0.001
1500	1200	50	0.001	0.001	0.871908	0.001	0.905847	0.001
1500	1200	100	0.200275	0.354629	0.001	0.490571	0.001	0.001
1500	1200	150	0.161492	0.116741	0.001	0.001	0.079901	0.161492
1500	1800	10	0.001	0.001	0.001	2.503642	0.001	0.001
1500	1800	50	0.001	0.001	1.079876	0.364958	0.364958	0.001
1500	1800	100	0.676026	0.001	0.001	0.671012	0.001	0.001
1500	1800	150	0.194169	0.001	0.001	0.001	0.208342	0.227138
2250	600	10	2.184921	2.002513	2.140776	2.112718	2.080461	2.222828
2250	600	50	0.172165	0.344329	0.509419	0.573648	0.472454	0.573648
2250	600	100	0.17439	0.206568	0.216305	0.201987	0.241836	0.277848
2250	600	150	0.107758	0.096579	0.113494	0.110376	0.12349	0.111614
2250	1200	10	0.001	3.086985	2.77611	0.001	0.001	4.046842
2250	1200	50	0.905847	0.461174	0.96393	0.71191	0.871908	0.919892
2250	1200	100	0.143083	0.484141	0.436489	0.484141	0.46835	0.143083
2250	1200	150	6.726946	0.166054	0.154177	0.167682	0.154177	0.167682
2250	1800	10	3.417987	3.596125	3.417987	23.04651	3.417987	3.46338
2250	1800	50	1.277088	1.216031	1.234885	1.265327	1.299245	1.302379
2250	1800	100	0.648838	0.001	0.648838	0.50214	0.475268	15.20192
2250	1800	150	0.220676	0.225677	0.222727	0.224391	0.218227	0.218227

The three way ANOVA analysis on the standard deviation of the error in fifty replicates or pulses at each state could not use the mathematical model in (i) due to lack

of degrees of freedom for error. Therefore, the interaction of three factors together was removed and ANOVA was carried out. The residual plot in Figure 3.48 shows that, the residual of the generalized linear model fitting for the dependent variables, standard deviation of error, data does not follow normal distribution, since the residual versus fitted value plot shows a distinct pattern.

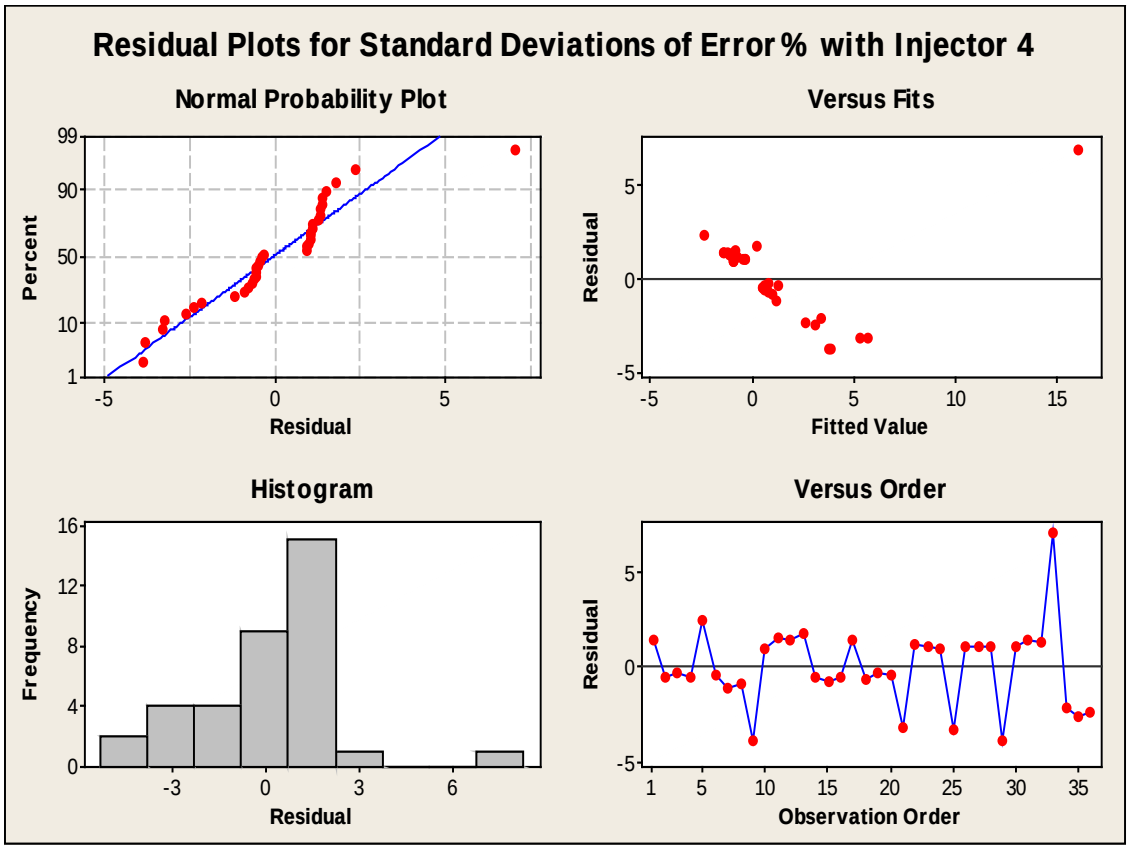

Figure 3.48 Residual plots of ANOVA of standard deviation of error with injectors

Thus, the standard deviations of errors were transformed to the natural logarithmic scale. In order to take natural log, the zero standard deviations were changed to 0.001. The natural log table is shown in Table 3.6 Natural log of standard deviations of error with injectors". The mathematical model for the ANOVA becomes,

$$Log(E) = \mu + S_i + P_j + F_k + SP_{ij} + SF_{ik} + PF_{jk} + \varepsilon_{m(ijk)} \text{.....(ii)}$$

Where, S = engine speed, P = common-rail pressure, F = fueling quantity, i, j, k are 1 through 50 and m=1, 2, 3, 4.

Table 3.6 Natural log of standard deviations of error with injectors

Eng Speed (rpm)	Pressure (bar)	Fueling (mg/stk)	Ln (ErStdInj 1)	Ln (ErStdInj 2)	Ln (ErStdInj 3)	Ln (ErStdInj 4)	Ln (ErStdInj 5)	Ln (ErStdInj 6)	RunOrder
750	600	10	-9.21034	-6.90776	0.789024	-9.21034	0.747975	-9.21034	13
750	600	50	-9.21034	-6.90776	-0.52716	-9.21034	-0.44172	-9.21034	6
750	600	100	-1.42271	-1.39149	-1.68979	-1.42271	-2.3562	-1.72982	22
750	600	150	-3.09974	-2.67387	-3.09974	-3.43601	-3.07933	-2.47336	23
750	1200	10	-9.21034	-6.90776	-9.21034	-9.21034	-9.21034	1.086631	8
750	1200	50	-1.30245	-0.3948	-0.02948	-0.13707	-9.21034	-9.21034	31
750	1200	100	-9.21034	-6.90776	-1.60806	-9.21034	-1.41586	-9.21034	14
750	1200	150	-2.52697	-6.90776	-9.21034	-1.85188	-9.21034	-9.21034	32
750	1800	10	-9.21034	-6.90776	-9.21034	-9.21034	1.253404	1.213666	34
750	1800	50	-9.21034	-0.04533	-9.21034	-9.21034	-9.21034	-9.21034	35
750	1800	100	-0.64203	-0.39152	-0.80946	-0.38581	-6.90776	-6.90776	17
750	1800	150	-6.90776	-6.90776	-2.22589	-2.09281	-1.53541	-2.75436	11
1500	600	10	-6.90776	-6.90776	0.49167	0.671048	0.43667	-0.13471	20
1500	600	50	-6.90776	-1.40263	-0.57351	-6.90776	-6.90776	-1.7593	1
1500	600	100	-2.69246	-2.69246	-1.52708	-2.69246	-1.72243	-1.56307	9
1500	600	150	-2.87995	-3.07933	-2.18345	-2.43334	-2.17029	-2.52836	5
1500	1200	10	1.344364	1.034993	-6.90776	-6.90776	-6.90776	-6.90776	19
1500	1200	50	-6.90776	-6.90776	-0.13707	-6.90776	-0.09889	-6.90776	28
1500	1200	100	-1.60806	-1.03668	-6.90776	-0.71218	-6.90776	-6.90776	12
1500	1200	150	-1.8233	-2.1478	-6.90776	-6.90776	-2.52697	-1.8233	2
1500	1800	10	-6.90776	-6.90776	-6.90776	0.917746	-6.90776	-6.90776	33
1500	1800	50	-6.90776	-6.90776	0.076846	-1.00797	-1.00797	-6.90776	3
1500	1800	100	-0.39152	-6.90776	-6.90776	-0.39897	-6.90776	-6.90776	27
1500	1800	150	-1.63903	-6.90776	-6.90776	-6.90776	-1.56857	-1.4822	7
2250	600	10	0.78158	0.694403	0.761169	0.747975	0.732589	0.79878	36
2250	600	50	-1.7593	-1.06616	-0.67449	-0.55574	-0.74982	-0.55574	4
2250	600	100	-1.74646	-1.57712	-1.53107	-1.59955	-1.4195	-1.28068	29
2250	600	150	-2.22787	-2.3374	-2.17601	-2.20386	-2.0916	-2.19271	24
2250	1200	10	-6.90776	1.127195	1.021051	-6.90776	-6.90776	1.397937	26
2250	1200	50	-0.09889	-0.77398	-0.03674	-0.3398	-0.13707	-0.0835	30
2250	1200	100	-1.94433	-0.72538	-0.82899	-0.72538	-0.75854	-1.94433	10
2250	1200	150	1.906121	-1.79544	-1.86965	-1.78569	-1.86965	-1.78569	25
2250	1800	10	1.229052	1.279857	1.229052	3.137515	1.229052	1.242245	21
2250	1800	50	0.244583	0.195592	0.210978	0.235331	0.261783	0.264193	18
2250	1800	100	-0.43257	-6.90776	-0.43257	-0.68888	-0.74388	2.721422	16
2250	1800	150	-1.51106	-1.48865	-1.50181	-1.49436	-1.52222	-1.52222	15

The residual plot in Figure 3.49Figure 3.48 shows the residual after fitting the log of standard deviation data to the generalized linear model in equation (ii). It shows that, the data satisfies the requirement of having natural distribution with the logarithmic transformation. Therefore, the ANOVA on the data is more acceptable.

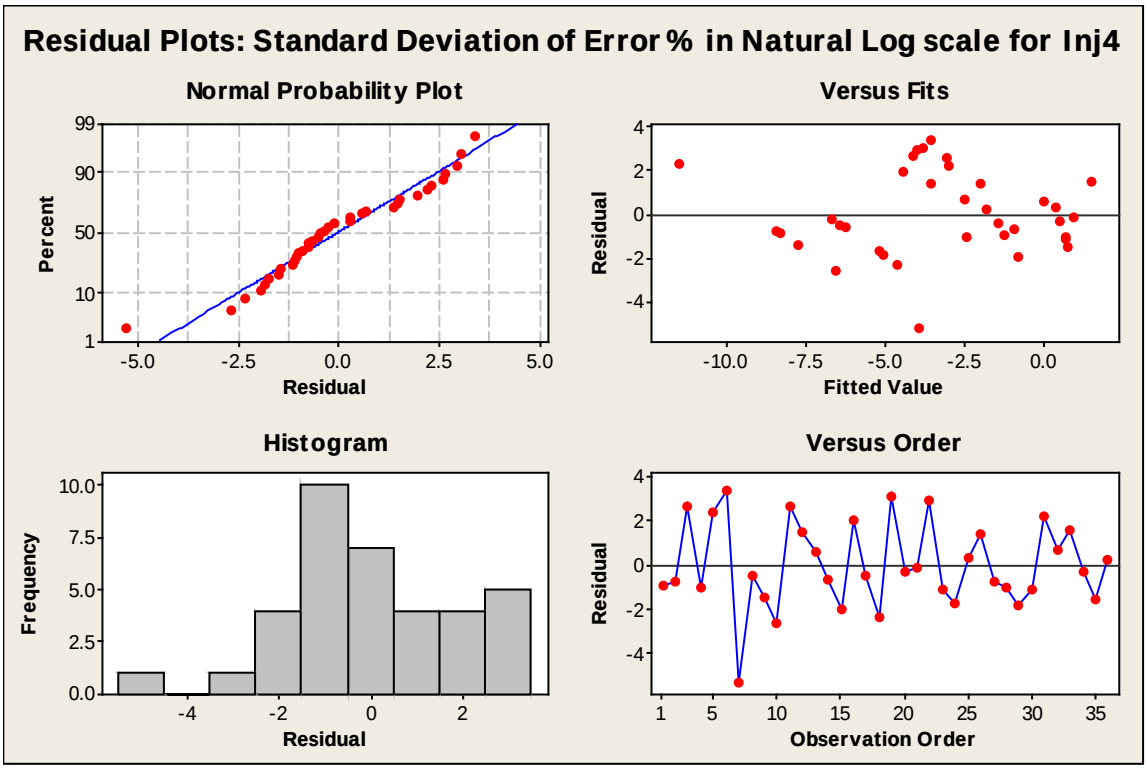

Figure 3.49 Residual plot of ANOVA of natural log of standard deviations with injectors

The Table 3.7 shows that, only the engine speed rejects the null hypothesis of ANOVA with 95% confidence interval. This means, the standard deviation in error percent data varies significantly as the engine speed varies. Other factors, such as, rail pressure and fueling quantity does not effect the change in variability. Therefore, the variability in error percent can be predicted with 95% statistical confidence that, the variability is normally distributed over all the values of the rail pressure and fueling quantities. However, the variability varies over different values of engine speeds, as seen in Figure 3.50. It shows that, the variability varies from standard deviation of error percentage from 0.004% to 0.368% over the range of engine speed from 750rpm to 2250rpm with injectors.

Table 3.7 ANOVA on log of standard deviation of error on injector 4

Source of Variation	Degrees of Freedom (df)	Sum of Squares (SS)	Mean Square (MS)	F	P
S	2	114.62	57.31	5.36	0.022*
P	2	25.07	12.54	1.17	0.342
F	3	22.05	7.35	0.69	0.577
S*P	4	17.35	4.34	0.41	0.801
S*F	6	67.67	11.28	1.06	0.439
P*F	6	102.98	17.16	1.61	0.228
Error	12	128.20	10.68		
Totals	35				
S	3.26848				
R-Sq	73.18%				
R-Sq(Adj)	21.77%				

Where, S = engine speed, P = common-rail pressure, F = fueling quantity
* P values less than 0.05, therefore, null hypothesis has been rejected.

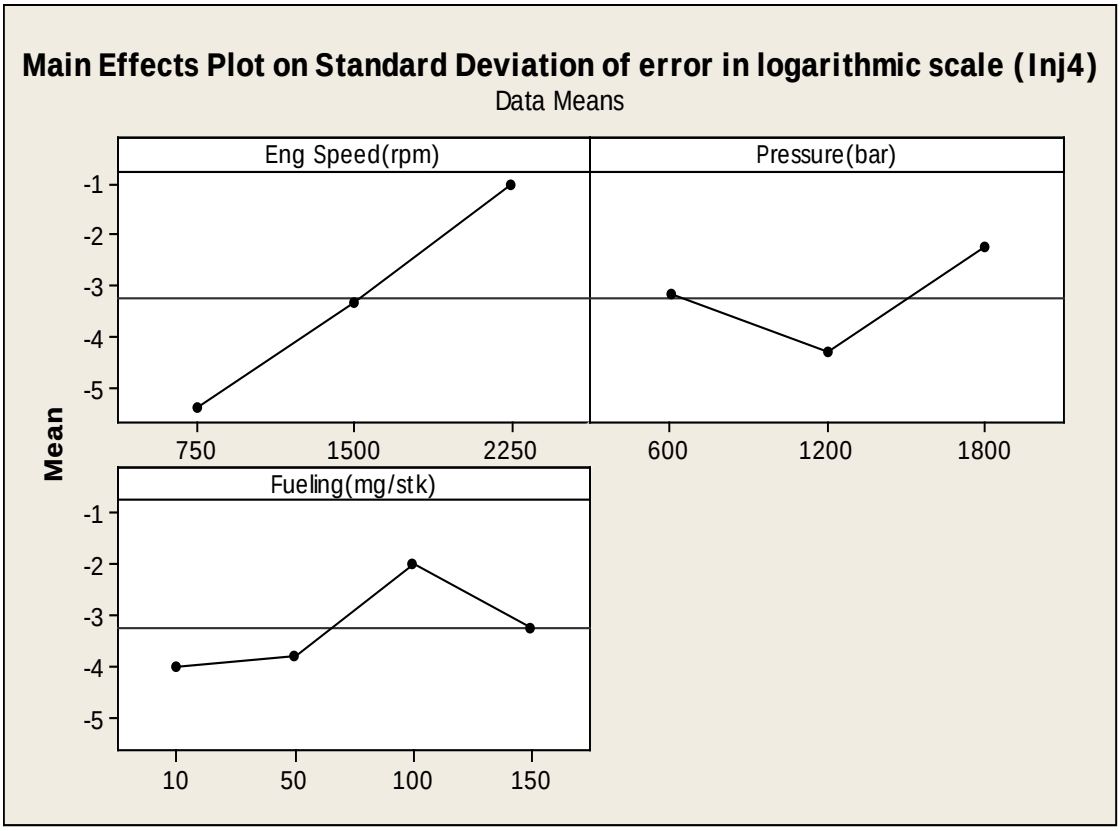

Figure 3.50 Main effect plot on the natural log of standard deviations of error in injector

2.7.2 Mixed Model ANOVA with Injectors as Random Factors

In order to find out the effect of various injectors on the variability, i.e. the variability over the six injectors, ANOVA with mixed model having three fixed factors and a random factor of injectors was carried out and the result is shown in Table 3.8. The mathematical model for mixed model ANOVA is,

$$Log(E) = \mu + S_i + P_j + F_k + I_l + SP_{ij} + SF_{ik} + SI_{il} + PF_{jk} + PI_{jl} + FI_{kl} + \varepsilon_{m(ijkl)} \ldots\ldots \text{(iii)}$$

Where, E=Estimate of standard deviation in error, S = engine speed, P = common-rail pressure, F = fueling quantity, i, j, k are 1 through 50, I=Random factor Injector Numbers, l=1,2,3,4,5,6 and m=1, 2, 3, 4.

Table 3.8 Mixed Model ANOVA of natural log of standard deviations of error with six injectors as random factors

Source of Variation	Degrees of Freedom (df)	Sum of Squares (SS)	Mean Square (MS)	F	P
S	1	77.7	77.7	8.32	0.004*
P	1	19.561	19.561	2.09	0.149
F	1	38.241	38.241	4.10	0.044*
I	5	105.482	21.096	2.26	0.050
S*P	1	15.614	15.614	1.67	0.198
S*F	1	67.092	67.092	7.18	0.008*
S*I	5	26.691	5.338	0.57	0.722
P*F	1	0.018	0.018	0.00	0.965
P*I	5	46.642	9.328	1.00	0.420
F*I	5	65.027	13.005	1.39	0.229
Error	189	1764.947	9.338		
Totals	215				
S	3.05587				
R-Sq	32.42%				
R-Sq(Adj)	23.13%				

Where, S = engine speed, P = common-rail pressure, F = fueling quantity, I= injector numbers.

*P values less than 0.05, therefore, null hypothesis has been rejected.

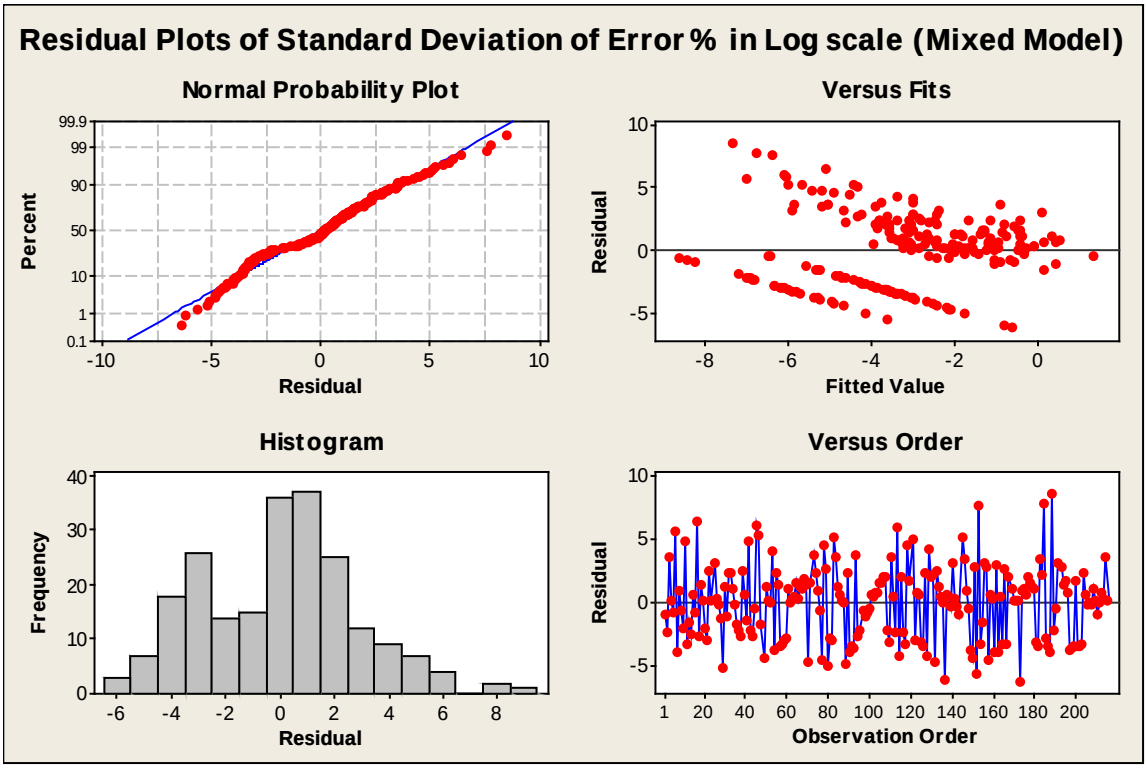

Figure 3.51 Residual plot for Mixed model ANOVA with six injectors

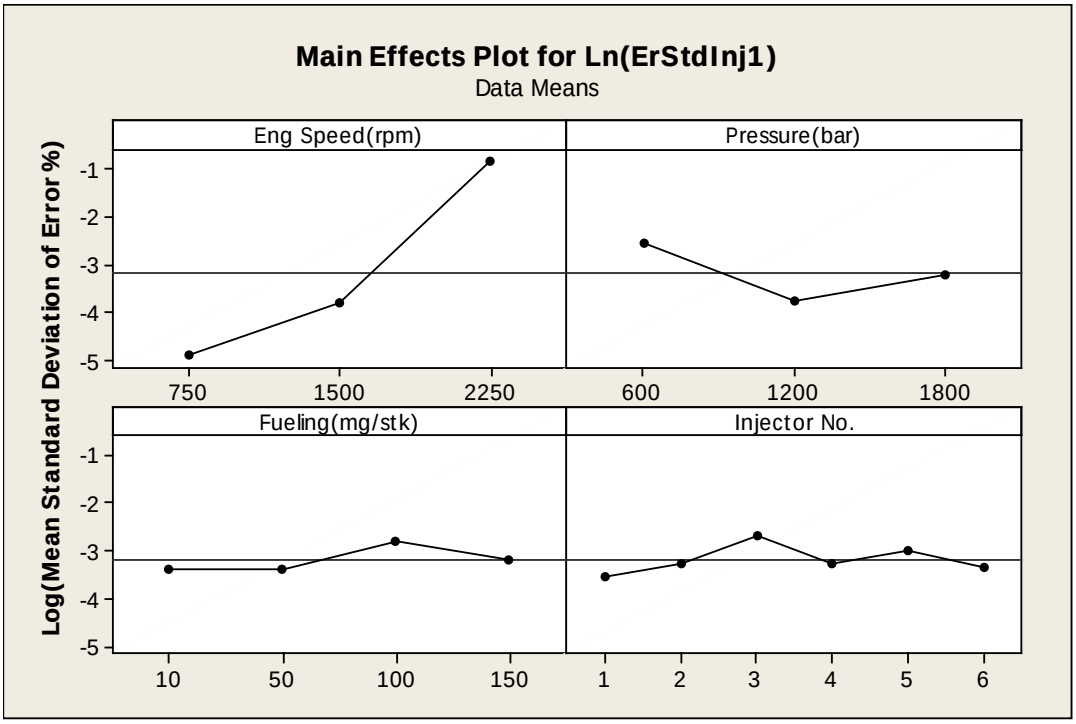

Figure 3.52 Main effect plots for mixed model ANOVA of natural log of standard deviations of error on with six injectors

The P values in Table 3.8 indicate that, if we consider multivariate ANOVA or mixed model ANOVA, the injectors narrowly escapes from rejecting the null hypothesis with 95% confidence interval. However, fueling quantity adds considerable amount of variability to the standard deviation of error that rejects the null hypothesis. Figure 3.51shows the residual plot for the mixed model ANOVA that, shows the normality of the data.

Figure 3.52 shows that, the standard deviation of error, i.e. variability of error is heavily dependent on engine speed ranging from 0.00745% to 0.45% error.

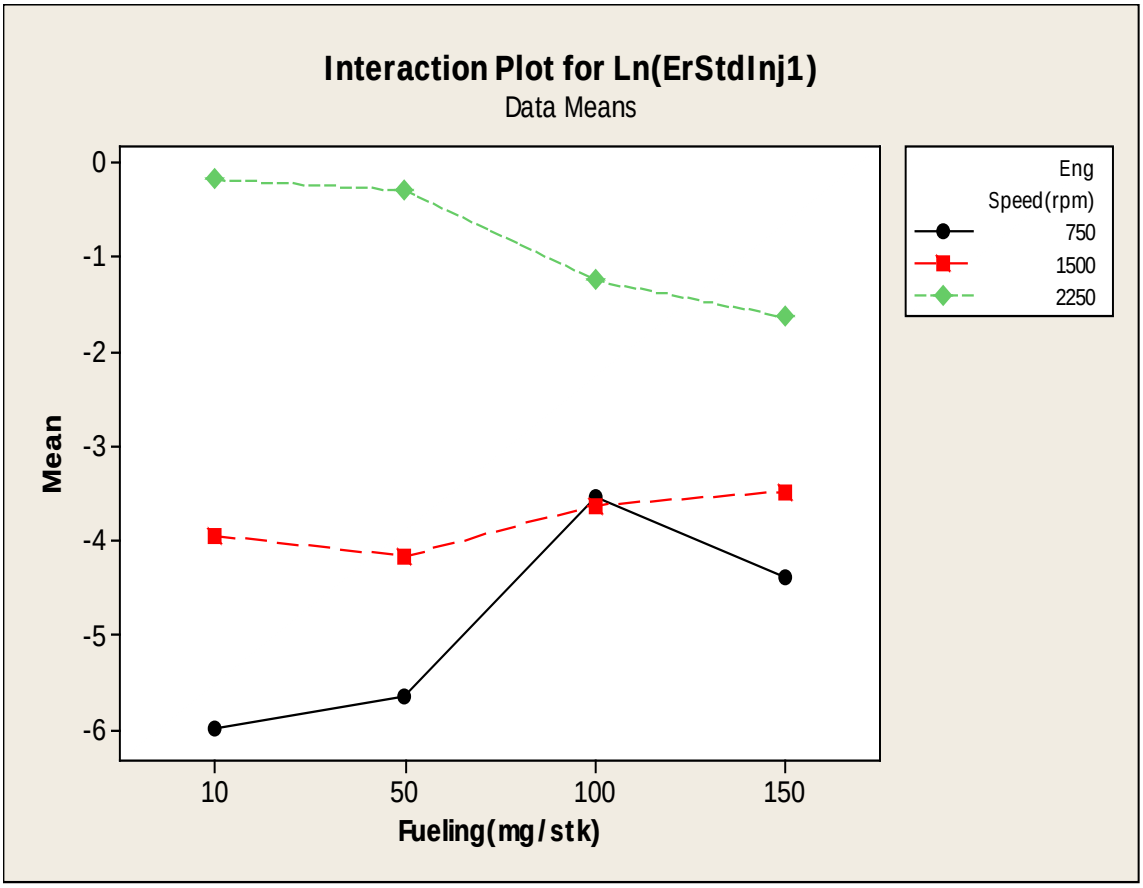

Figure 3.53 Interactions of engine speed and fueling on mixed model ANOVA on injectors

Figure 3.53 shows the interaction that rejects null hypothesis of the mixed model ANOVA, i.e. the interaction of engine speed and fueling quantity. This figure in addition

to the Figure 3.54 indicates that, the variability of error is more influenced by the engine speed than the fueling quantity.

From Table 3.8 it is observed that, the effect of engine speed, fueling quantity and their interaction is the dominating factor in the variability of error across the range of operation with all six injectors. Therefore, ANOVA was carried out on these two factors and the main effects are shown in Figure 3.54. The engine speed is evidently the dominating factor in the variability of the error in fueling quantity monitoring in the system.

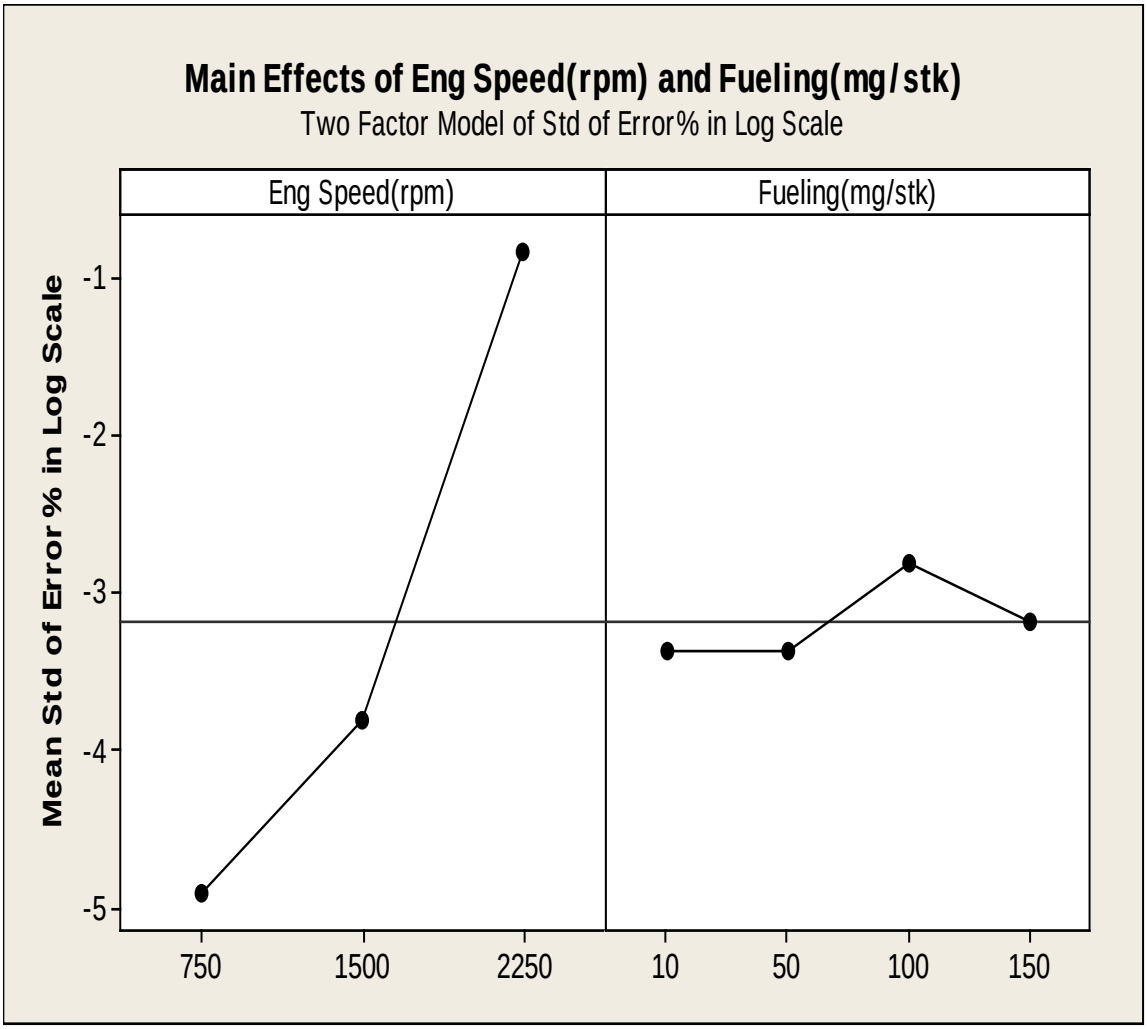

Figure 3.54 Main effect of engine speed and fueling on natural log of standard deviation of error with six injectors

2.7.3 Design of Experiment and Mixed Model ANOVA with Inductors

The fourth inductor has been chosen to represent the similar results obtained for all six inductors in the DOE.

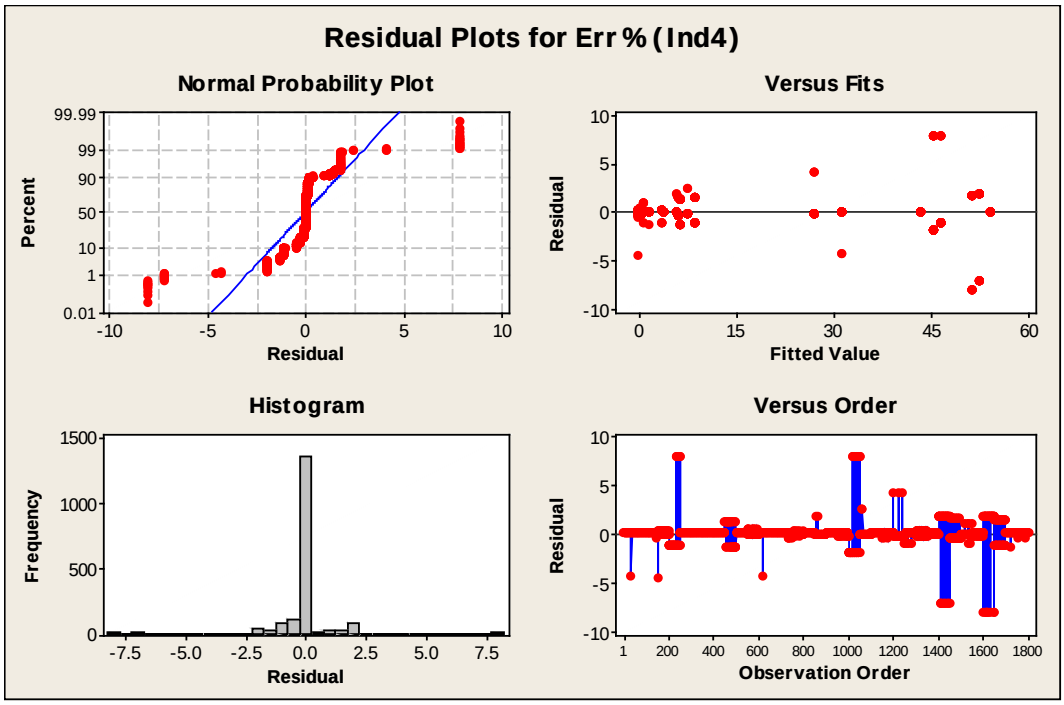

Figure 3.55 Three-way ANOVA DOE for Inductor 4

Table 3.9 ANOVA for error percentage in monitoring of fueling quantity with Inductors

Source of Variation	Degrees of Freedom (df)	Sum of Squares (SS)	Mean Square (MS)	F	P
S	2	387	194	116.48	0
P	2	13527	6764	4071.22	0
F	3	553868	184623	111128.96	0
S*P	4	922	231	138.80	0
S*F	6	791	132	79.38	0
P*F	6	25059	4177	2513.99	0
S*P*F	12	2107	176	105.68	0
Error	1756	2917	2		0
Totals	1791				0
S	1.28893				
R-Sq	99.51%				
R-Sq(Adj)	99.50%				

Where, S = engine speed, P = common-rail pressure, F = fueling quantity,

The residual plot in Figure 3.55 shows that the error percentage in fueling quantity monitoring is not very well normally distributed and the ANOVA result is shown in Table 3.9. The P values indicate that all the factors and their interactions reject the null hypothesis of ANOVA. This result led to further investigation of the variability in standard deviation, in order to find out if an effort towards finding a model that will estimate the error at various values in factors based on the mean values is going to be effective in order to correct the inherent variability.

The mean error percentage at each level of the three factors shown in Figure 3.56 indicates that, the mean is varying within 0% to 41% error. The interaction of engine speed and pressure in Figure 3.57 shows that the effect of pressure is higher than the engine speed.

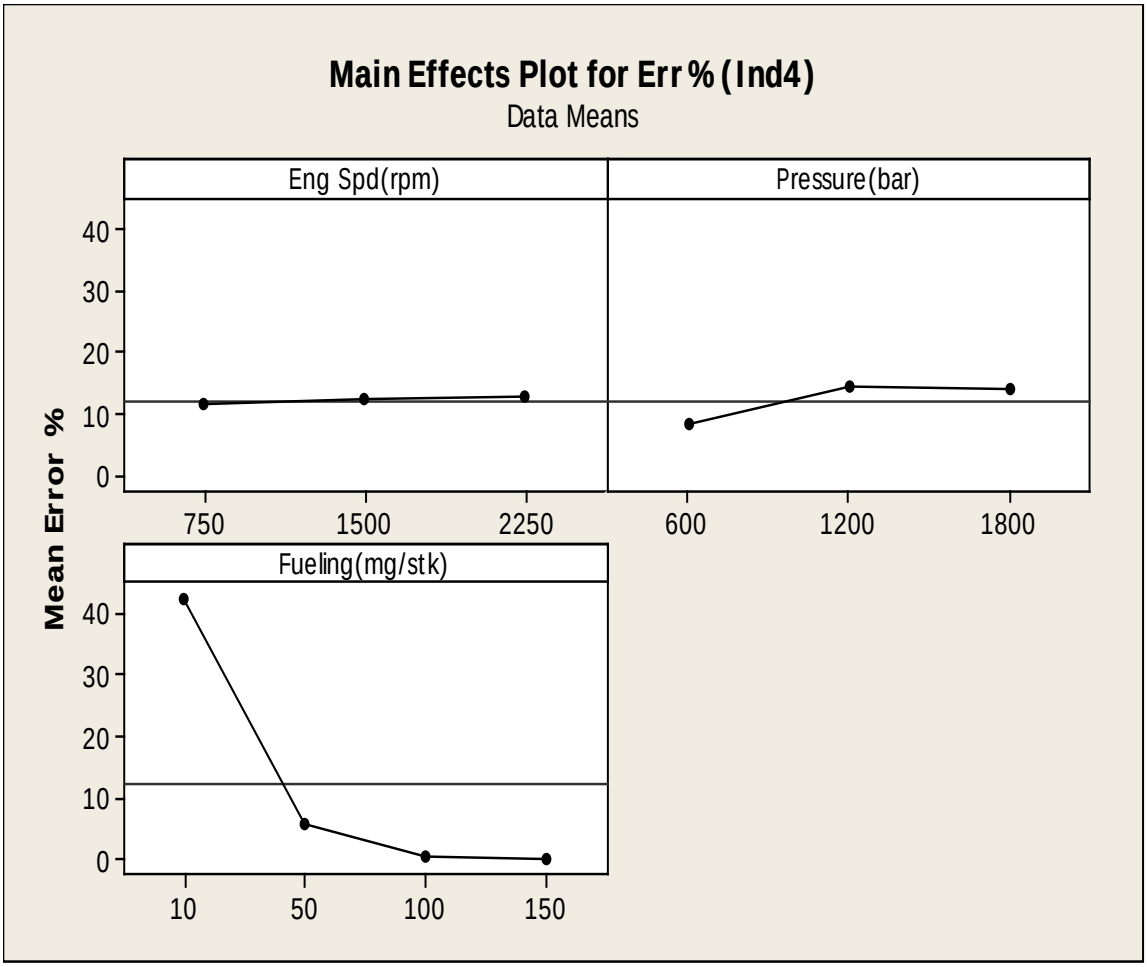

Figure 3.56 Main effect plots on the mean of error percentage with inductors

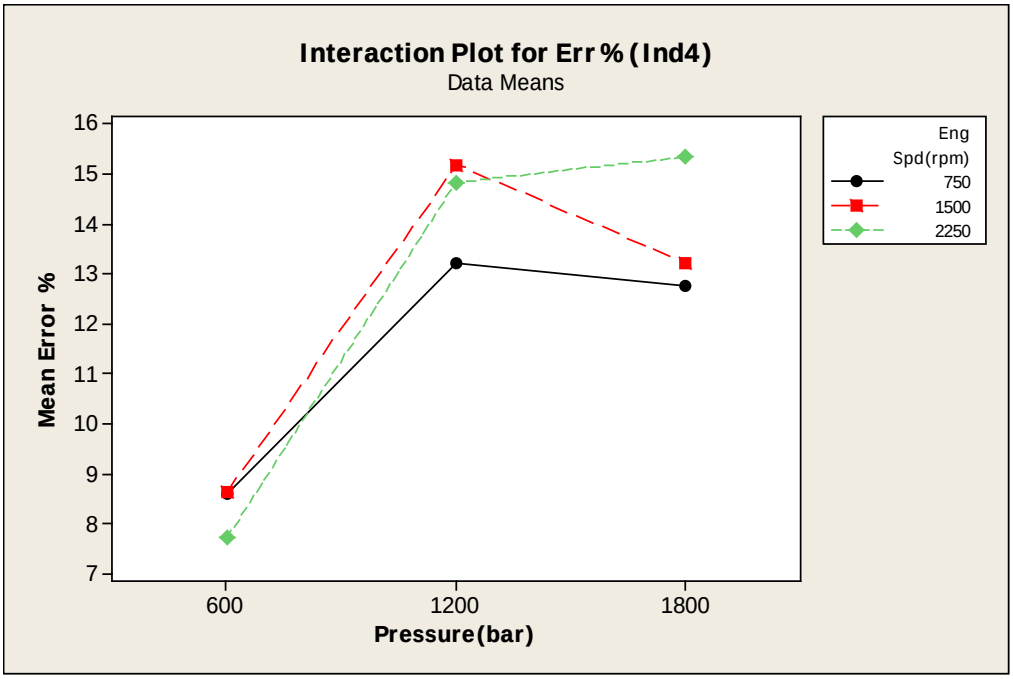

Figure 3.57 Interaction of pressure and engine speed on error percent with inductors

Figure 3.58 shows that, the error varies over different fueling quantity while the interaction with engine speed does not effect that much. The error is dominated by fueling quantity compared to engine speed.

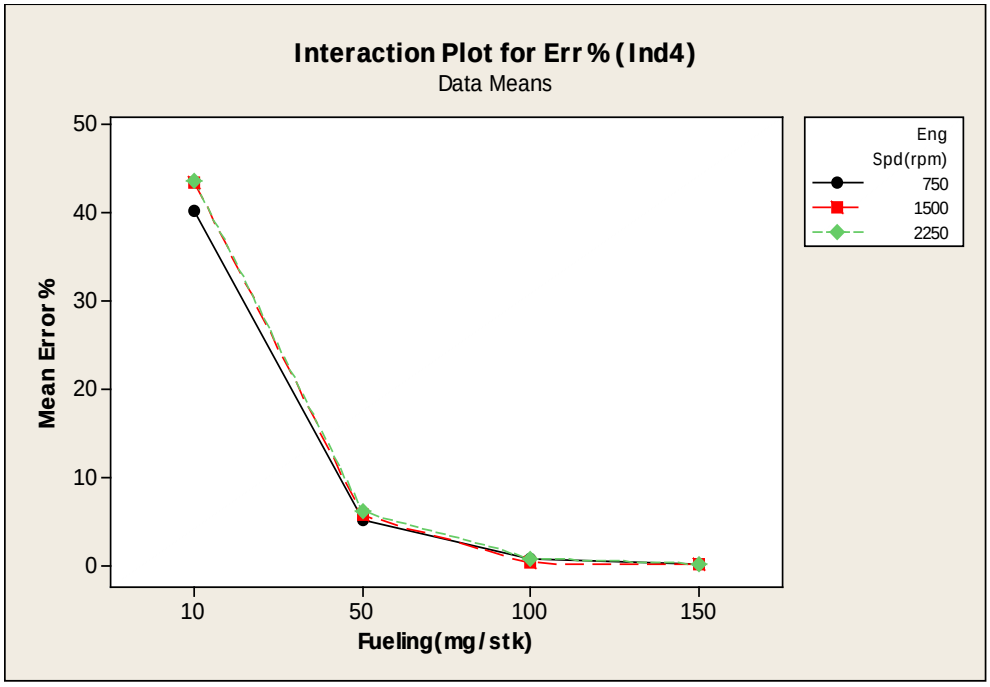

Figure 3.58 Interaction of fueling and engine speed on error percentage with inductors

Figure 3.59 shows the interaction between pressure and fueling in case of inductors, which is evidently dominated by fueling quantity.

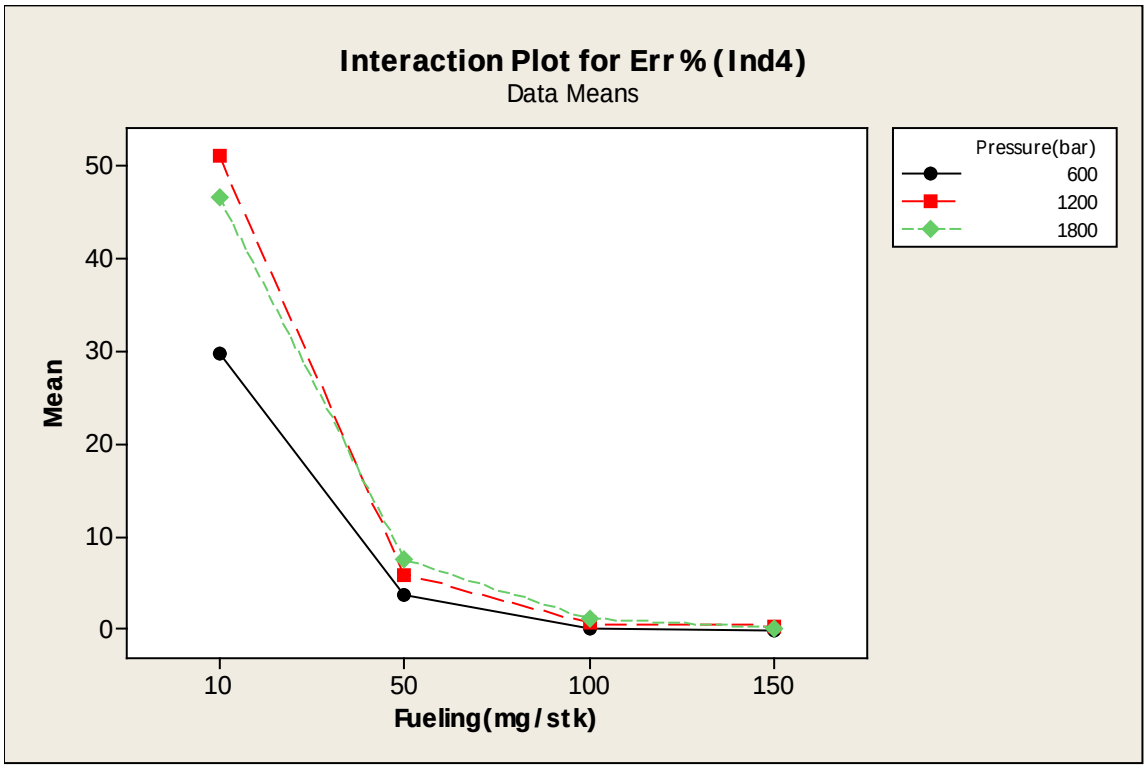

Figure 3.59 Interaction of fueling and pressure on error percentage with inductors

Results above shows promise that, error can be modeled and corrected only if the variability, i.e. the standard deviations at each of the factor levels are not too high. Therefore, standard deviations at each factor levels were calculated for 50 replicates, i.e. 50 pulses and is shown in Table 3.10.

Table 3.10 Standard deviations of error among 50 replicates using inductors

EngSpd (rpm)	Pressure (bar)	Fueling (mg/stk)	StdErr (Ind1)	StdErr (Ind2)	StdErr (Ind3)	StdErr (Ind4)	StdErr (Ind5)	StdErr (Ind6)
750	600	10	0.001	1.4493	0.001	0.6244	0.001	0.001
750	600	50	0.001	0.001	0.001	0.001	0.6144	0.4919
750	600	100	0.001	0.0677	0.0677	0.0677	0.0677	0.1935
750	600	150	0.0883	0.1301	0.001	0.6694	0.1146	0.1084
750	1200	10	0.001	0.001	1.3698	2.9495	3.6306	0.001
750	1200	50	0.001	0.001	0.001	0.001	0.001	0.001
750	1200	100	0.001	0.5106	0.001	0.001	0.2427	0.2003
750	1200	150	0.167	0.0471	0.0799	0.001	0.001	0.001
750	1800	10	1.2856	0.001	0.001	0.001	0.001	0.001
750	1800	50	0.365	0.001	0.001	1.3024	0.001	0.001
750	1800	100	0.001	0.001	0.001	0.001	0.001	0.001
750	1800	150	0.001	0.0891	0.0636	0.1667	0.001	0.0636
1500	600	10	1.4493	1.0592	2.1849	0.6244	0.001	0.001
1500	600	50	0.3336	0.241	1.73913	0.001	0.3996	0.1722
1500	600	100	0.001	0.1858	0.001	0.1451	0.1181	0.001
1500	600	150	0.1178	0.096	0.0883	0.0901	0.1196	0.1318
1500	1200	10	0.001	4.5055	0.001	0.001	2.9495	2.6543
1500	1200	50	0.2719	0.001	0.001	0.3805	0.001	0.001
1500	1200	100	0.2773	0.001	0.001	0.001	0.001	0.3747
1500	1200	150	0.1476	0.001	0.0913	0.1437	0.001	0.0471
1500	1800	10	0.001	3.5281	0.001	3.9794	0.001	0.001
1500	1800	50	0.001	0.001	0.001	0.5108	1.1946	0.001
1500	1800	100	0.6277	0.3253	0.5262	0.001	0.001	0.001
1500	1800	150	0.1994	0.0891	0.001	0.108	0.001	0.001
2250	600	10	2.0025	2.1127	2.0805	1.0592	0.001	0.001
2250	600	50	0.292	0.4231	0.6323	0.3689	0.6144	0.5522
2250	600	100	0.2322	0.1935	0.2411	0.2416	0.001	0.001
2250	600	150	0.0877	0.092	1.1022	0.0989	0.001	0.001
2250	1200	10	0.001	4.2997	4.564	3.6306	0.001	0.001
2250	1200	50	0.9426	0.7119	0.9426	0.8044	0.001	0.001
2250	1200	100	0.4234	0.5073	0.3173	0.3517	0.001	0.5044
2250	1200	150	0.1677	0.001	0.1233	0.1542	0.001	0.001
2250	1800	10	4.5584	0.001	2.9079	3.8221	4.3502	5.611
2250	1800	50	0.5108	1.1133	1.216	1.294	1.216	1.2349
2250	1800	100	0.5021	0.6389	0.5479	0.1918	0.6389	0.6008
2250	1800	150	0.2197	0.2154	0.1994	0.0891	0.001	0.001

The three way ANOVA analysis on the standard deviation of the error in fifty pulses at each state could not use the mathematical model in equation (i) due to lack of degrees of freedom for error. Therefore, the interaction of three factors together was removed and ANOVA was carried out using the model in equation (ii). The residual plot in Figure 3.60 shows that, the standard deviation of error data does not follow normal distribution well enough, since the residual versus fitted value plot shows a distinct pattern.

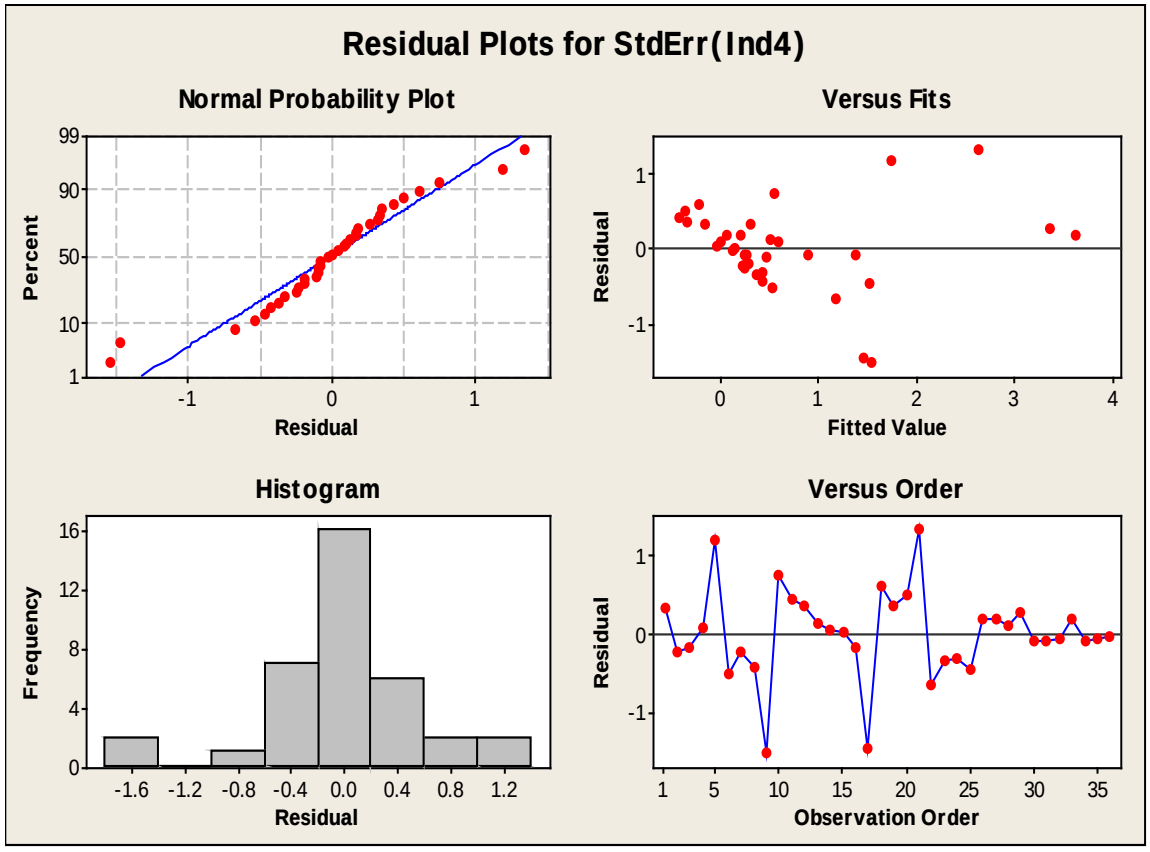

Figure 3.60 Residual plots of ANOVA of standard deviation of error with inductors

Thus, the standard deviations in error were transformed to their natural logarithm. In order to take natural log, the zero standard deviations were changed to 0.001. The natural log table is shown in Table 3.11. The mathematical model for the ANOVA becomes,

$$Log(E) = \mu + S_i + P_j + F_k + SP_{ij} + SF_{ik} + PF_{jk} + \varepsilon_{m(ijk)} \ldots\ldots\ldots\ldots\ldots\ldots (ii)$$

Where, S = engine speed, P = common-rail pressure, F = fueling quantity, i, j, k are 1 through 50 and m=1, 2, 3, 4.

Table 3.11 Natural Log of standard deviations of error with inductors

EngSpd (rpm)	Pressure (bar)	Fueling (mg/stk)	Ln(StdErr Ind1)	Ln(StdErr Ind2)	Ln(StdErr Ind3)	Ln(StdErr Ind4)	Ln(StdErr Ind5)	Ln(StdErr Ind6)	RunOrder
750	600	10	-6.90776	0.371081	-6.90776	-0.47096	-6.90776	-6.90776	13
750	600	50	-6.90776	-6.90776	-6.90776	-6.90776	-0.48711	-0.70948	6
750	600	100	-6.90776	-2.69267	-2.69267	-2.69267	-2.69267	-1.64248	22
750	600	150	-2.42702	-2.03945	-6.90776	-0.40137	-2.16631	-2.22193	23
750	1200	10	-6.90776	-6.90776	0.314665	1.081636	1.289398	-6.90776	8
750	1200	50	-6.90776	-6.90776	-6.90776	-6.90776	-6.90776	-6.90776	31
750	1200	100	-6.90776	-0.67217	-6.90776	-6.90776	-1.41593	-1.60794	14
750	1200	150	-1.78976	-3.05548	-2.52698	-6.90776	-6.90776	-6.90776	32
750	1800	10	0.251226	-6.90776	-6.90776	-6.90776	-6.90776	-6.90776	34
750	1800	50	-1.00786	-6.90776	-6.90776	0.264209	-6.90776	-6.90776	35
750	1800	100	-6.90776	-6.90776	-6.90776	-6.90776	-6.90776	-6.90776	17
750	1800	150	-6.90776	-2.418	-2.75514	-1.79156	-6.90776	-2.75514	11
1500	600	10	0.371081	0.057514	0.78157	-0.47096	-6.90776	-6.90776	20
1500	600	50	-1.09781	-1.42296	0.553385	-6.90776	-0.91729	-1.7591	1
1500	600	100	-6.90776	-1.68308	-6.90776	-1.93033	-2.13622	-6.90776	9
1500	600	150	-2.13877	-2.34341	-2.42702	-2.40684	-2.1236	-2.02647	5
1500	1200	10	-6.90776	1.505299	-6.90776	-6.90776	1.081636	0.976181	19
1500	1200	50	-1.30232	-6.90776	-6.90776	-0.96627	-6.90776	-6.90776	28
1500	1200	100	-1.28266	-6.90776	-6.90776	-6.90776	-6.90776	-0.98163	12
1500	1200	150	-1.91325	-6.90776	-2.3936	-1.94003	-6.90776	-3.05548	2
1500	1800	10	-6.90776	1.260759	-6.90776	1.381131	-6.90776	-6.90776	33
1500	1800	50	-6.90776	-6.90776	-6.90776	-0.67178	0.177811	-6.90776	3
1500	1800	100	-0.46569	-1.12301	-0.64207	-6.90776	-6.90776	-6.90776	27
1500	1800	150	-1.61244	-2.418	-6.90776	-2.22562	-6.90776	-6.90776	7
2250	600	10	0.694396	0.747967	0.732608	0.057514	-6.90776	-6.90776	36
2250	600	50	-1.231	-0.86015	-0.45839	-0.99723	-0.48711	-0.59384	4
2250	600	100	-1.46016	-1.64248	-1.42254	-1.42047	-6.90776	-6.90776	29
2250	600	150	-2.43383	-2.38597	0.097308	-2.31365	-6.90776	-6.90776	24
2250	1200	10	-6.90776	1.458545	1.518199	1.289398	-6.90776	-6.90776	26
2250	1200	50	-0.05911	-0.33982	-0.05911	-0.21766	-6.90776	-6.90776	30
2250	1200	100	-0.85944	-0.67865	-1.14791	-1.04498	-6.90776	-0.68439	10
2250	1200	150	-1.78558	-6.90776	-2.09313	-1.8695	-6.90776	-6.90776	25
2250	1800	10	1.516972	-6.90776	1.067431	1.3408	1.470222	1.724729	21
2250	1800	50	-0.67178	0.107329	0.195567	0.257738	0.195567	0.21099	18
2250	1800	100	-0.68896	-0.44801	-0.60166	-1.6513	-0.44801	-0.50949	16
2250	1800	150	-1.51549	-1.53526	-1.61244	-2.418	-6.90776	-6.90776	15

The residual plot with the transformation in Figure 3.61 shows that, the data satisfies the requirement of having natural distribution with the logarithmic transformation. Therefore, the ANOVA on the data is more acceptable.

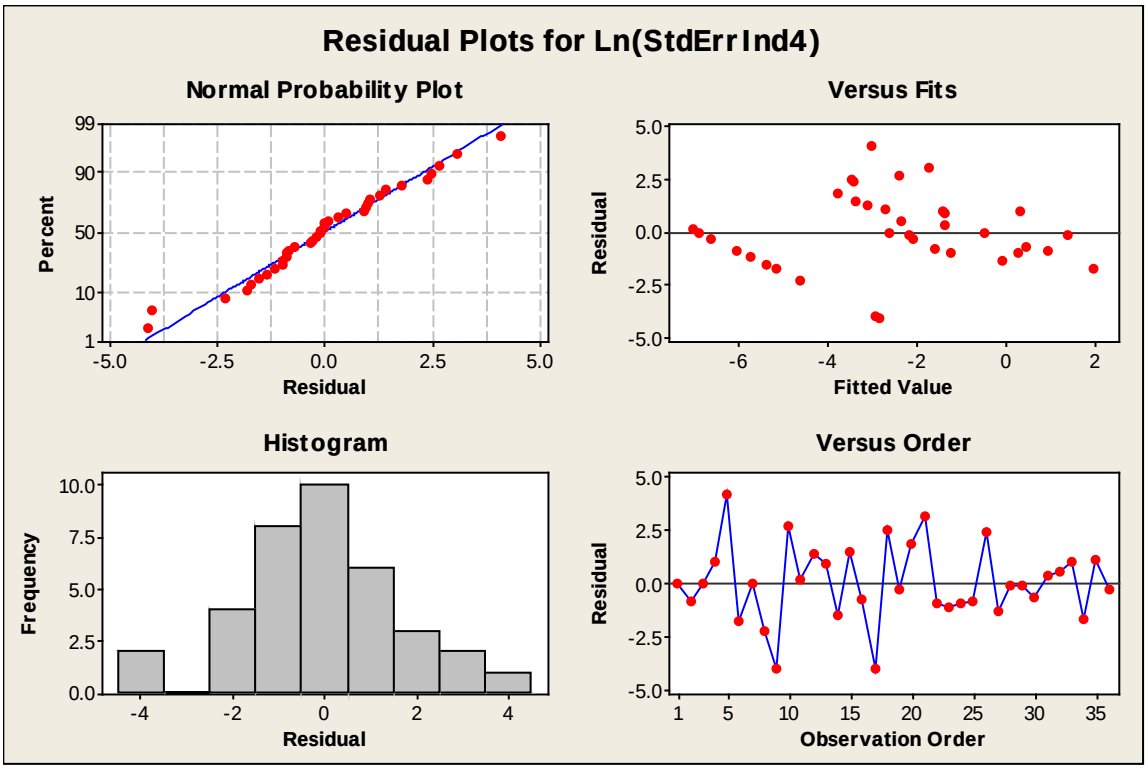

Figure 3.61 Residual plot of ANOVA of natural log of standard deviations with inductors

The Table 3.12 shows that, the null hypothesis cannot be rejected for any of the terms in ANOVA with 95% confidence interval. This signifies that the variation in the standard deviations in error percent belongs to the same normal distribution with a single mean and it does not vary over different values or levels of factors with 95 percent statistical significance. The P values are more than the value of 0.05 signifies that, the probability of making a type I error if the null hypothesis is rejected is more than 5 percent.

Table 3.12 ANOVA on log of standard deviation of error on inductor 4

Source of Variation	Degrees of Freedom (df)	Sum of Squares (SS)	Mean Square (MS)	F	P
S	2	60.581	30.291	3.27	0.074
P	2	7.564	3.782	0.41	0.674
F	3	39.840	13.280	1.43	0.282
S*P	4	12.792	3.198	0.34	0.843
S*F	6	17.142	2.857	0.31	0.921
P*F	6	55.312	9.219	0.99	0.472
Error	12	111.297	9.275		
Totals	35				
S	3.04544				
R-Sq	63.45%				
R-Sq(Adj)	0.00%				

Where, S = engine speed, P = common-rail pressure, F = fueling quantity

Figure 3.62 show that, the variability varies from standard deviation of error percentage from 0.018% to 0.4781% over the range of operation with inductors, which is similar to the injectors. This finding points out the fact that, if the error can be corrected, cheaper solution of using inductors will perform as good as expensive injectors.

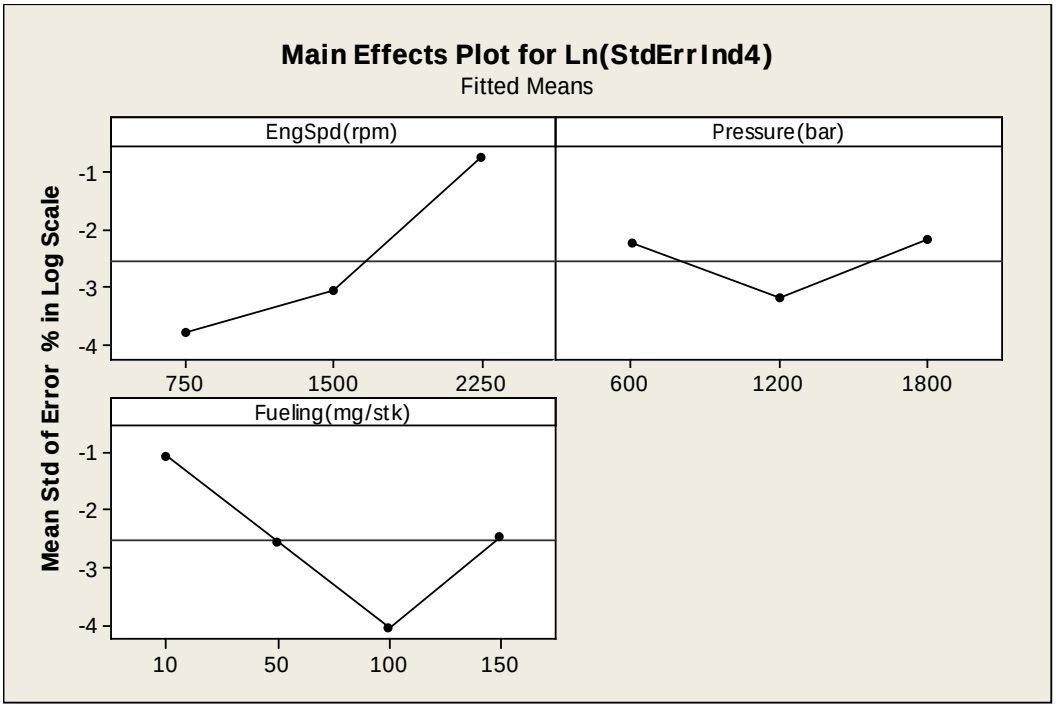

Figure 3.62 Main effect plot on the natural log of standard deviations of error in inductors

2.7.4 Mixed Model ANOVA with Inductors as Random Factors

In order to find out the effect of various inductors on the variability, i.e. the variability over the six inductors, ANOVA with mixed model having three fixed factors and a random factor of inductors was carried out and the result is shown in Table 3.13. The mathematical model for mixed model ANOVA is,

$$Log(E) = \mu + S_i + P_j + F_k + I_l + SP_{ij} + SF_{ik} + SI_{il} + PF_{jk} + PI_{jl} + FI_{kl} + \varepsilon_{m(ijkl)} \ldots\ldots \text{(iii)}$$

Where, E=Estimate of standard deviation in error, S = e ngine speed, P = common-rail pressure, F = fueling quantity, i, j, k are 1 through 50, I=Random factor Injector Numbers, l=1,2,3,4,5,6 and m=1, 2, 3, 4.

The P values in Table 3.13 indicate that, if we consider multivariate ANOVA or mixed model ANOVA, the interaction between engine speed and pressure, engine speed and fueling, engine speed and inductors rejects null hypothesis, thus they add additional variability distribution of error to the system.

Table 3.13 Mixed Model ANOVA of natural log of standard deviations of error with six inductors as random factors

Source of Variation	Degrees of Freedom (df)	Sum of Squares (SS)	Mean Square (MS)	F	P
S	1	8.829	8.829	1.11	0.293
P	1	37.259	37.259	4.70	0.031*
F	1	23.699	23.699	2.99	0.085
I	5	45.737	9.147	1.15	0.334
S*P	1	47.726	47.726	6.02	0.015*
S*F	1	53.812	53.812	6.79	0.010*
S*I	5	104.057	20.811	2.63	0.025*
P*F	1	1.731	1.731	0.22	0.641
P*I	5	18.115	3.623	0.46	0.808
F*I	5	27.159	5.432	0.69	0.635
Error	189	1498.407	7.928		
Totals	215				
S	2.81568				
R-Sq	29.43%				
R-Sq(Adj)	19.72%				

Where, S = engine speed, P = common-rail pressure, F = fueling quantity, I= Injector Numbers, *P values less than 0.05, therefore, null hypothesis has been rejected.

Figure 3.63 shows the residual plot for the mixed model ANOVA, that shows the normality of the data.

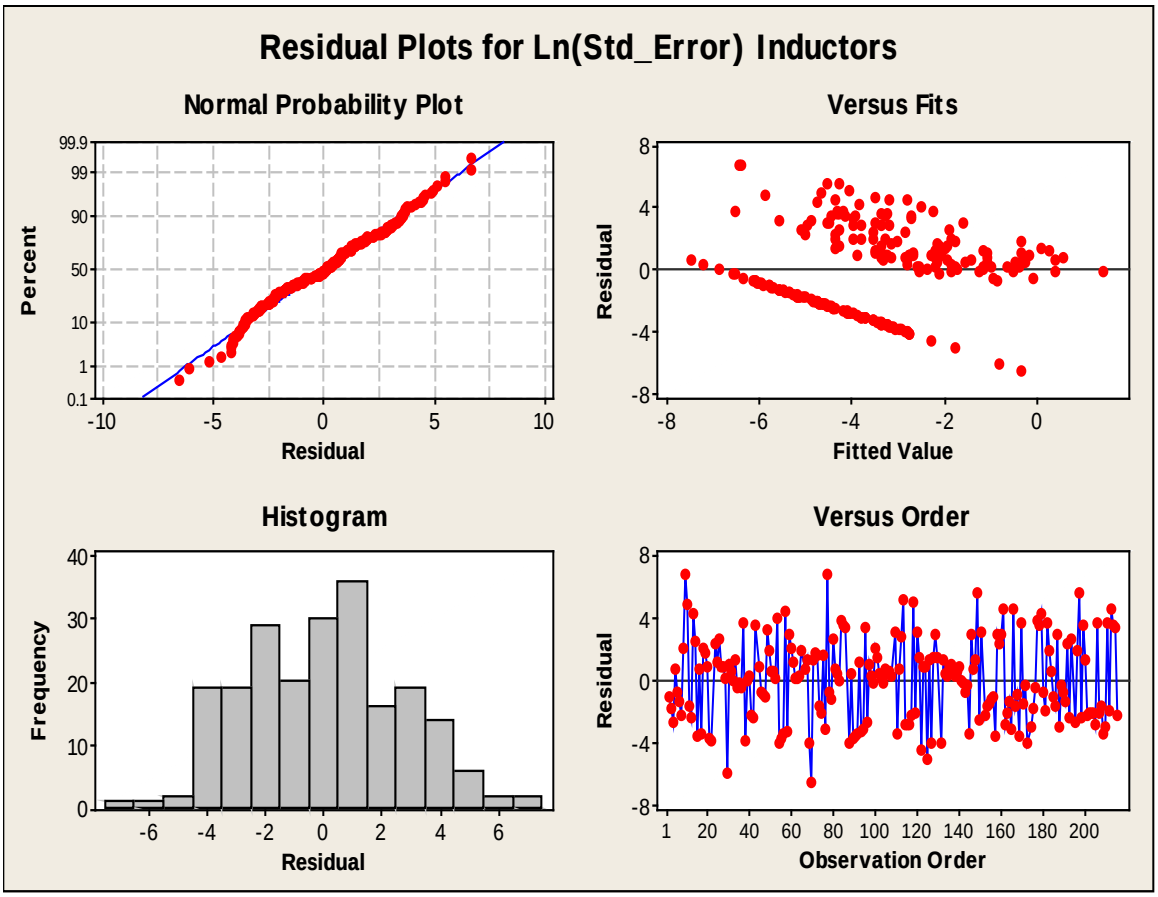

Figure 3.63 Residual plot for Mixed model ANOVA with six inductors

Figure 3.64 shows that, the standard deviation of error, i.e. variability of error is heavily dependent on engine speed ranging from 0.004892% to 0.45% error. Therefore, if the error is corrected based on mean error, the variability of error would fall in this range. The variability of error with inductors is very similar to injectors, thus, if error correction effort is employed, use of inductors can be justifiable due to cost savings. The figure also points out the fact that, the variability is different from inductor to inductor, however, it is not statistically significant. The fifth and sixth inductors have less variability than others, while the fourth inductor has the highest variability. The Table 3.13 shows that the interaction adds significantly different variability distribution than the whole variability in the process.

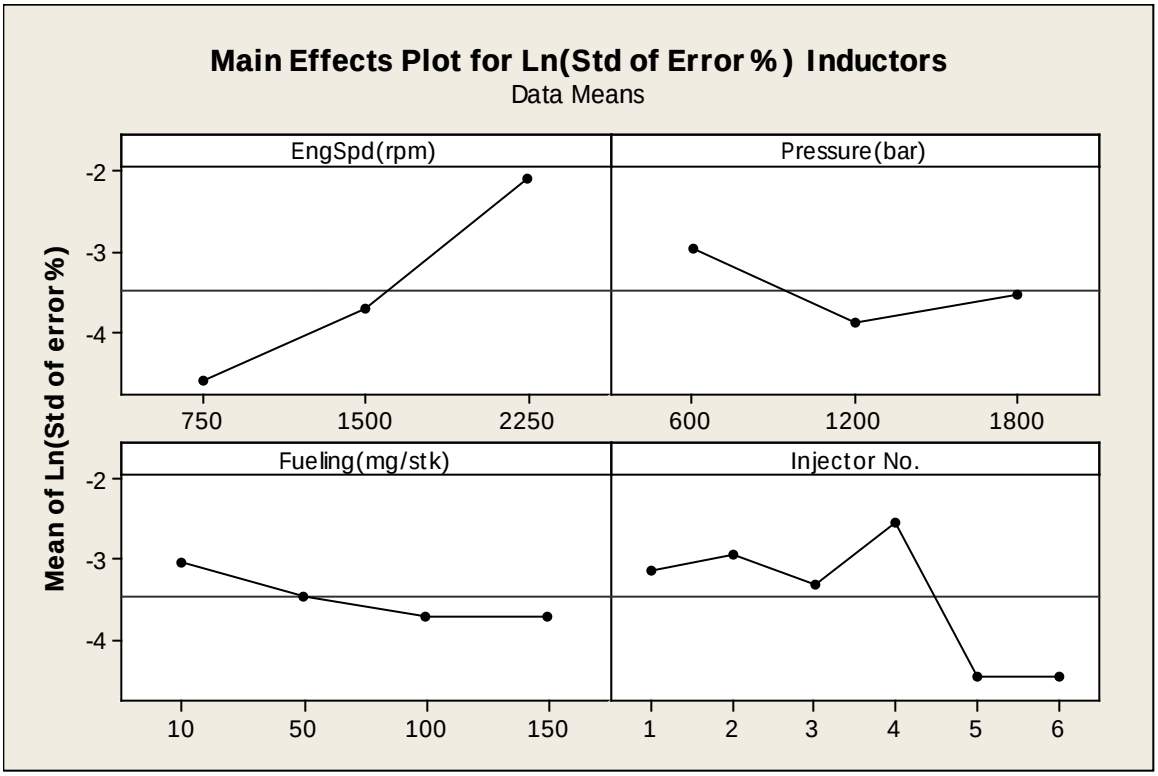

Figure 3.64 Main effect plots for mixed model ANOVA of natural log of standard deviations of error percent with six inductors

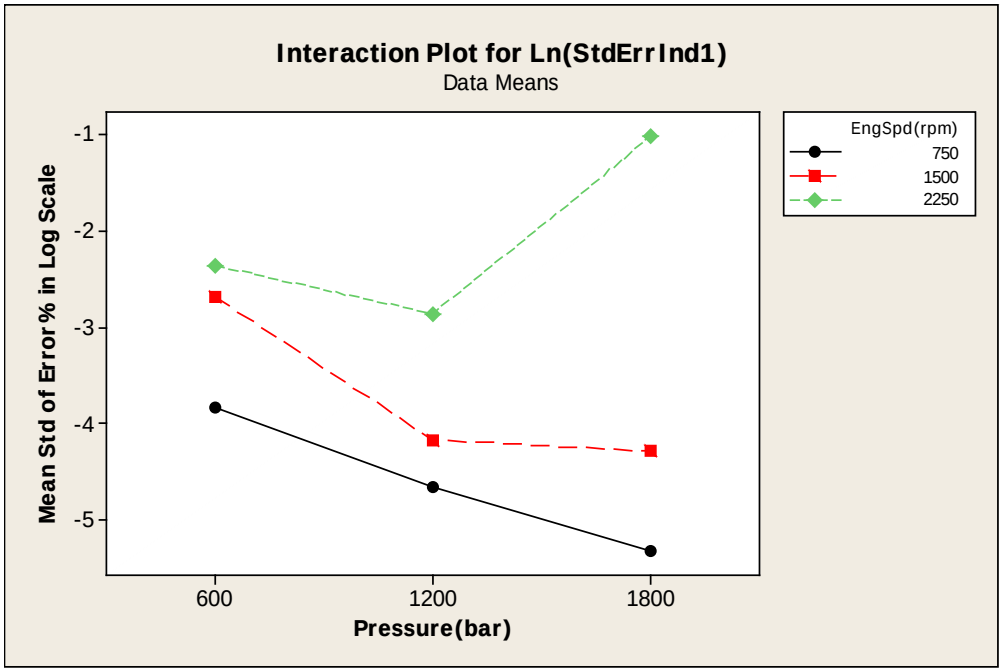

Figure 3.65 Interactions of engine speed and pressure on mixed model ANOVA on inductors

Significant interactions are plotted in Figure 3.65, Figure 3.66 and Figure 3.67. Figure 3.65 shows that the variability of error is more significantly changing due to engine speed. At higher engine speed, the variability is higher and goes as high as 0.3679%.

Figure 3.66 shows the interaction between engine speed and fueling. It shows that the engine speed is again the dominating factor affecting the variability of the system. The higher the engine speed is, the higher the variability in the system. However, at high fueling values, the effect of engine speed becomes insignificant and the variability is converges to a low value.

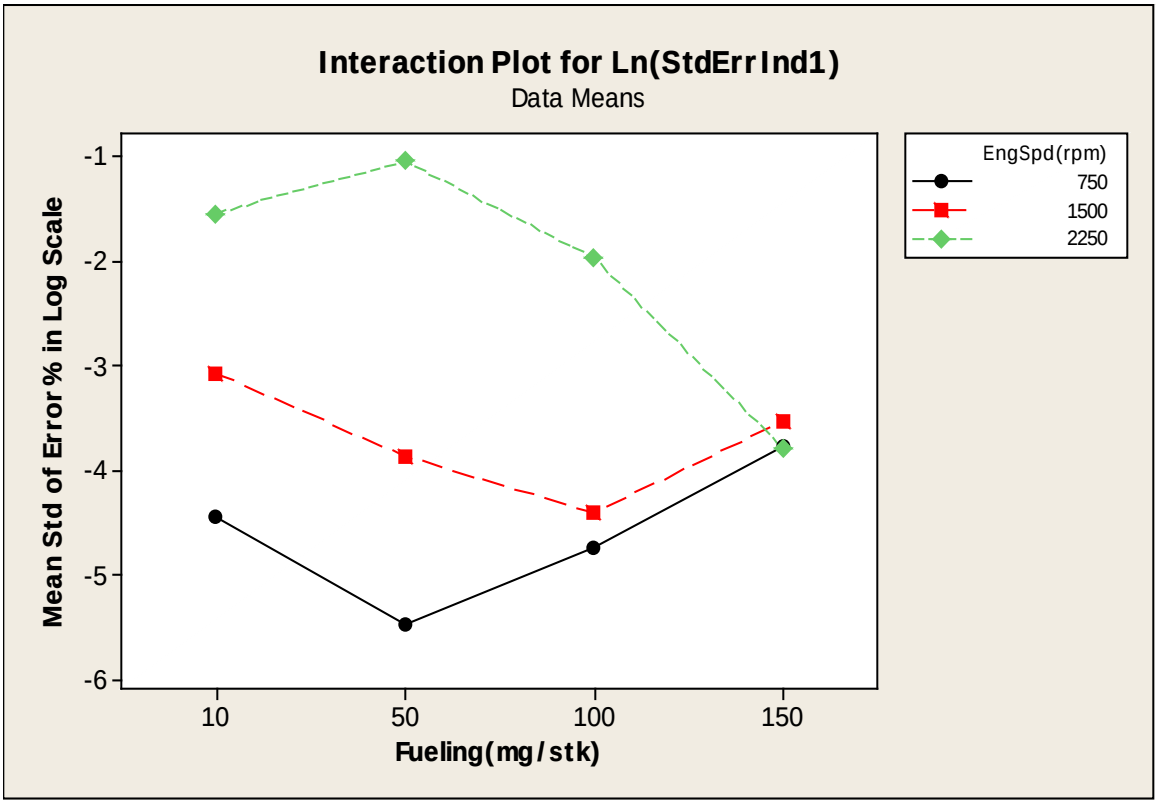

Figure 3.66 Interactions of engine speed and fueling on mixed model ANOVA on inductors

Figure 3.67 shows the interaction between different inductors at varying engine speeds. The fifth and sixth inductors show least variability over entire range of engine speeds. The fifth inductor shows least change in variability over different engine speeds.

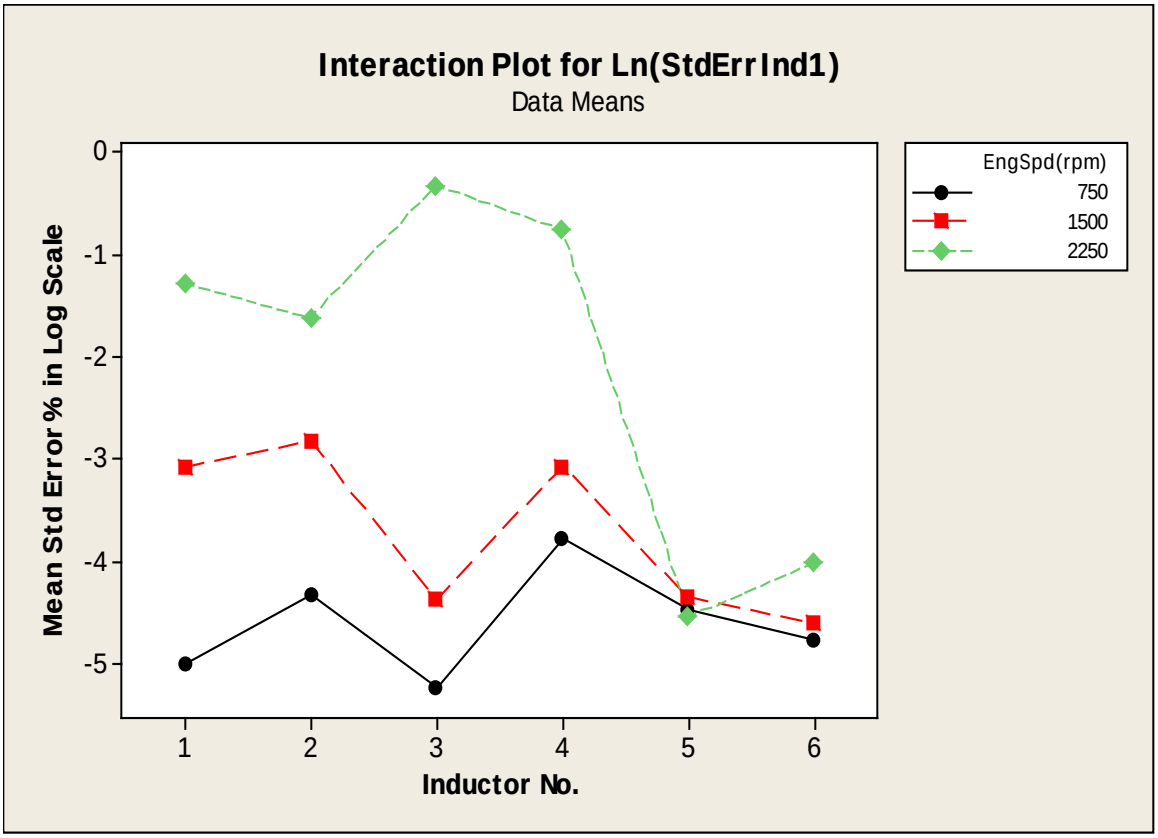

Figure 3.67 Interactions of engine speed and inductors in mixed model ANOVA on inductors

In summary, the mean standard deviation at each value of the factors are below 0.0608 percent, provided the engine is not running over 1500 rpm. The higher engine speed causes the variability to be higher all the inductors except the fifth one. It also signifies that, the inductors are significantly different in terms of variability. Therefore, each of the inductors will be required to be tested with the test sequence used in this research before using on the HIL bench.

2.8 Comparison between and Injector and Inductor Performance

Six injectors and six inductors were used in this research and it has been found that, the variability of error is similar. However, the mean error percents are much higher with inductors than with real production injectors when used as load on the HIL bench. Figure 3.68 shows that, the error percent is distinctly higher with inductors than with the

injectors, however, the consistency of the error with both the injectors and inductors points out the fact that, the error can be corrected.

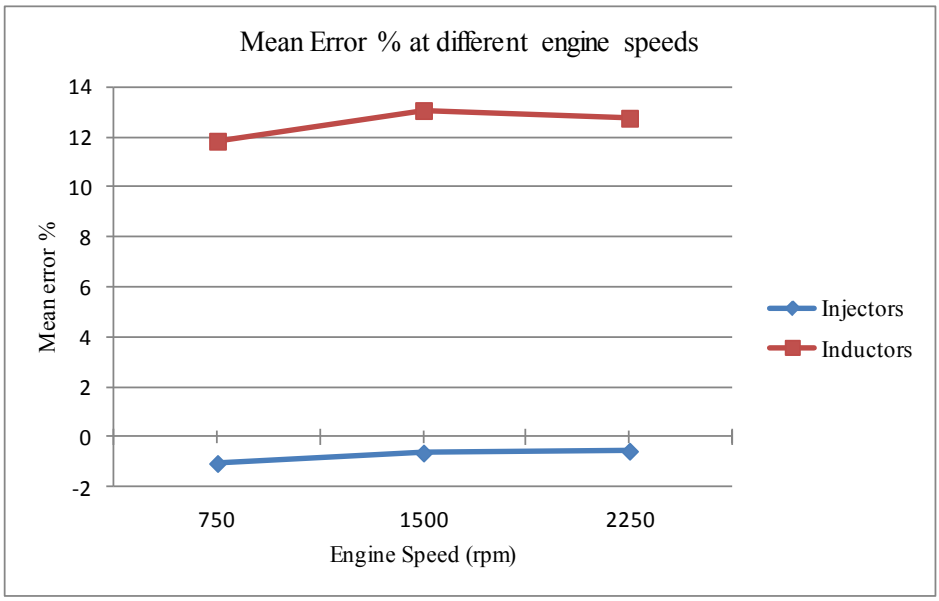

Figure 3.68 Comparing error percent against engine speed for injectors and inductors

Figure 3.69 shows the difference in mean error percents is significant between injectors and inductors and the error varies over a larger range in response to the common-rail pressure with inductors than the injectors.

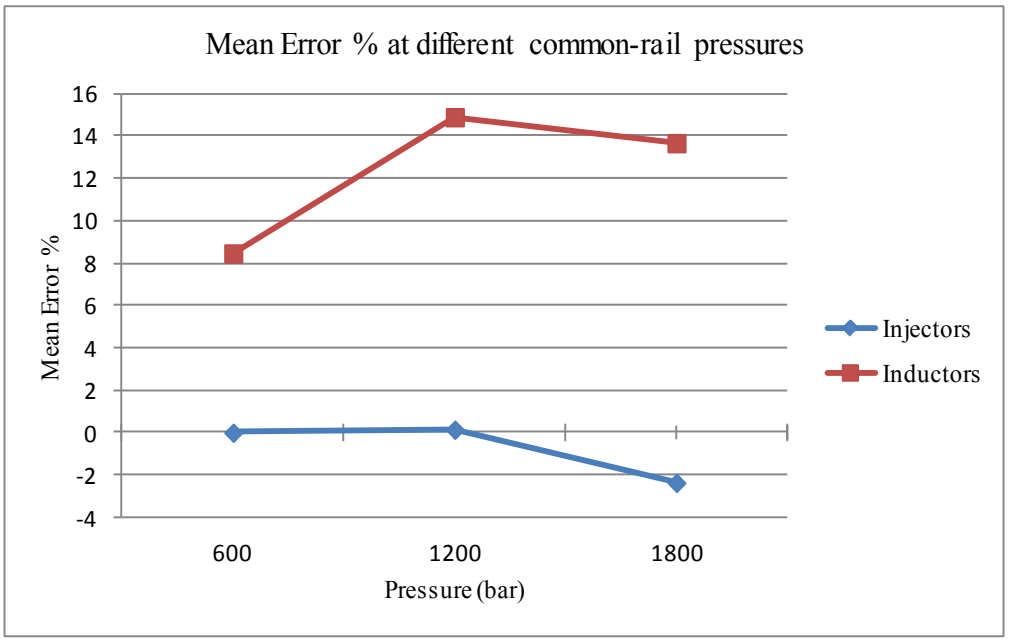

Figure 3.69 Comparing error percent against bar pressure for injectors and inductors

Figure 3.70 shows the large influence of fueling quantity on the mean of error percents with inductors as opposed to injectors. However, the mean error shows a consistent trend that can be corrected with a regression algorithm.

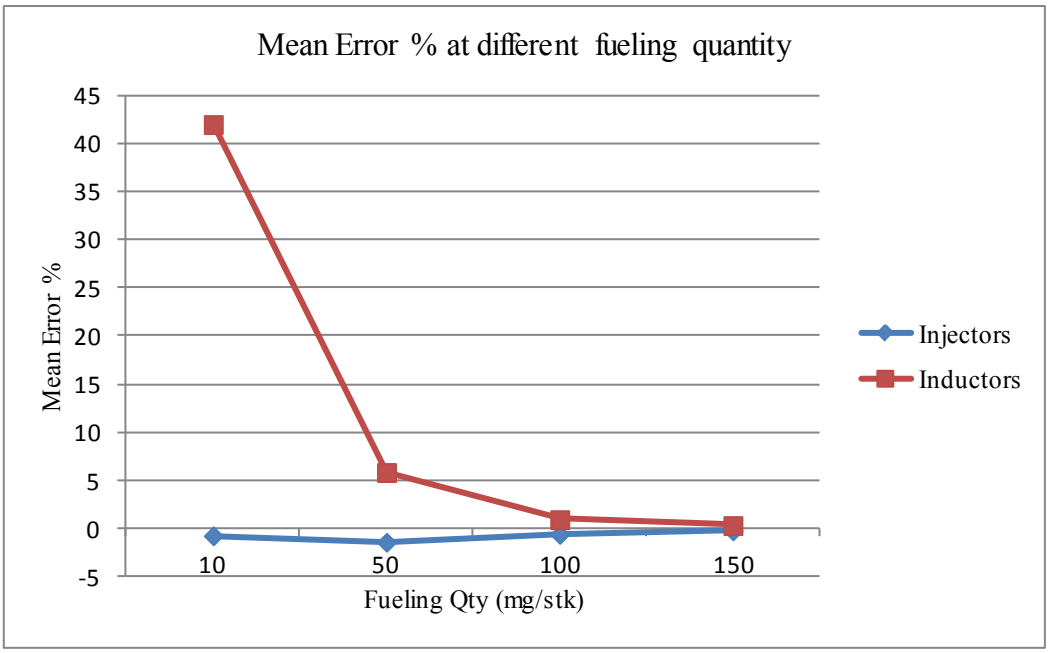

Figure 3.70 Comparing error percent against fueling quantity for injectors and inductors

Previous analysis of variability showed that, the variability of standard deviation of error percent with injectors at different engine speeds is significantly (95% statistical confidence) different from the variability of the whole process of variability, considering the fixed factors. However, incorporating the six injectors and carrying out mixed model ANOVA exposed the fact that, interaction of engine speed and fueling add significantly different variability distribution compared to the normally distributed variability of the whole process of standard deviation. It signifies that, if the engine speed and fueling do not vary, the standard deviation of error maintains the same distribution around the mean standard deviations of error percent. Interaction of engine speed and fueling generates statistically significant different distribution of standard deviation of error percent, i.e. varying pressure or using different injectors do not contribute to the variability of the standard deviation of error percent. On the other hand, the inductors with only the fixed factor model shows that all the fixed factors fall under the same normal distribution of standard deviation of error percent. However, when the mixed model of ANOVA was

carried out, it pointed out that, the interaction of engine speed with all other three factors, i.e. pressure, fueling quantity and inductor number add different distribution that is statistically significant. Therefore, the system's variability depends on all the variable factors, including different inductors. The standard deviation of all the values of standard deviations of error percent with injectors in logarithmic scale is 3.48534, while with inductors, the standard deviations of all the values of standard deviations of error percent in logarithmic scale is 3.14255.

Figure 3.71, Figure 3.72 and Figure 3.73 show the mean standard deviation of error percentage changing with engine speed, pressure and fueling quantity, comparing injectors with inductors with ANOVA of fixed factors. Figure 3.71 shows that, variability is increasing with rising engine speed, while the inductor's variability is not much higher than injector's.

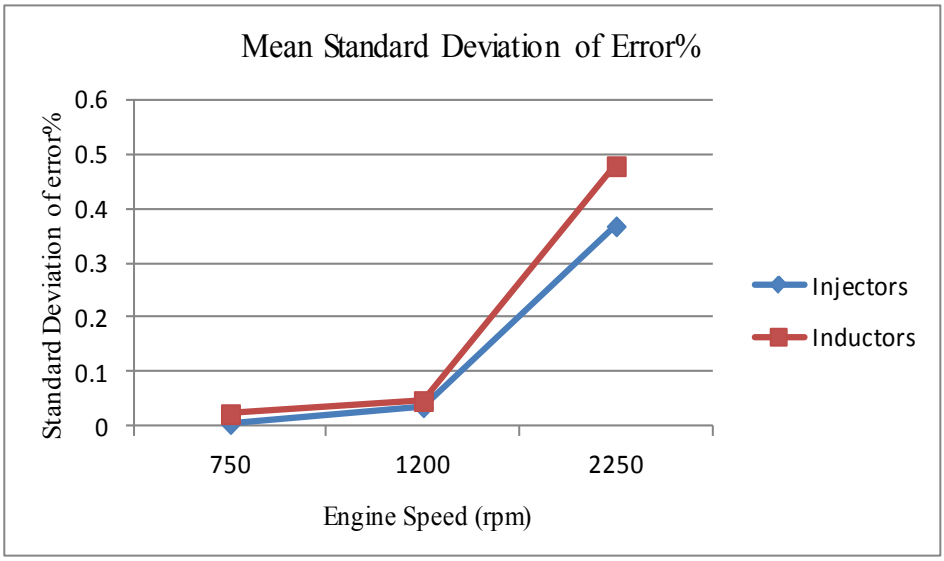

Figure 3.71 Comparing standard deviation of error percent with engine speed

Variability with respect to different common-rail pressure is less than other two factors, the maximum variability observed is 0.115 percent while the maximum variability with inductors are 0.48 percent and 0.35 percent with respect to engine speed and fueling quantity respectively. Therefore, pressure did not reject the null hypothesis

for neither injectors nor inductors with ANOVA with standard deviation of error percent as dependent variable.

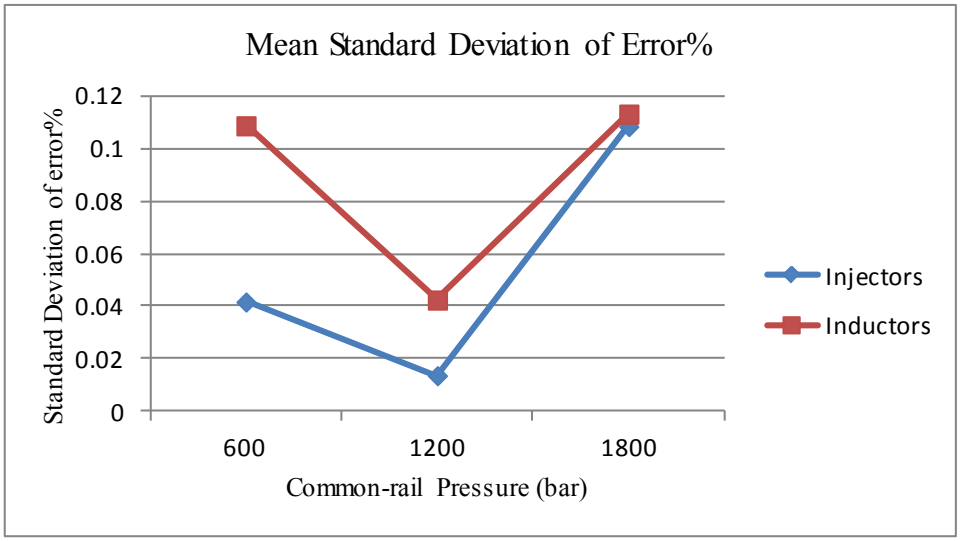

Figure 3.72 Comparing standard deviation of error percent with pressure

Variability is higher at lower fueling quantity with inductors, while, with injectors fueling does not contribute to the variability of the standard deviation of error percent as much.

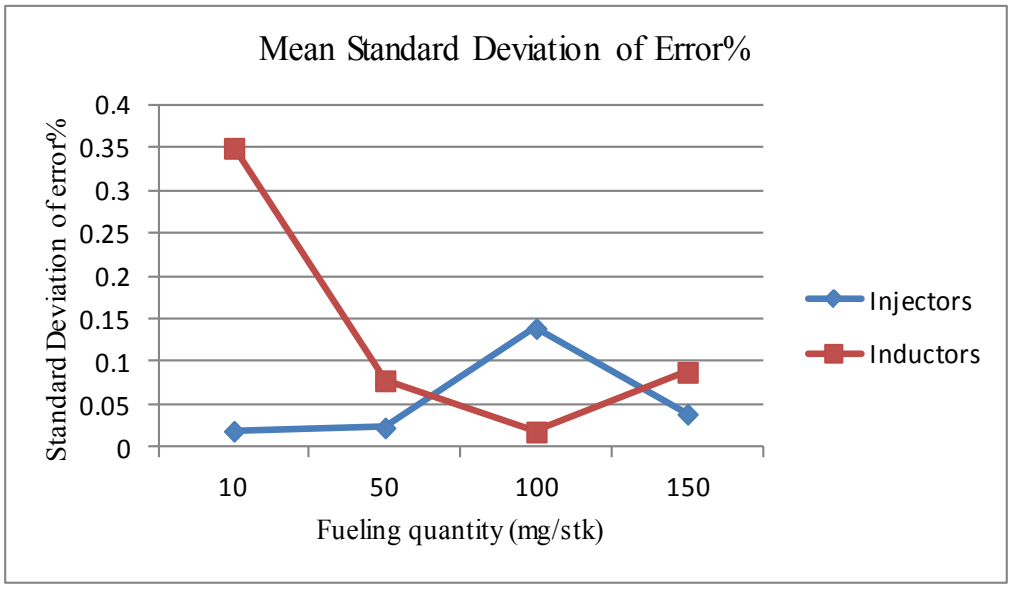

Figure 3.73 Comparing standard deviation of error percent with pressure

Mixed model ANOVA takes the contribution of six injectors and six inductors to the variance of the distribution of standard deviation of error into account. The mixed model ANOVA signifies that, with the injectors, only the interaction of engine speed and fueling rejects null hypothesis, thus, different combinations of engine speed and fueling contributes to varying distribution of standard deviation of error percent. On the other hand, with inductors, the variability of error % is dependent on the interaction of engine speed and fueling, engine speed and pressure, engine speed and inductor number with 95% statistical significance.

Having the information of mean standard deviation is not enough until we are aware of how much the variance varies over the period of operation. 10,800 pulses have been logged with the six injectors and 10,800 pulses were logged with the six inductors. There were some extreme overlying points with inductors that were removed before carrying out the ANOVA. The standard deviation of error percents at each of the 36 steady states have been plotted in the scatter plot in Figure 3.74 for injectors, classified at engine speeds of 750rpm, 1500rpm and 2250rpm. It is observed that, the three steady state points at which the variability is very high are at 2250 rpm.

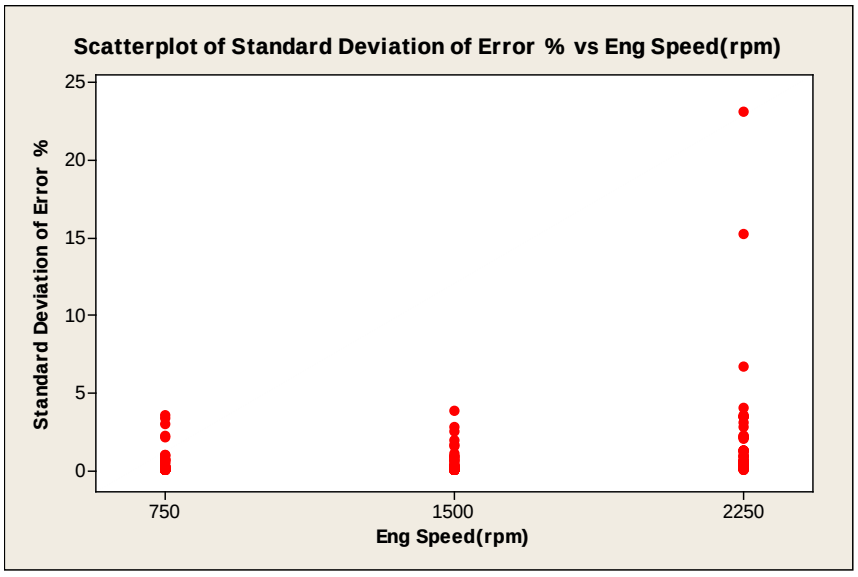

Figure 3.74 Scatterplot of standard deviation of error percent from 216 data points classified based on engine speed with injectors as load

Figure 3.75 shows similar scatter plot of the same data at four fueling quantities of 10 mg/stk, 50mg/stk, 100mg/stk and 150mg/stk. Maximum standard deviation was observed at lowest fueling quantity of 10mg/stk.

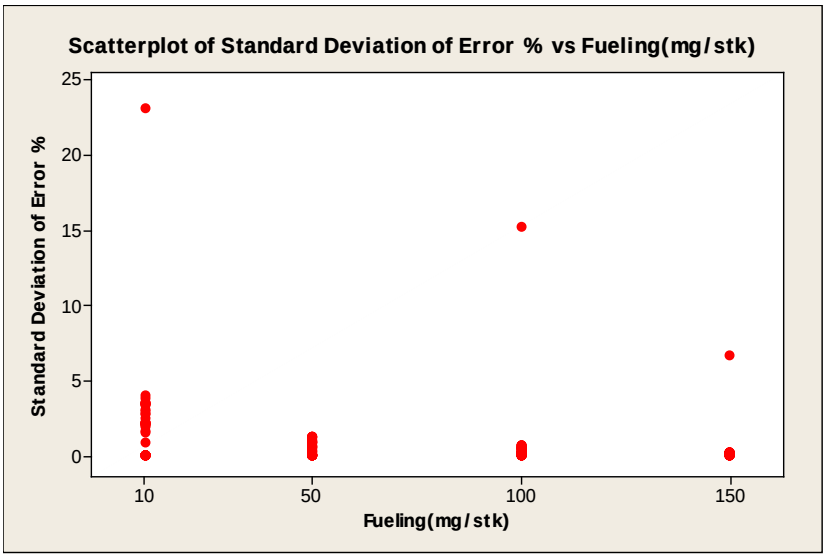

Figure 3.75 Scatterplot of standard deviation of error percent from 216 data points classified based on fueling quantity with injectors as load

Figure 3.76 shows the scatter plot at three values of common-rail pressures of 600 bar, 1200 bar and 1800 bar. The maximum standard deviation is at 1800 bar pressure.

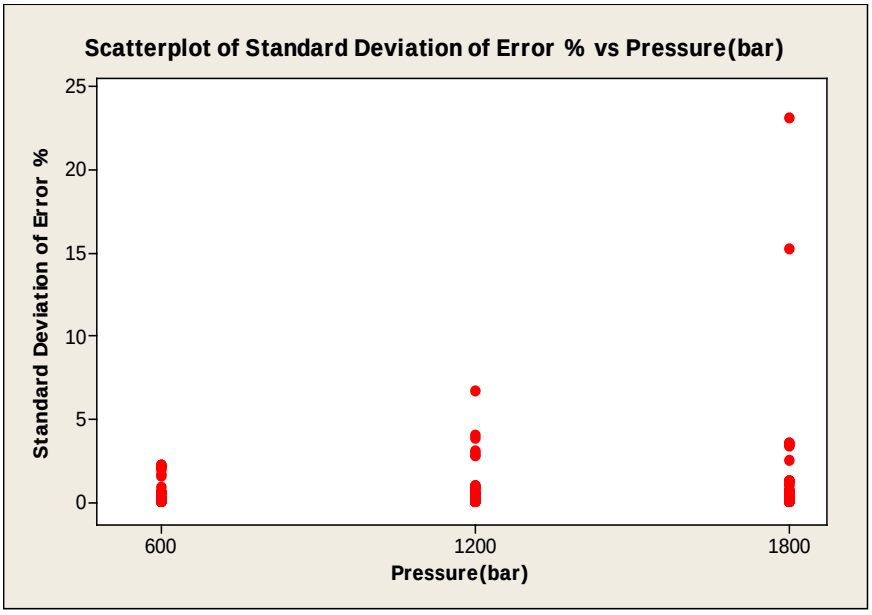

Figure 3.76 Scatterplot of standard deviation of error percent from 216 data points classified based on pressure with injectors as load

Figure 3.77 overlays three scatter plots in one for inductors; classified based on the different values of the fixed factors, i.e, three values of engine speeds of 750rpm, 1500rpm and 2250rpm, three values of common-rail pressures of 600 bar, 1200 bar and 1800 bar, four fueling quantities of 10 mg/stk, 50mg/stk, 100mg/stk and 150mg/stk. With injectors, if the three extreme values are ignored, the error percent varies with the maximum standard deviation value of 4.30063%. It is noticed that, all three extreme variability occurred at 2250 rpm engine speeds. On the other hand, Figure 3.77 does not have any extreme values with the inductors, however, three to four extreme outlying data points had to be removed for each of the inductors from 1800 pulses for each inductor data, in order to carry out the ANOVA analysis. Six steady states with inductors as load have standard deviation of error percent higher than the maximum value of 4.30063% observed with injectors. Therefore, it is observed that, even if the mean of the standard deviation values are closer to the values of injectors, the inductors were found to have six states that represent 300 pulses out of 10800 pulses that had higher variance than injectors. In case of injectors, only three states having 2250rpm engine speed had higher variability than the 4.30063%.

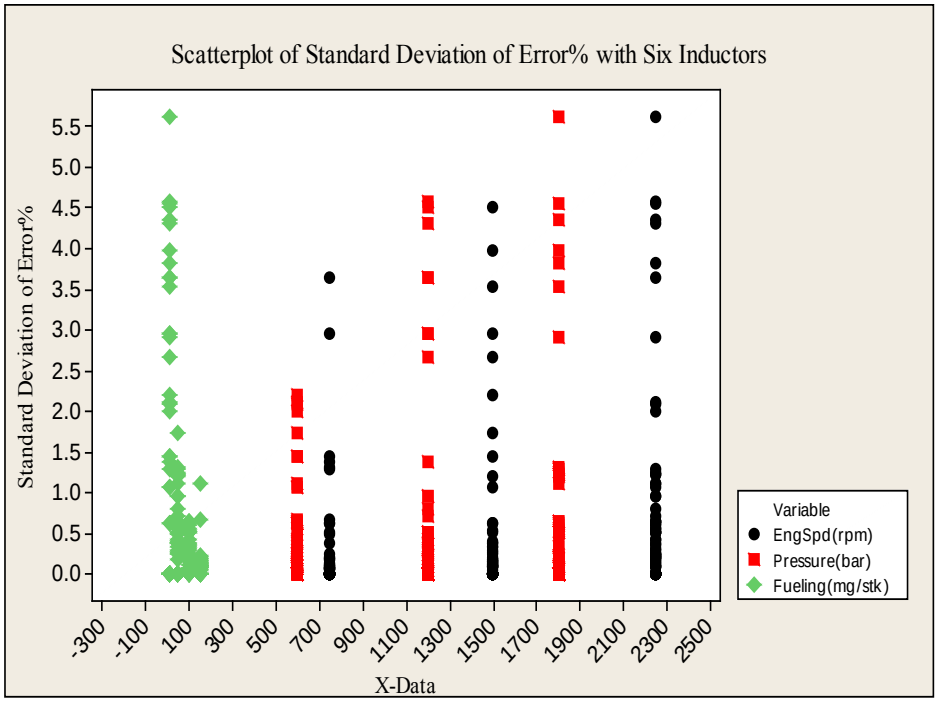

Figure 3.77 Scatterplot of standard deviation of error percent from 216 data points classified with fixed factors base on 90000 pulses with inductors

3. DISCUSSION

The research involved development of a bench setup that is capable of testing injector performance for fueling quantity monitoring, with automated test sequence that goes over all the predefined steady state operating points. It uses custom steps in NI Teststand to establish communication through CUTY and CAN bus to override parameter values on ECM, as well as, monitor the CAN bus to make sure that the correct values are being registered by the ECM from the emulated sensors. The bench uses FPGA personality to model the engine crank shaft rotation by generating high speed EPS/ESS signal, in addition to pressure sensor signal. The bench is capable of monitoring the analog injector pulse, using double thresholds to capture the fueling ontime and feed the engine model running on real time computer with the correct value of fueling quantity through high speed DMA transfer using FIFO method. Future research can be carried out on this bench with different types of injectors, such as, injectors using piezoelectric technology, without using the expensive resource, i.e. the fully capable closed loop test development bench. The research shows the high amount of error that persists if single AI module is used for more than one injector monitoring. There are certain regions of operation with low error, therefore, the cheaper solution can be selected for an application that does not operate in high error region or in cases when the tests carried out are not susceptible to this high error. Statistical analysis was carried out on the system that uses one module allowing data acquisition at 125 kHz on each injector with differential input, which is the most expensive solution proposed to implement on the closed loop HIL test bench. The research also compares the performance of the system with the production injector and the inductors load cells that emulates the injectors. The statistical analysis shows that, the expensive injectors can be replaced by inductor load cells if an error correction algorithm is incorporated into the system, since it showed

about 40% error at lower fueling quantity, which may potentially cause unstable solution when engine idling condition will be simulated on the bench. On the other hand, the injectors perform with very low error percent, i.e. -2.38045% to 0.13551% error with less than 4% standard deviations, unless the system is used at as high an engine speed as 2250 rpm. The mixed model ANOVA, which is a relatively new technique to carry out multivariate ANOVA exposed the fact that, the variability of the error percent varies with 95% statistical confidence, over different interaction values of engine speed and fueling quantity when the production quality injectors are used. With inductors, the value varies with the impact of all four variables, i.e. interaction of engine speed and fueling quantity, engine speed and pressure, engine speed and different inductors. This analysis shows that, the variability of the error percent is not influenced by the common-rail pressure or different injectors, which is not the case with inductors. However, the variability is not very different with injectors or inductors in terms of standard deviation of error percent, i.e. if the variability range is acceptable for a particular HIL test application, the inductors can be used, provided the error correction algorithm is incorporated into the system. Higher error percent at lower fueling quantity compared to higher fueling quantity at a constant rail pressure is due to the fact that, the data acquisition rate was constant, and the highest data acquisition rate available was data point at every 8 micro seconds. This exposes the limitation on the best accuracy that can be expected from the system. However, if a sensitivity analysis on the engine model shows that it is not sensitive to the amount of error inherent in the system, the system can be implemented to deliver the fueling quantity to the model that simulates the engine.

4. CONCLUSIONS

In conclusion, the proposed system uses high speed data acquisition of analog injector pulse and data transfer with DMA. Therefore, it is capable of reducing the latency involved in the delivery of fueling quantity in closed loop HIL tests on the current benches, compared to current method of delivery from the CAN message. The experimental data validates the fact that, the most reliable solution is the most costly one to implement, using 125kHz sampling rate with production injectors as loads. However, high engine speed causes higher variability in error. The inductors cannot emulate the electromechanical characteristics of the injector stators perfectly, however, the error showed smoothly varying offset without additional variability. Therefore, the inductors can be used with proper error correction algorithm.

5. FUTURE WORK

Since the fueling injection monitoring in the proposed system is carried out at hardware level speed with the FPGA, a windowing algorithm can be developed to sequentially deliver the fueling injection taking place at all the injectors with only one analog input module, provided it is synchronized with the crank angle position of the crank shaft of the engine. In addition, sensitivity analysis on the engine model should be carried out to determine if the model is sensitive to the error found in the proposed system prior to implementation. Using improved hardware that allows higher data acquisition rate will improve the accuracy in the fuel quantity delivered by the system.

LIST OF REFERENCES

LIST OF REFERENCES

1. Introduction to FPGA technology: top five benefits, http://zone.ni.com/devzone/cda/tut/p/id/6984

2. L. M. Reyneri, B. Bbllei, E. Bussolino, F. Gregoretti and L. Mari, F. Renga, "Simulink-based codesign and cosimulation of a common rail injector test bench," *Journal of Circuits, Systems and Computers*, Vol. 12, No. 2, pp. 171-202, April 2003.

3. G. Saldaña-González, H. Salazar-Ib argüen, O. M. Martínez Bravo and E. Moreno-Barbosa, "2D image reconstruction with a FPGA-based archit ecture in a gamma camera application," *20th International Conference on Electronics Communications and Computers*, pp. 102-105, 2010.

4. T. Pozniak and T. Krzysztof, "FPGA-base d, specialized trigger and data acquisition systems for high-energy physics experim ents," *Measurement Science and Technology*, Vol. 21, No. 6, 2010.

5. M. Turqueti, J. Saniie and E. Oruklu, "MEMS acoustic array embedded in an FPGA based data acquisition and signal processing system ," *Midwest Symposium on Circuits and Systems*, pp. 1161-1164, 2010.

6. N. Guerassi and P. Dupraz, 1998. "A Common Rail Injection System for High Speed Direct Injection Diesel Engines," *SAE Technical Paper 980803*.

7. "NI cRIO-9014 controller," http://sine.ni.com/nips/cds/view/p/lang/en/nid/203500; Last accessed November 2011.

8. "NI cRIO-9111 chassis," http ://sine.ni.com/nips/cds/view/p/lang/en/nid/206762; Last accessed November 2011

9. "NI 9205 analog input module," http://sine.ni.com/nips/cds/view/p/lang/en/nid/208800; Last accessed November 2011

10. "NI 9264 analog output module," http://sine.ni.com/nips/cds/view/p/lang/en/nid/208807; Last accessed November 2011.

11. "NI 9401, 8 channel, 5 V/TTL h igh speed biderictional digital I/O m odule," http://sine.ni.com/nips/cds/view/p/lang/en/nid/208809; Last accessed November 2011.

12. A. Kulas, P. Zalewski and T. Hortobagyi , P. D eVita, "Effects of added trunk load and corresponding trunk position adapta tions on lower extrem ity biomechanics during drop-landings," *Journal of Biomechanics*, Vol 41, No. 1, pp. 180-185, 2008.

13. A. Mohammadi, A. Tehrani and E. Emanian, D. Karimi, "Statistical analysis of wire electrical discharge turning on m aterial removal rate, " *Journal of Materials Processing Technology*, Vol. 205, No. 1-3, pp. 283-289, August 26, 2008.

APPENDIX

APPENDIX: ADDITIONAL EXPERIMENTAL RESULTS

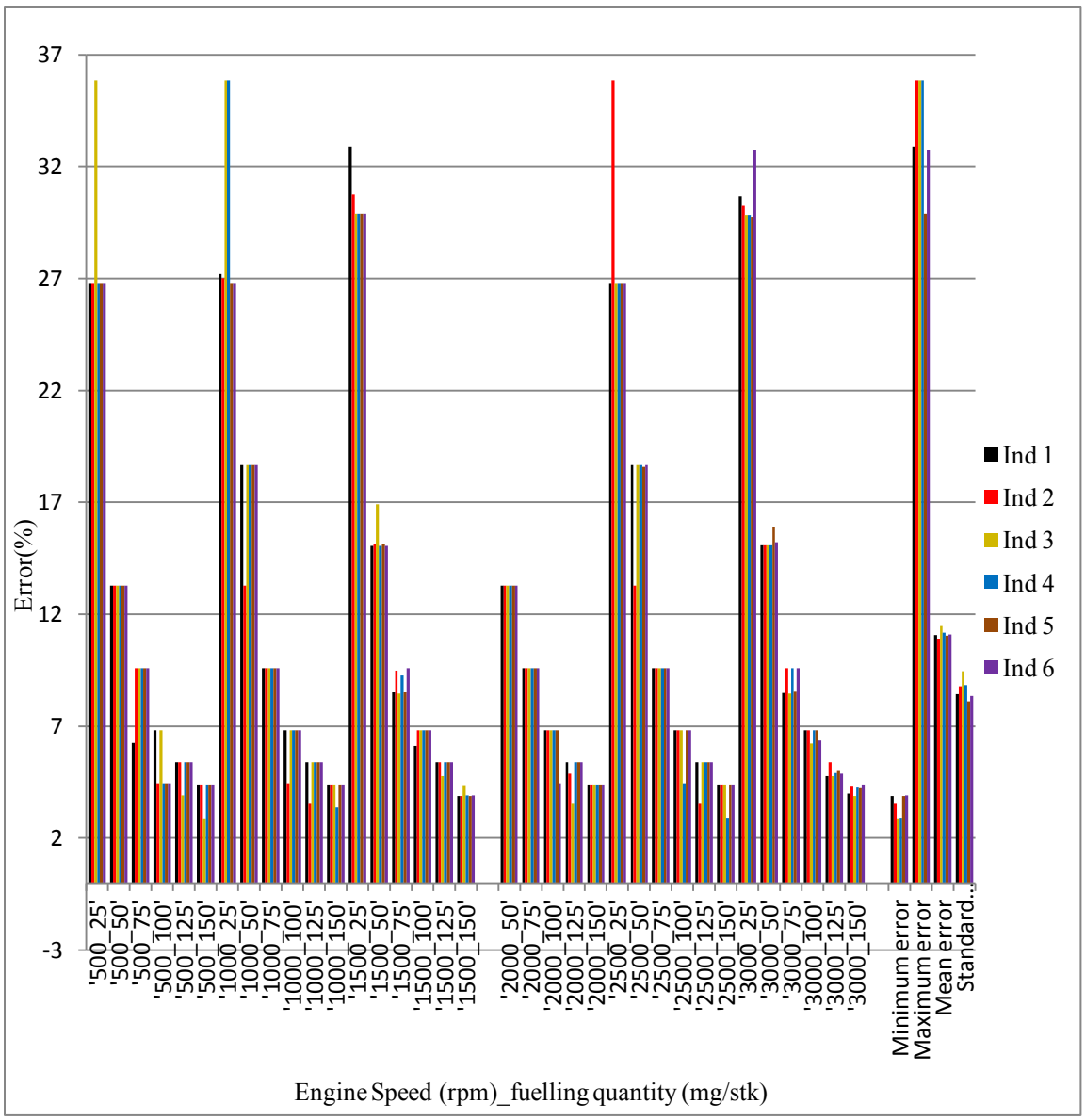

Figure A.1 Error percentage with single threshold at zero volts (inductor) with 20.8kHz sampling rate at 1V precision

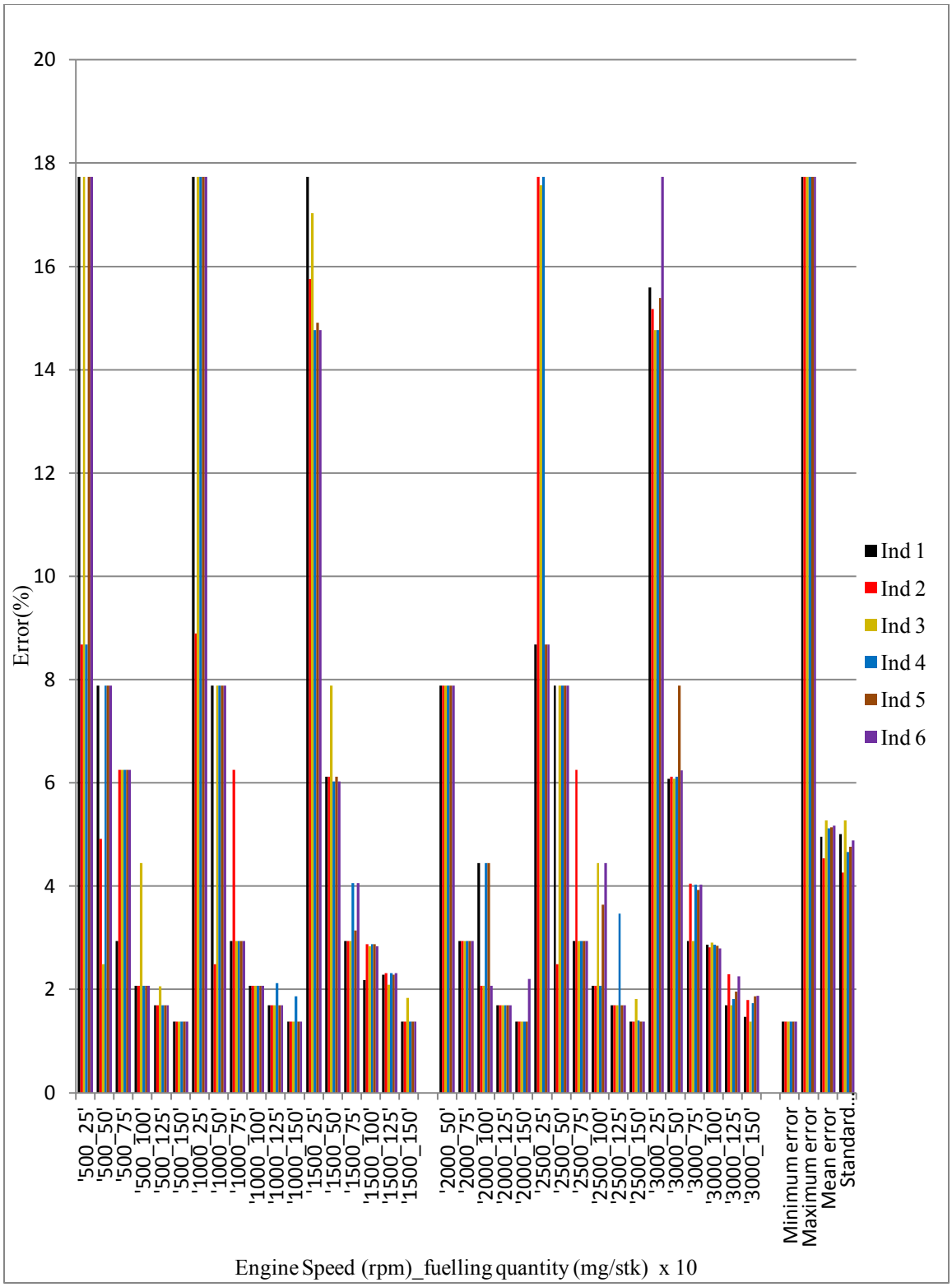

Figure A.2 Error percentage with single threshold at 1V (inductor) with 20.8kHz sampling rate at 1V precision

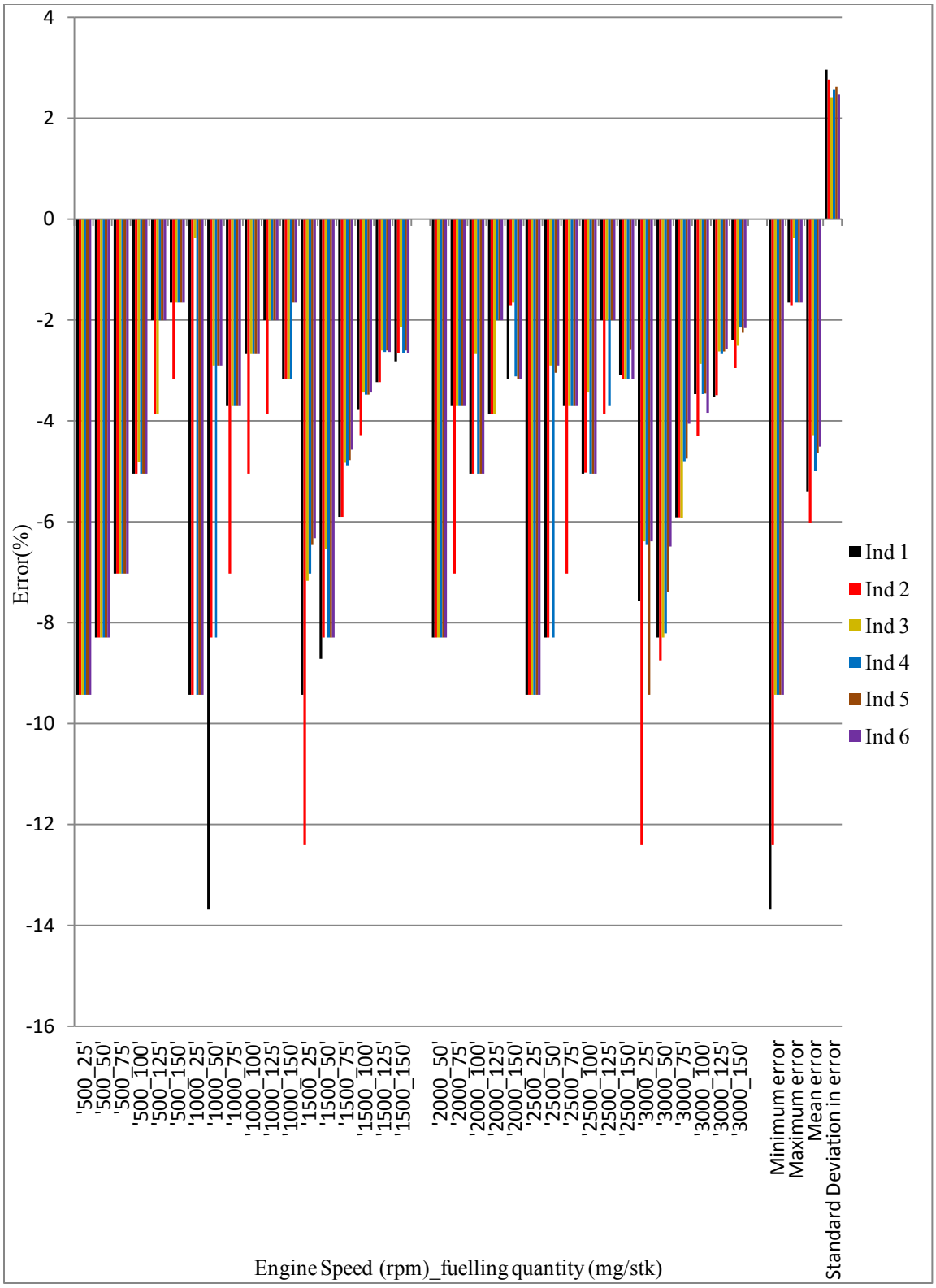

Figure A.3 Error percentage with single threshold at 3V (Inductor) with 20.8kHz sampling rate at 1V precision

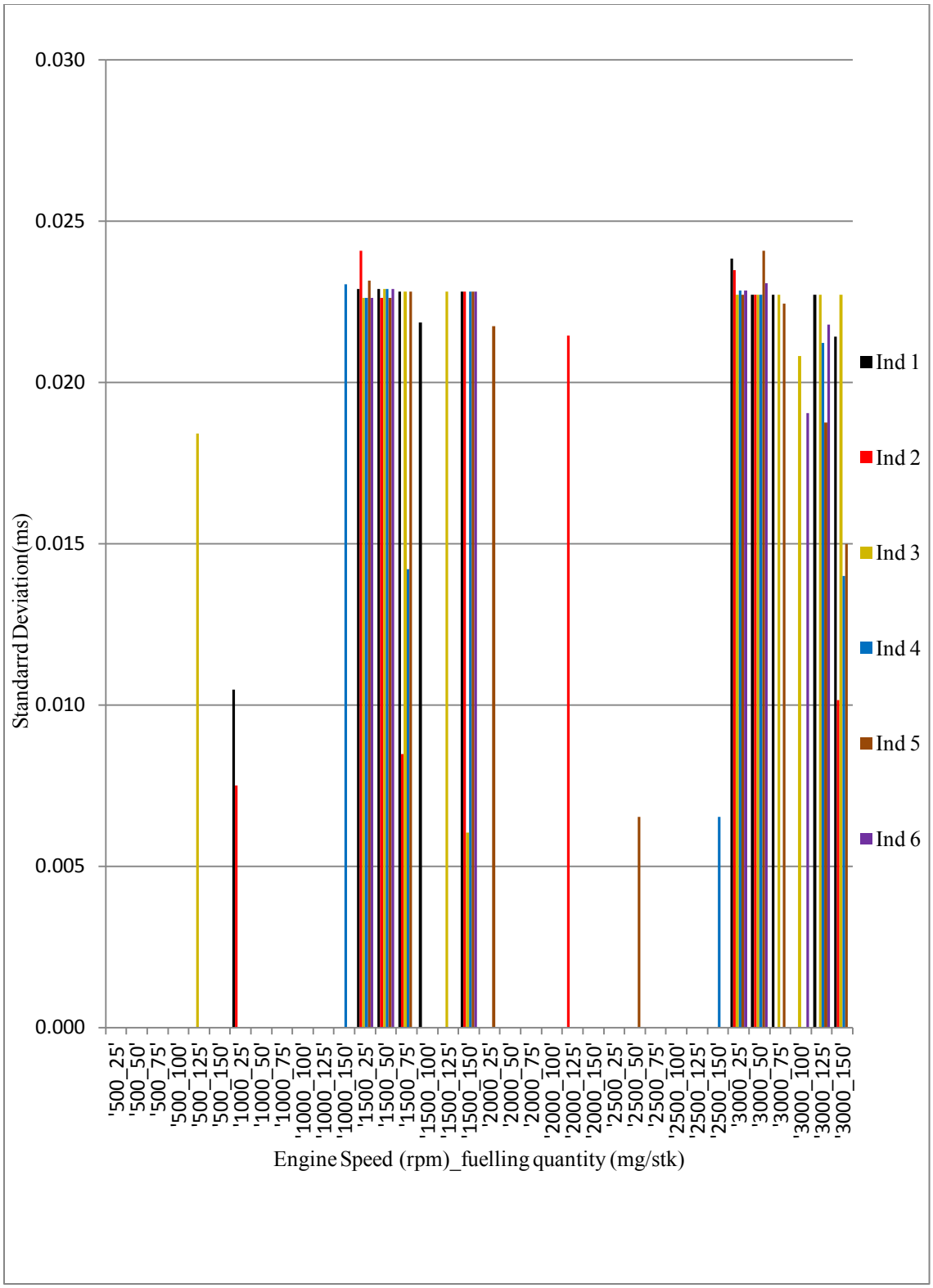

Figure A.4 Single threshold at 0V (Inductor) – Standard Deviation (Ontime) with 20.8kHz sampling rate at 1V precision

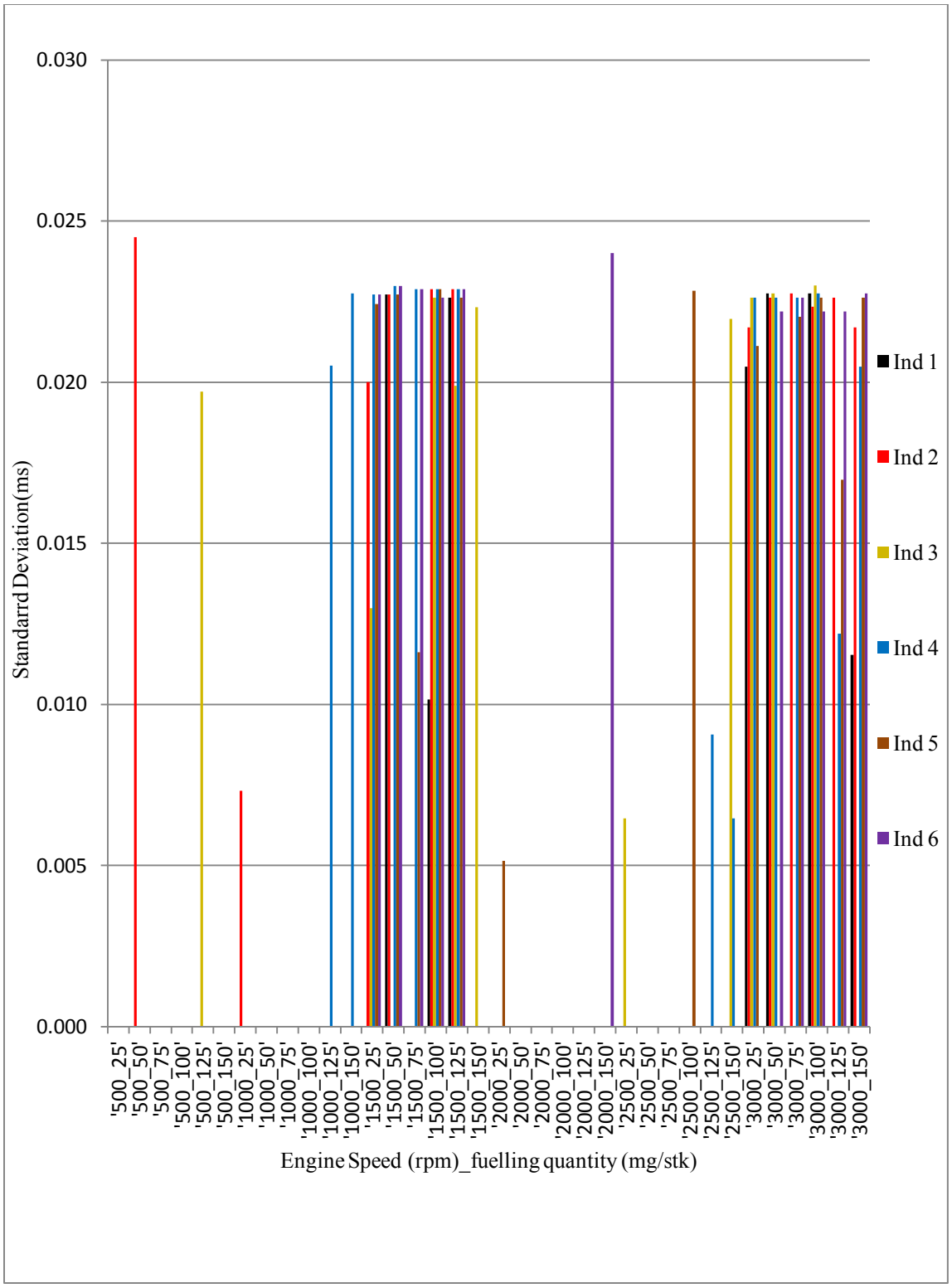

Figure A.5 Single threshold at 1V (Inductor) – Standard Deviation (Ontime) with 20.8kHz sampling rate at 1V precision

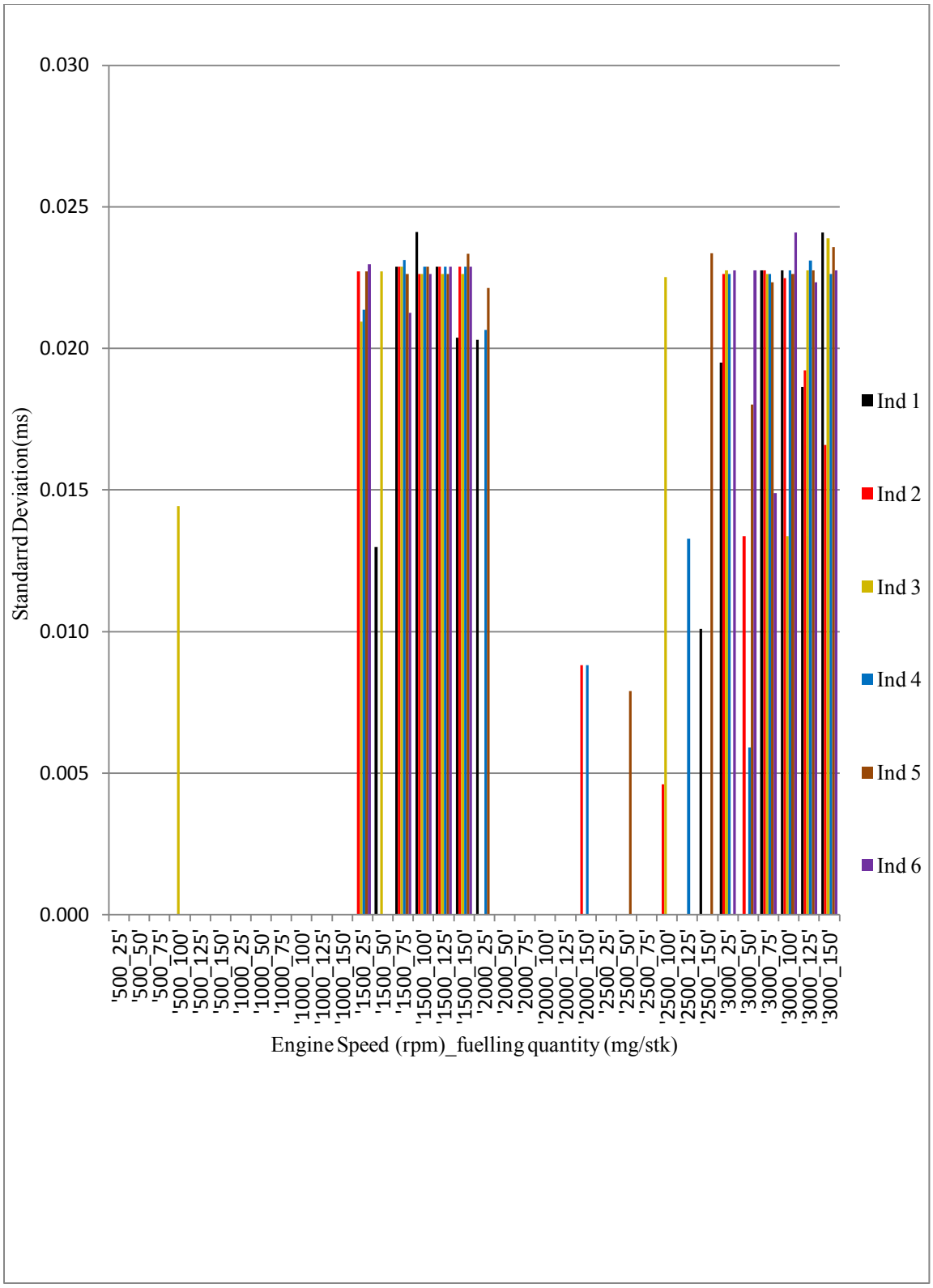

Figure A.6 Single threshold at 3V (Inductor) – Standard Deviation (Ontime) with 20.8kHz sampling rate at 1V precision

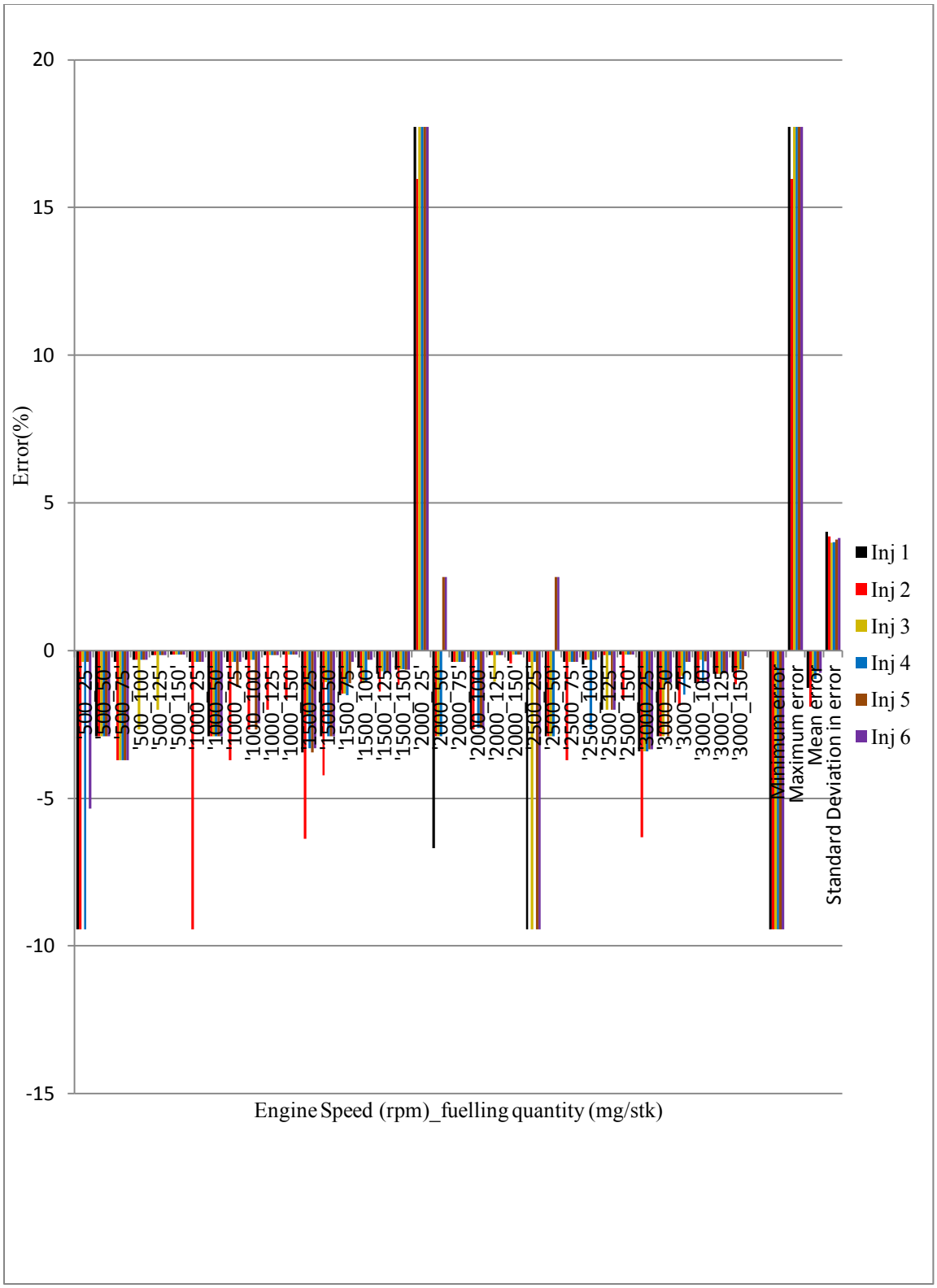

Figure A.7 Error Percentage with single threshold at 0V (Injector) with 20.8kHz sampling rate at 1V precision

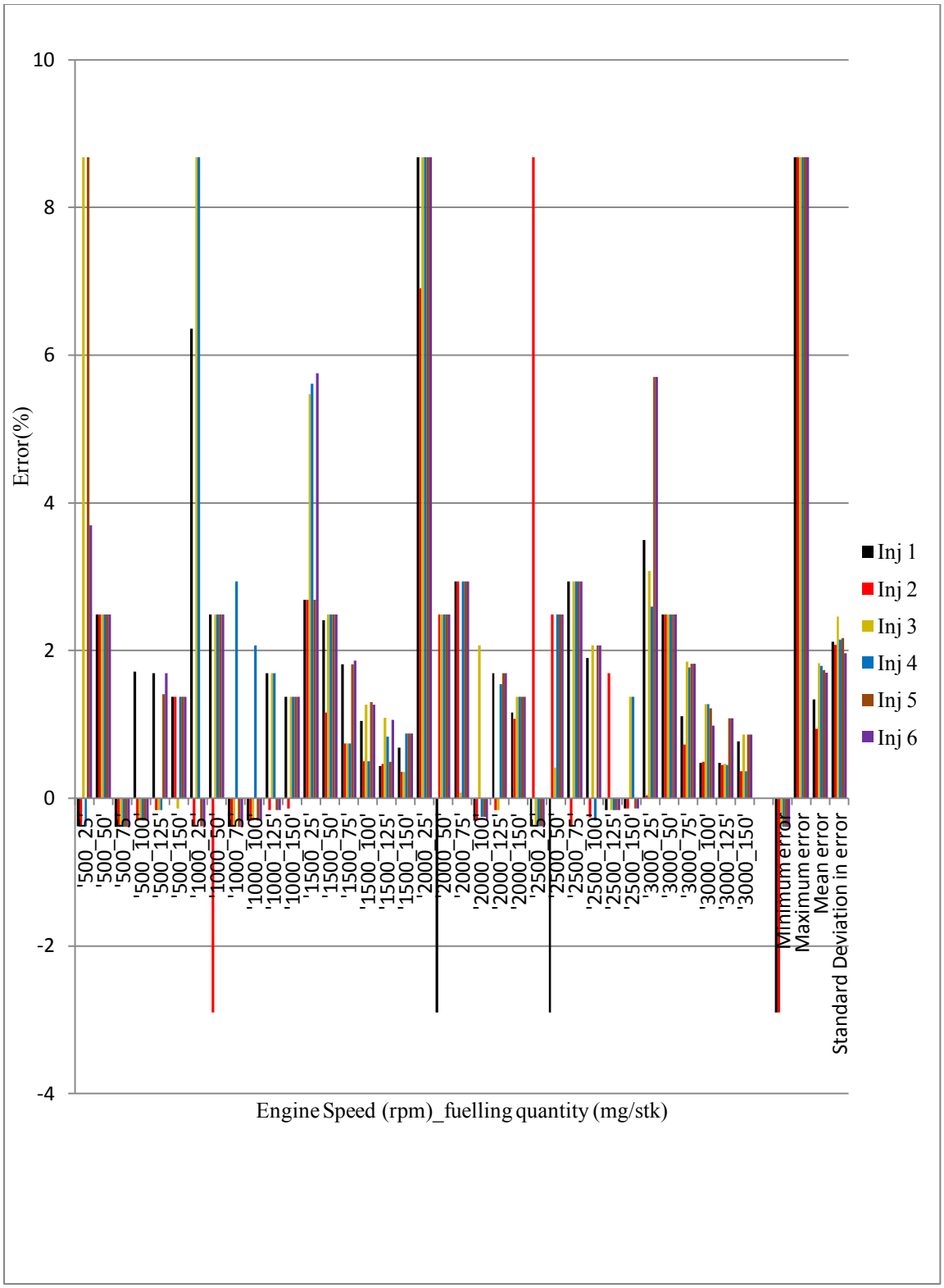

Figure A.8 Error Percentage with single threshold at 1V (Injector) with 20.8kHz sampling rate at 1V precision

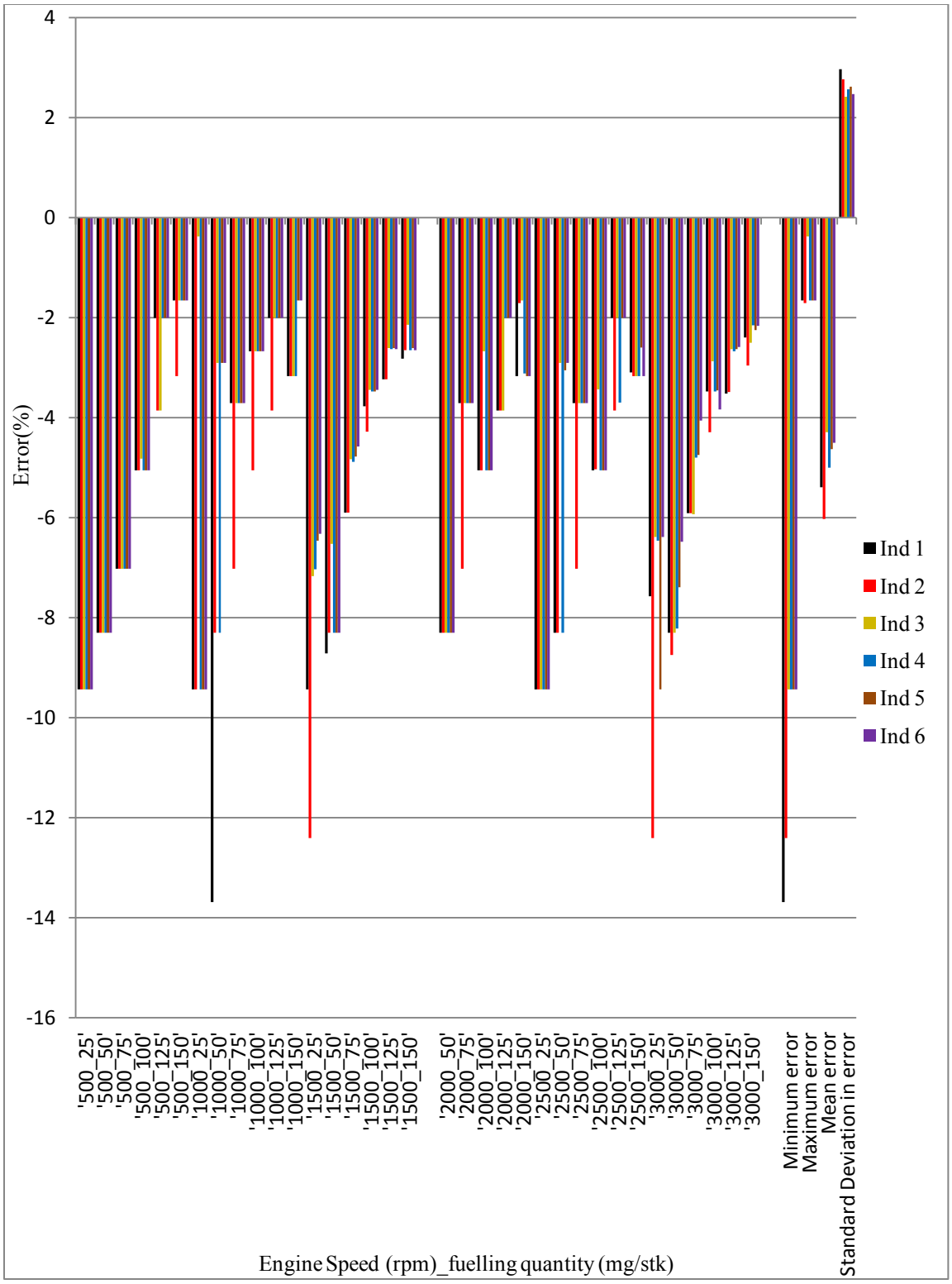

Figure A.9 Error Percentage with single threshold at 3V (Injector) with 20.8kHz sampling rate at 1V precision

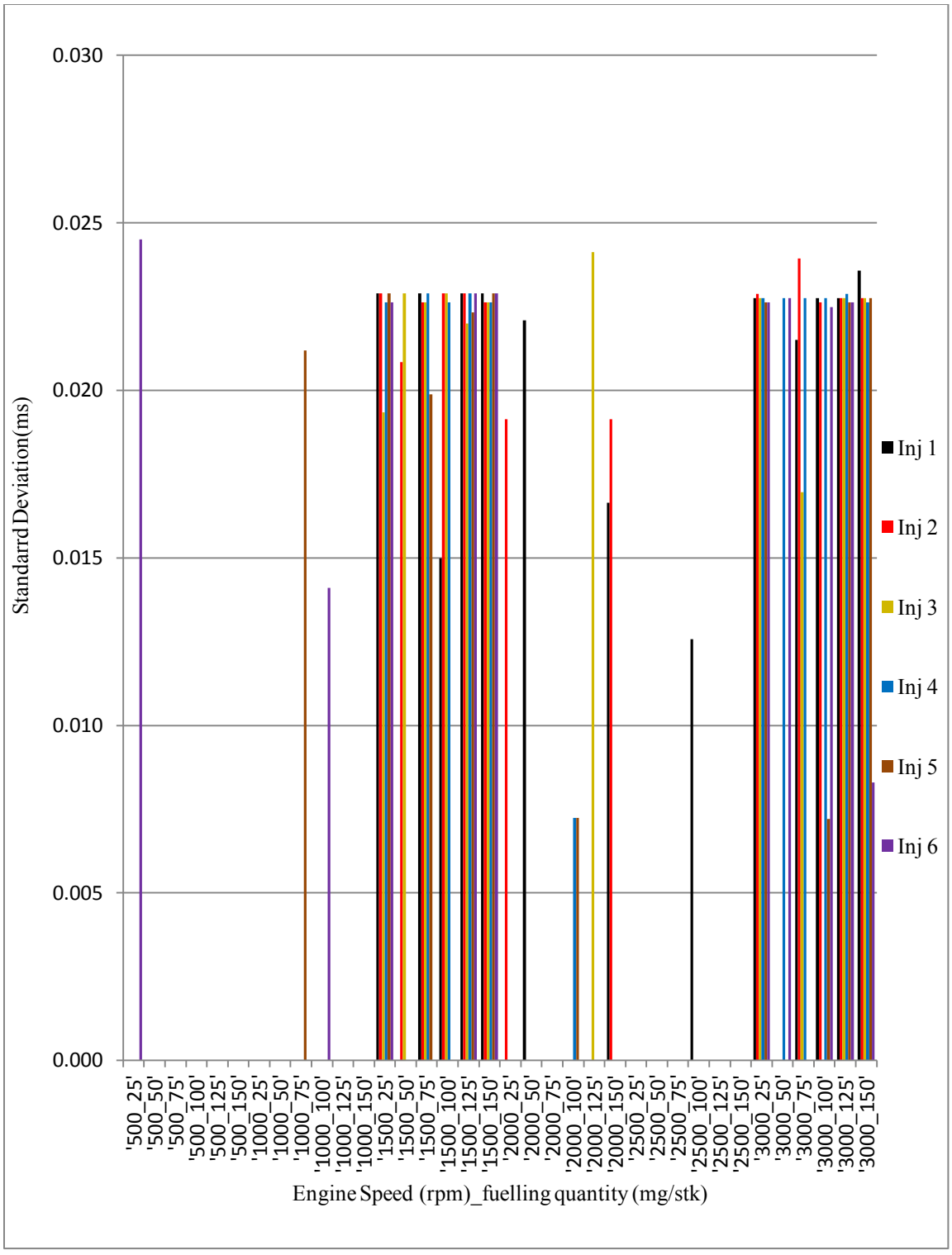

Figure A.10 Single threshold at 0V (Injector) – Standard Deviation (Ontime) with 20.8kHz sampling rate at 1V precision

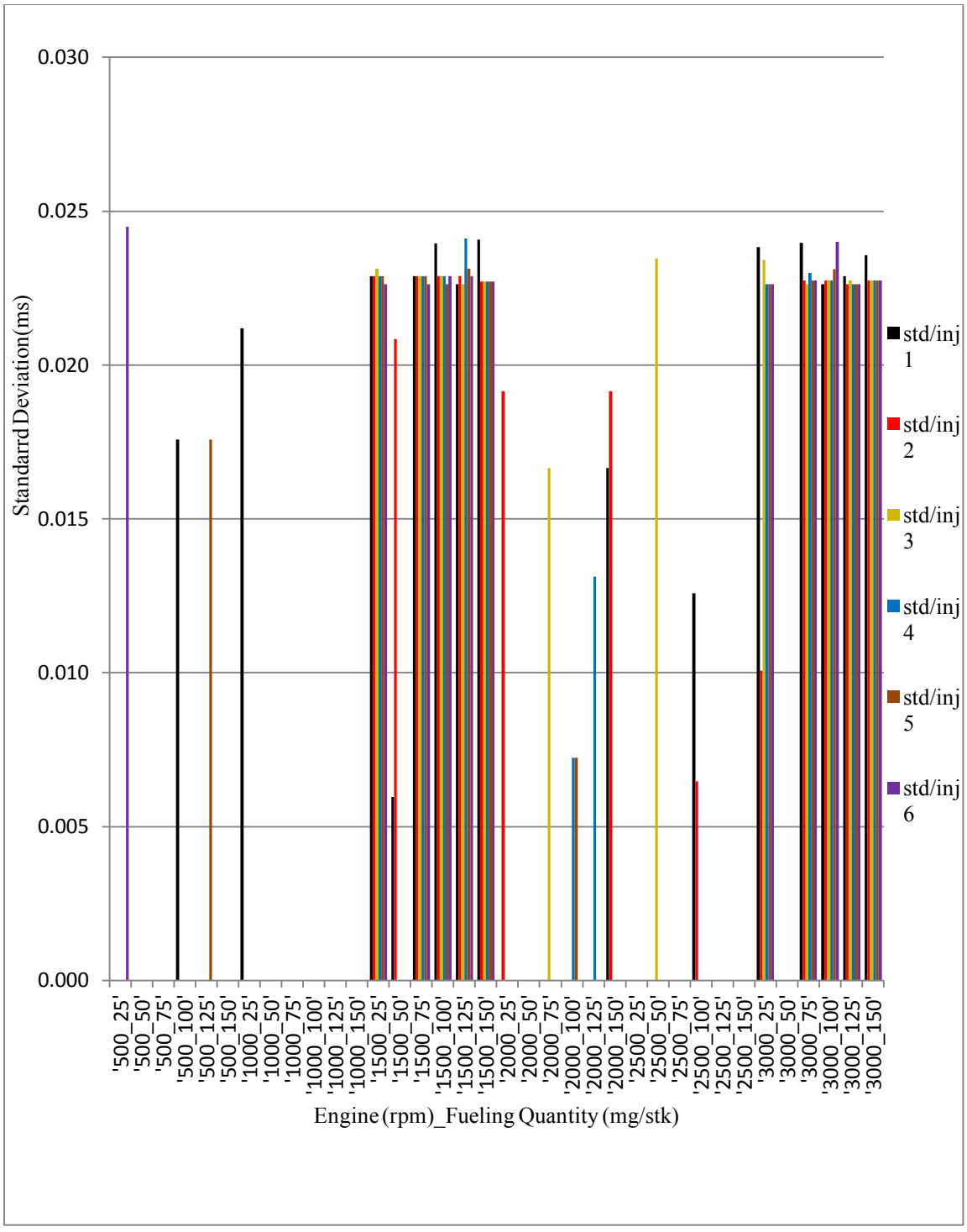

Figure A.11 Single threshold at 1V (Injector) – Standard Deviation (Ontime) with 20.8kHz sampling rate at 1V precision

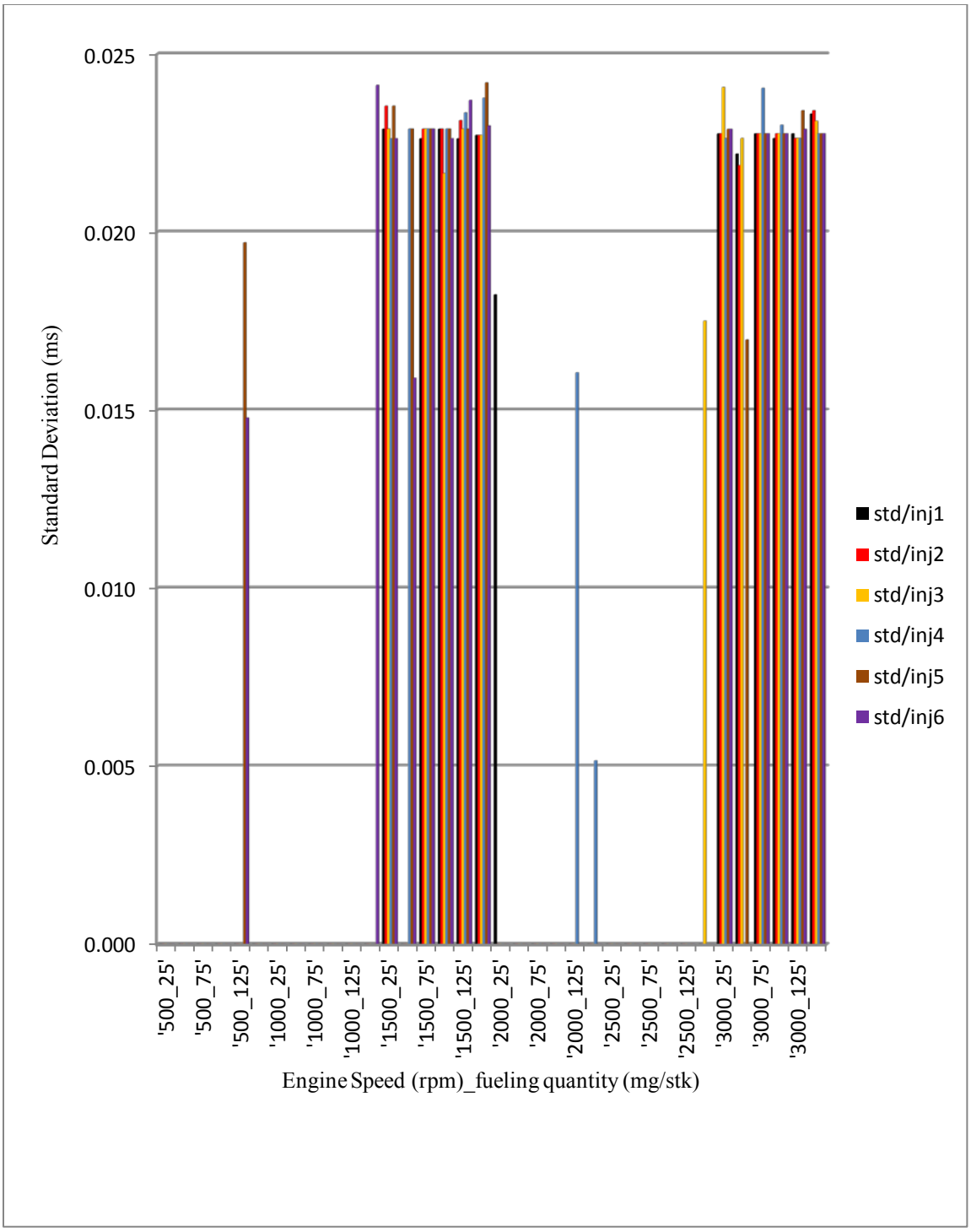

Figure A.12 Single threshold at 3V (Injector) – Standard Deviation (Ontime) with 20.8kHz sampling rate at 1V precision

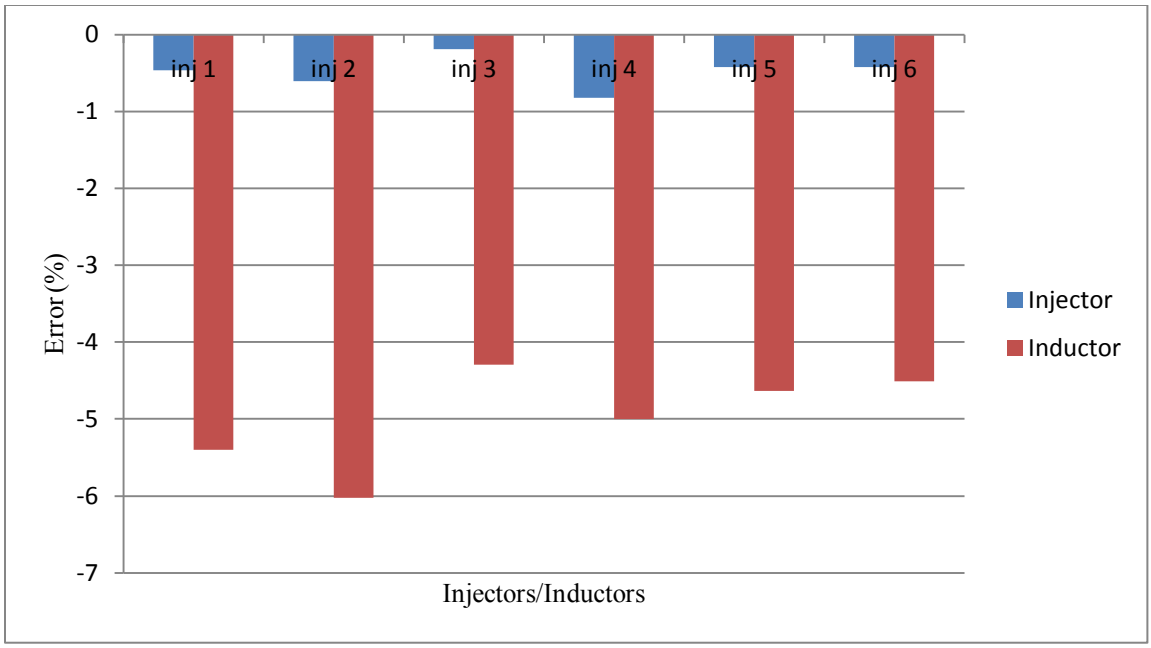

Figure A.13 Mean error percent using Threshold at 3V with 20.8kHz sampling rate at 1V precision

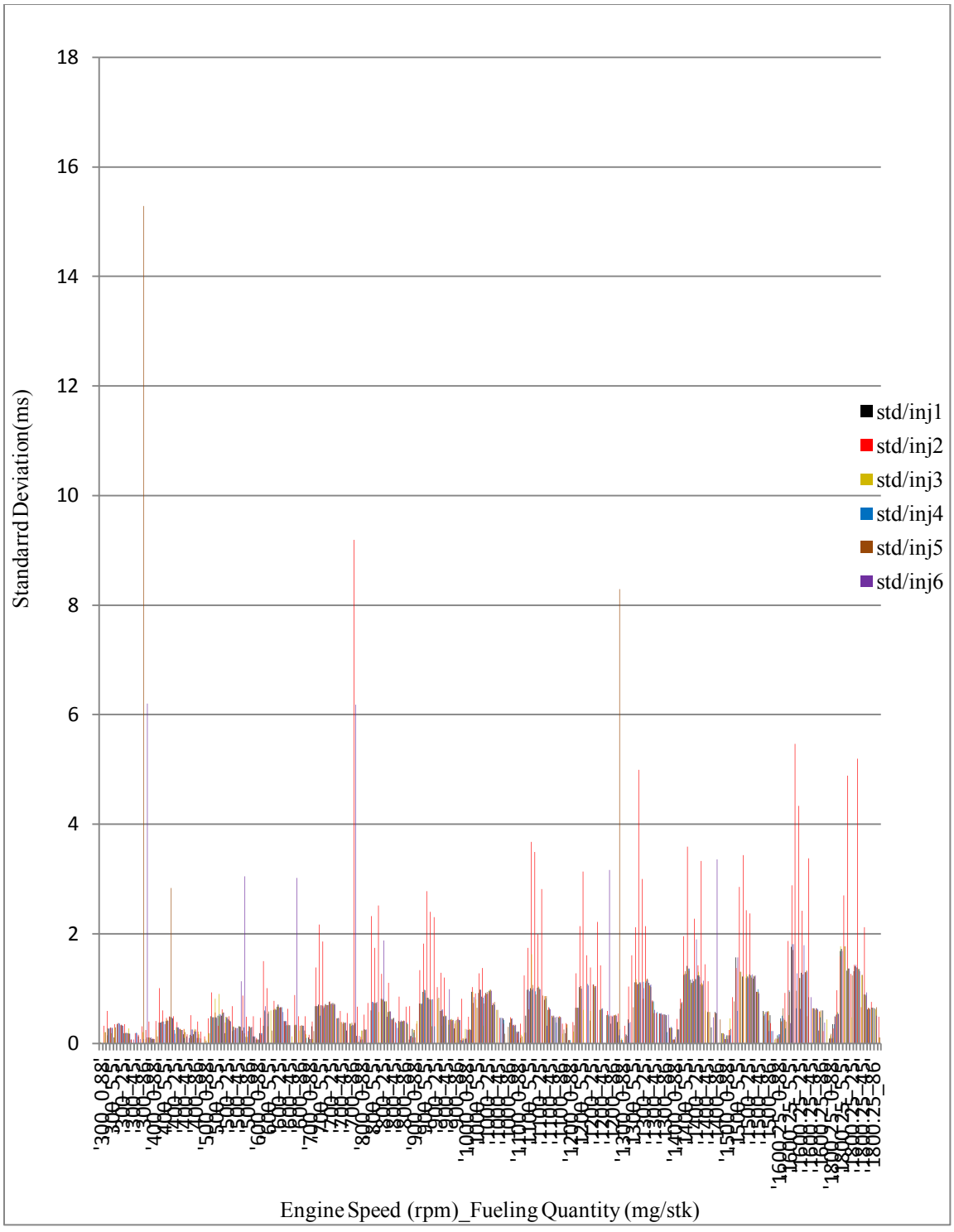

Figure A.14 Standard Deviation (Shot to Shot Variability) 1500rpm with injector at a higher sampling rate of 41.6kHz.

Experimetation at higher precision of 0.0156V and higher sampling rate of 125KHz per channel

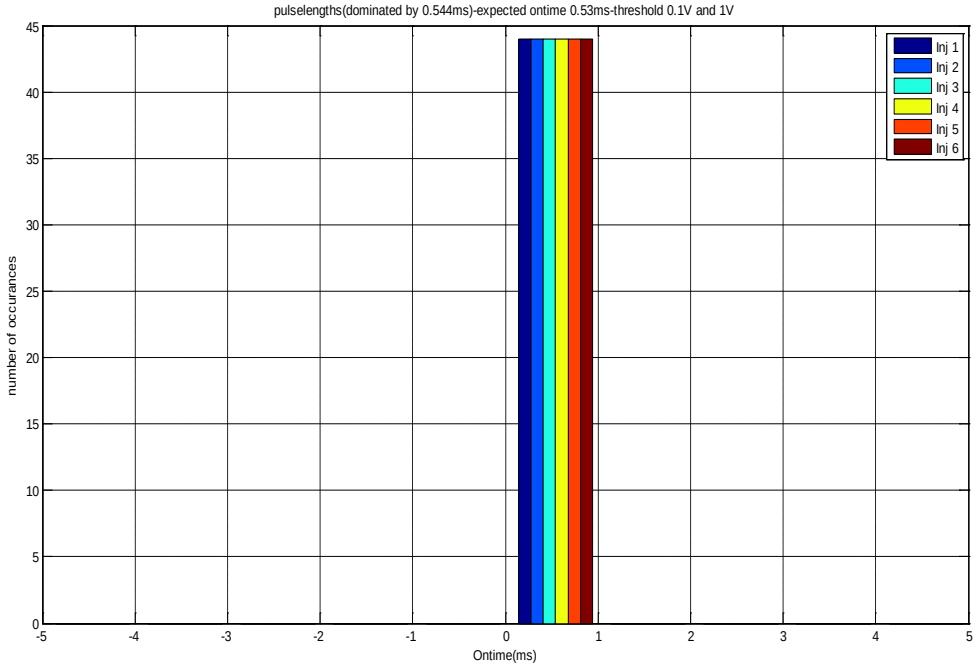

Figure A.15 Histogram of captured ontime (ms) with injectors with thresholds at 0.1V and 1V

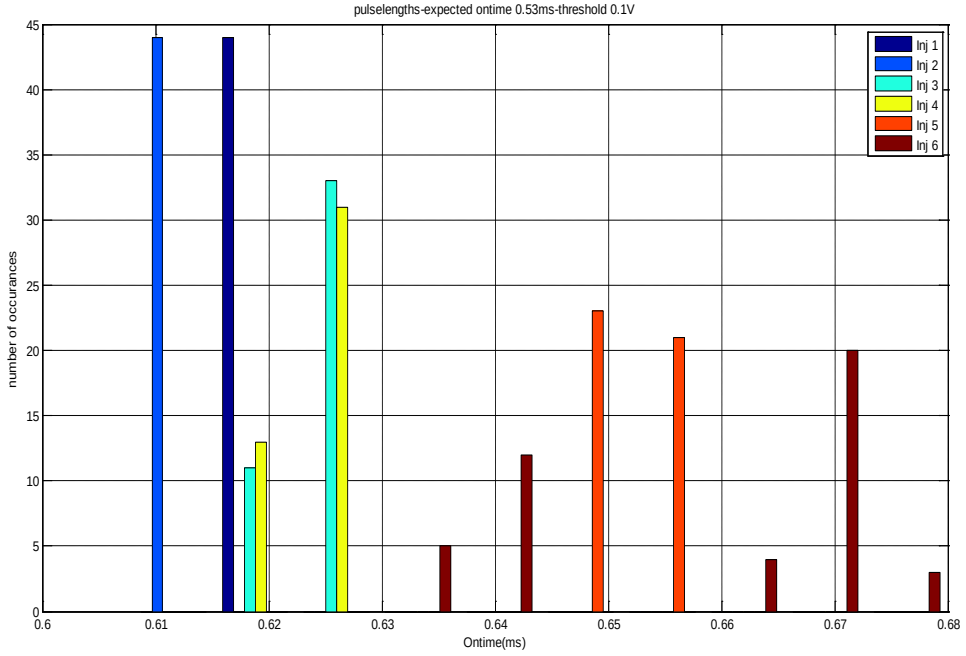

Figure A.16 Histogram of captured ontime (ms) with injectors with threshold at 0.1V

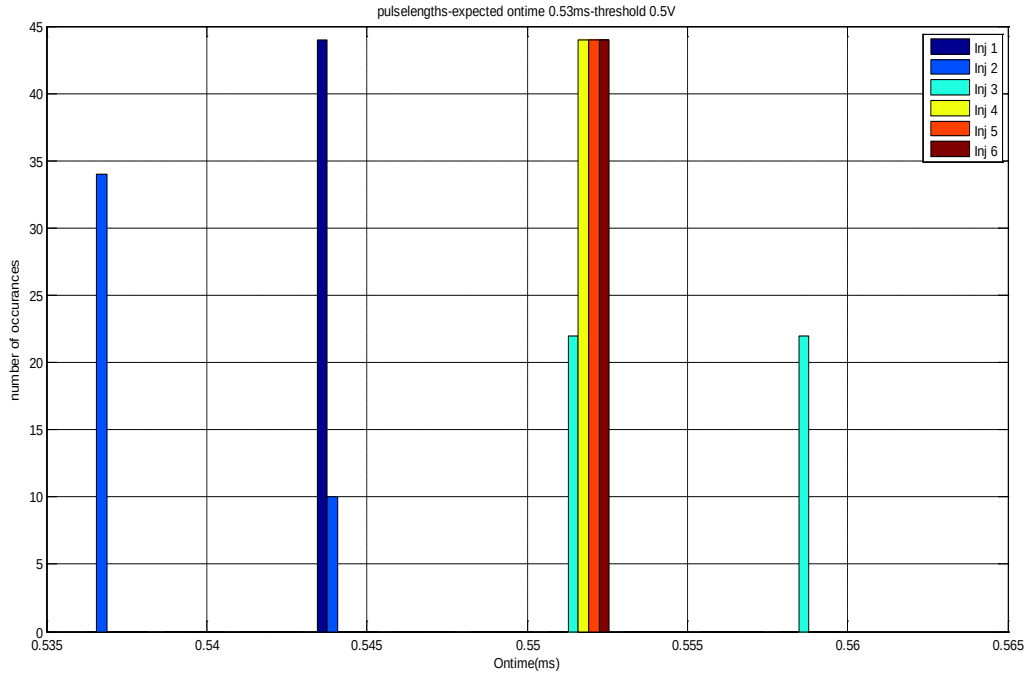

Figure A.17 Histogram of captured ontime (ms) with injectors with threshold at 0.5V

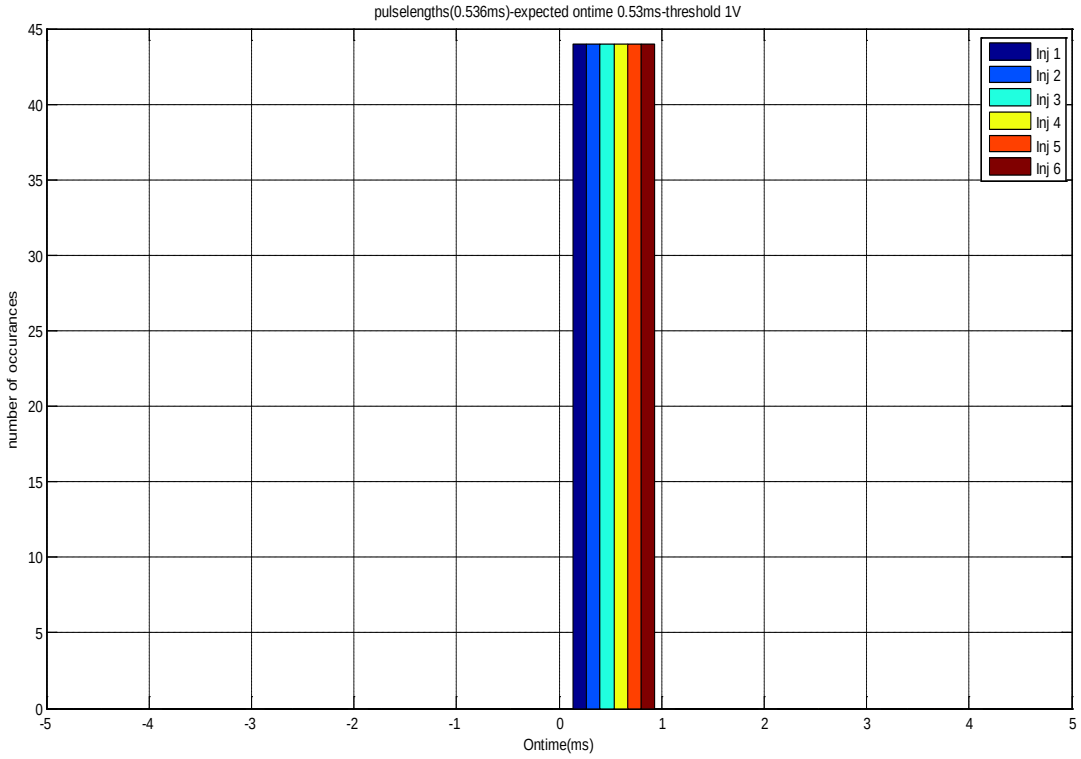

Figure 6.18 Histogram of captured ontime (ms) with injectors with threshold at 1V

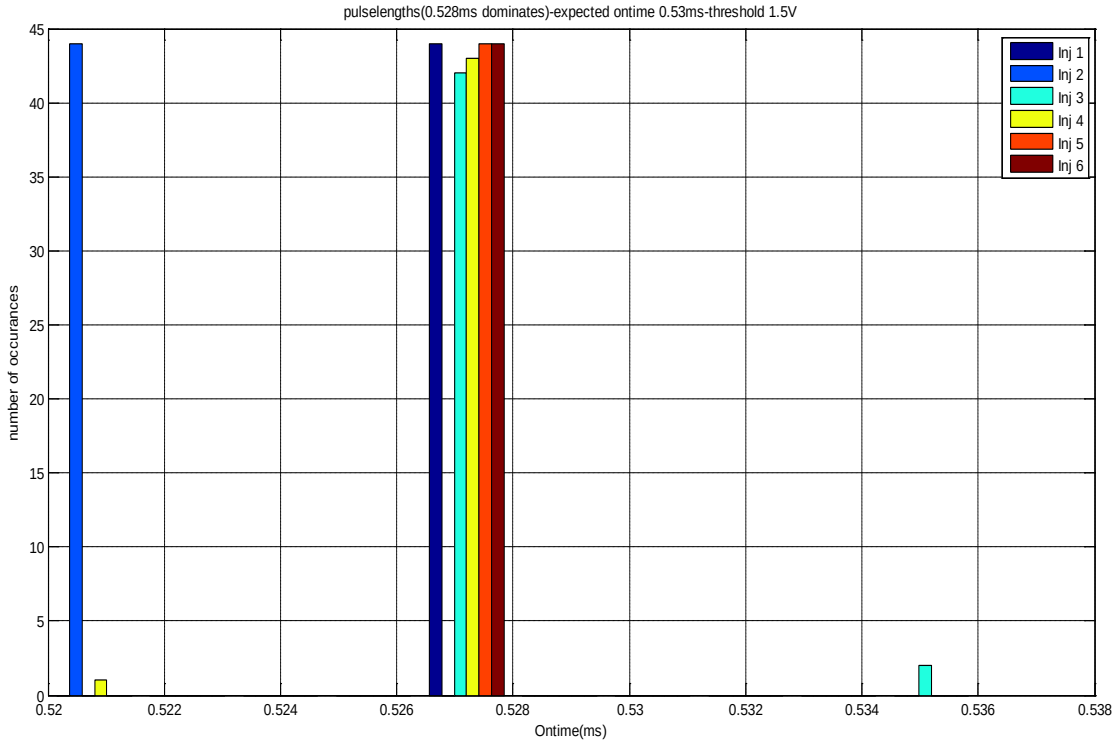

Figure A.19 Histogram of captured ontime (ms) with injectors with threshold at 1.5V

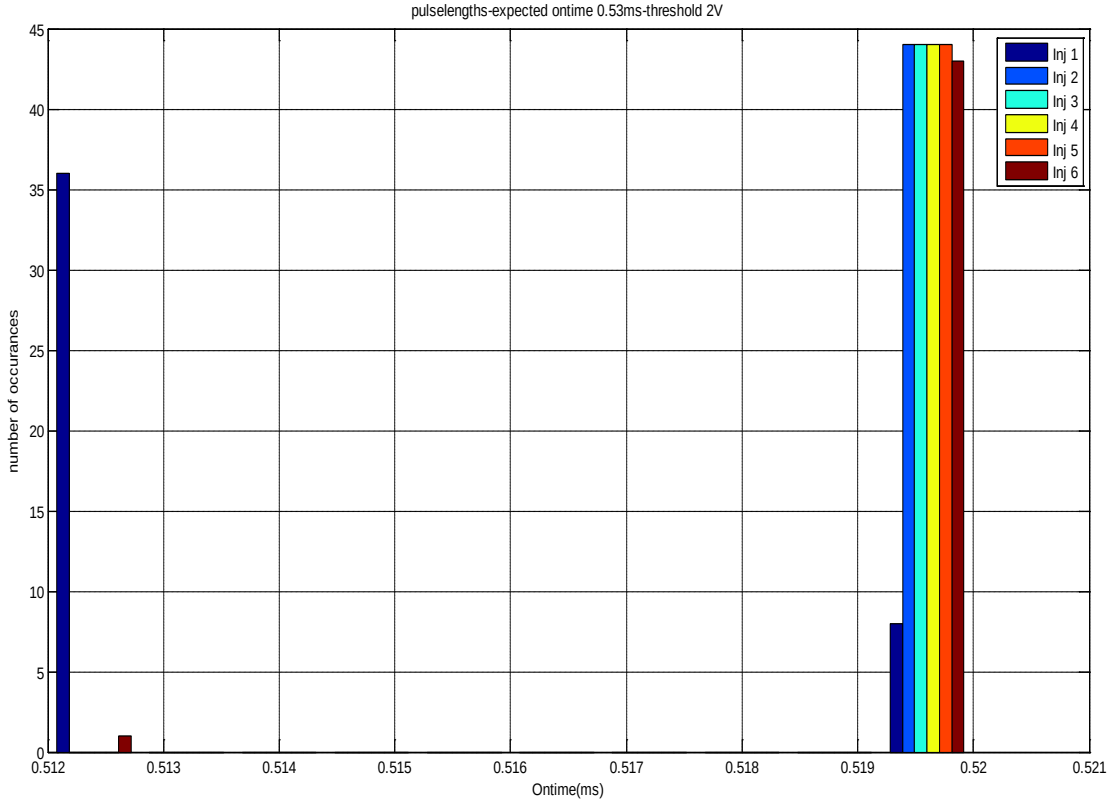

Figure A.20 Histogram of captured ontime (ms) with injectors with threshold at 2V

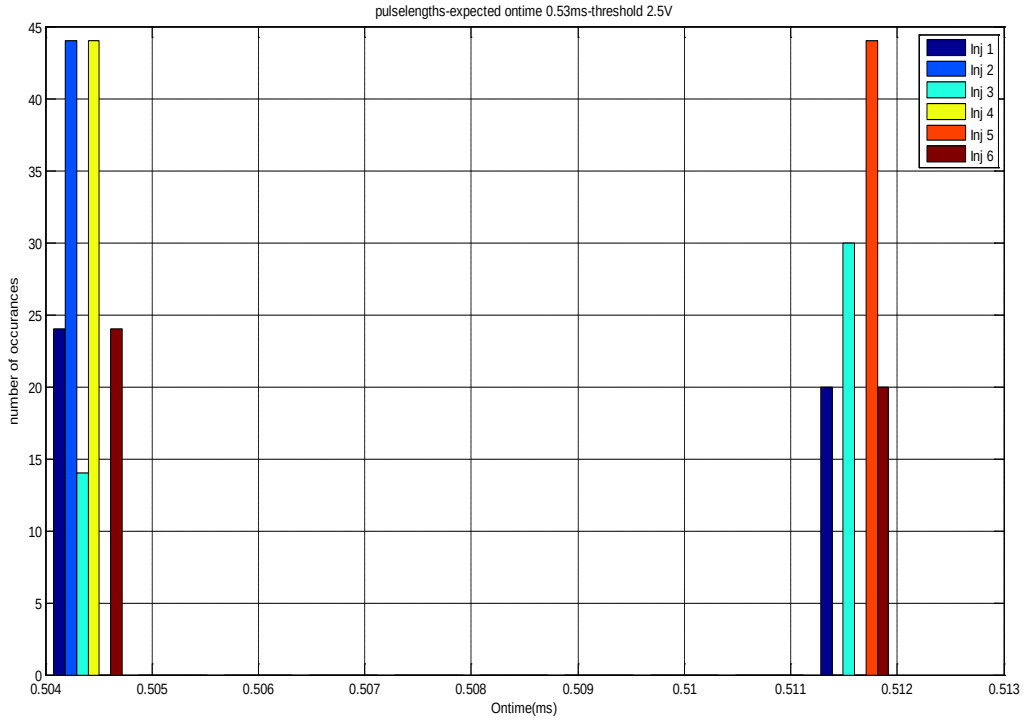

Figure A.21 Histogram of captured ontime (ms) with injectors with threshold at 2.5V

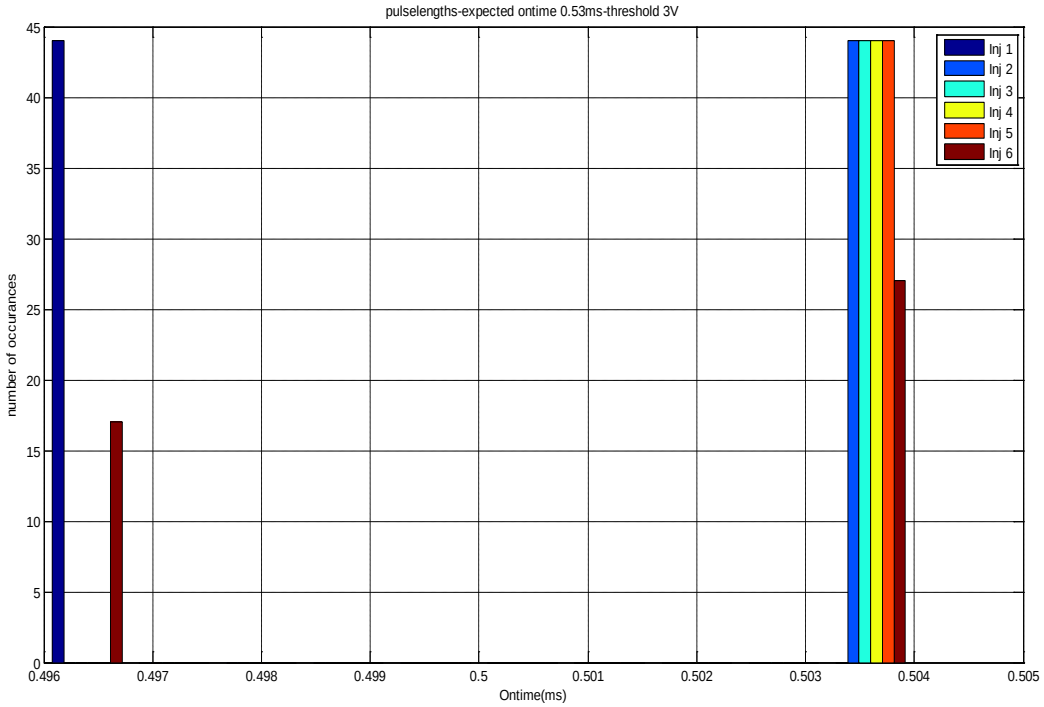

Figure A.22 Histogram of captured ontime (ms) with injectors with threshold at 3V

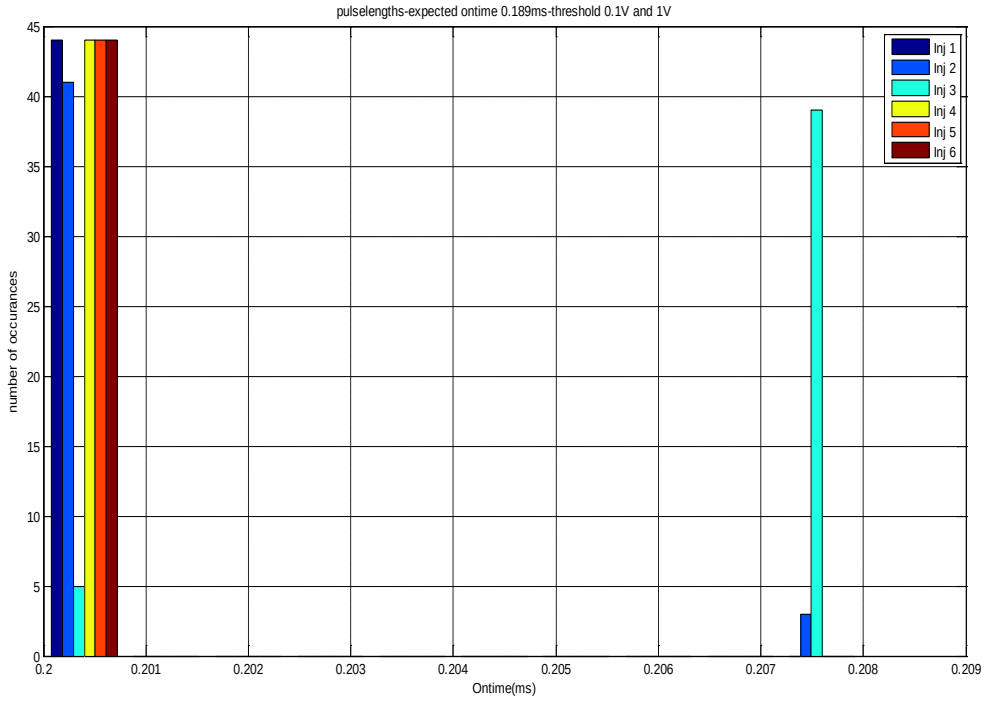

Figure A.23 Histogram of captured ontime (ms) with injectors with threshold at 0.1V and 1V

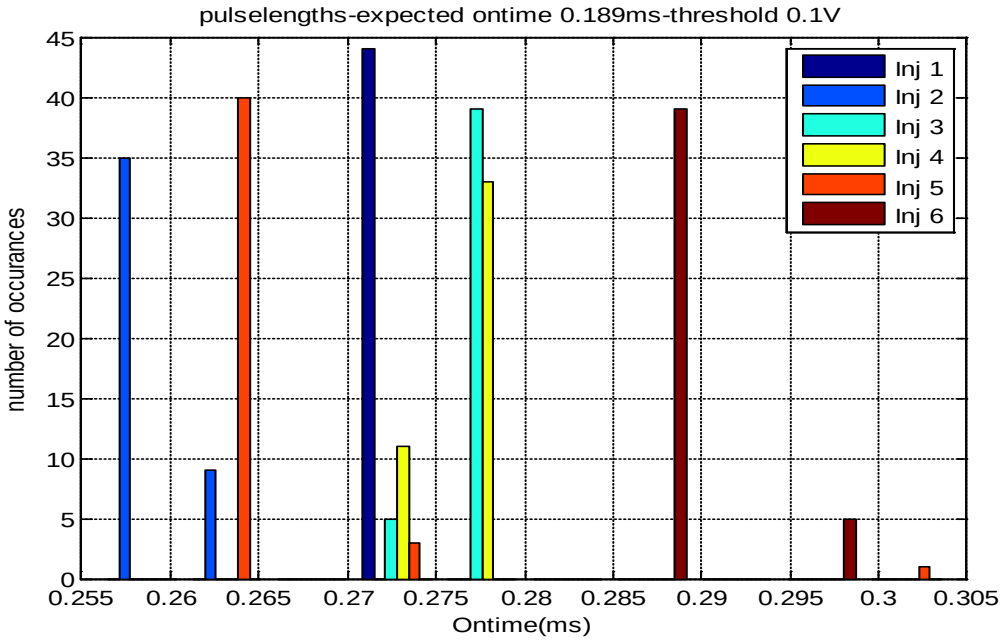

Figure A.24 Histogram of captured ontime (ms) with injectors with threshold at 0.1V

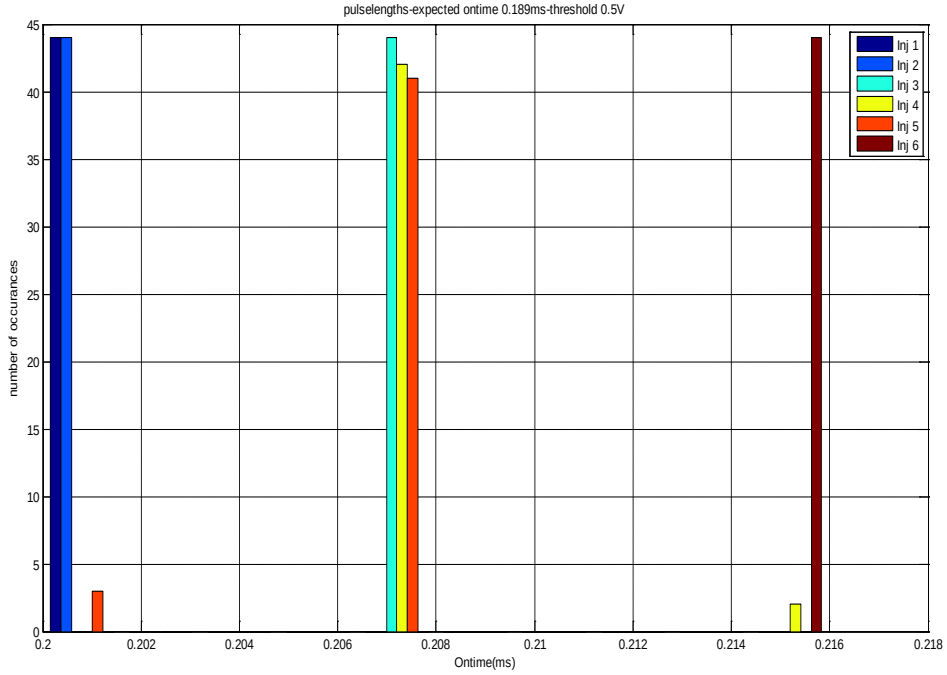

Figure A.25 Histogram of captured ontime (ms) with injectors with threshold at 0.5V

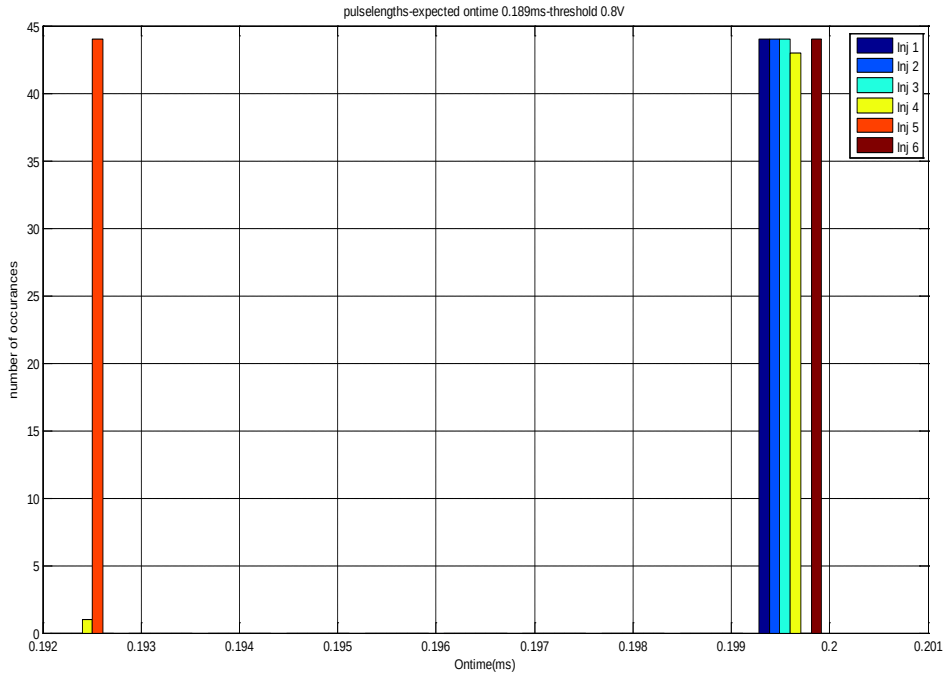

Figure A.26 Histogram of captured ontime (ms) with injectors with threshold at 0.5V

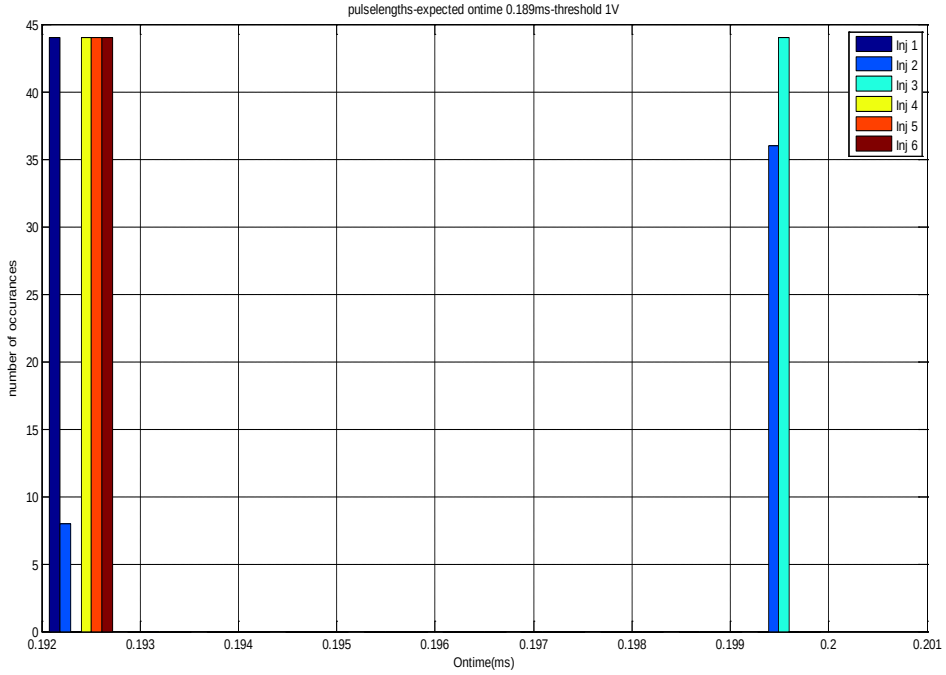

Figure A.27 Histogram of captured ontime (ms) with injectors with threshold at 1V

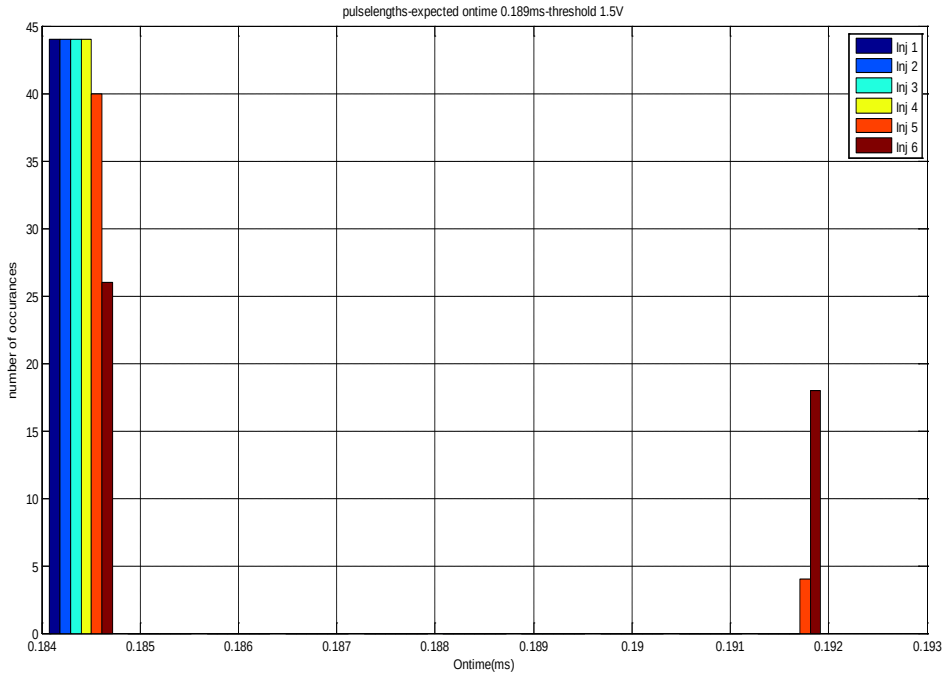

Figure A.28 Histogram of captured ontime (ms) with injectors with threshold at 1.5V

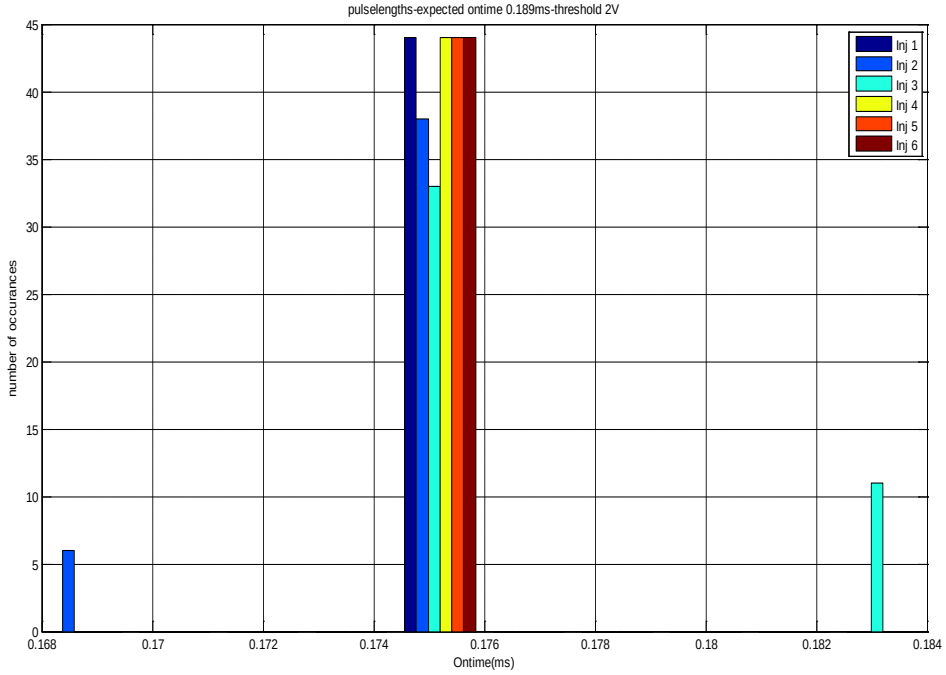

Figure A.29 Histogram of captured ontime (ms) with injectors with threshold at 2V

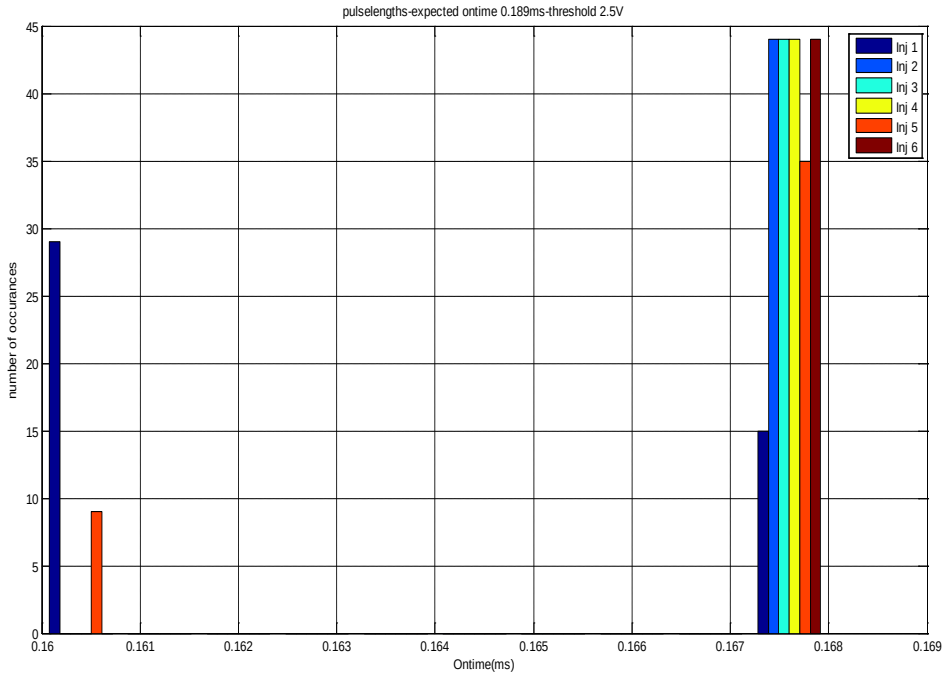

Figure A.30 Histogram of captured ontime (ms) with injectors with threshold at 2.5V

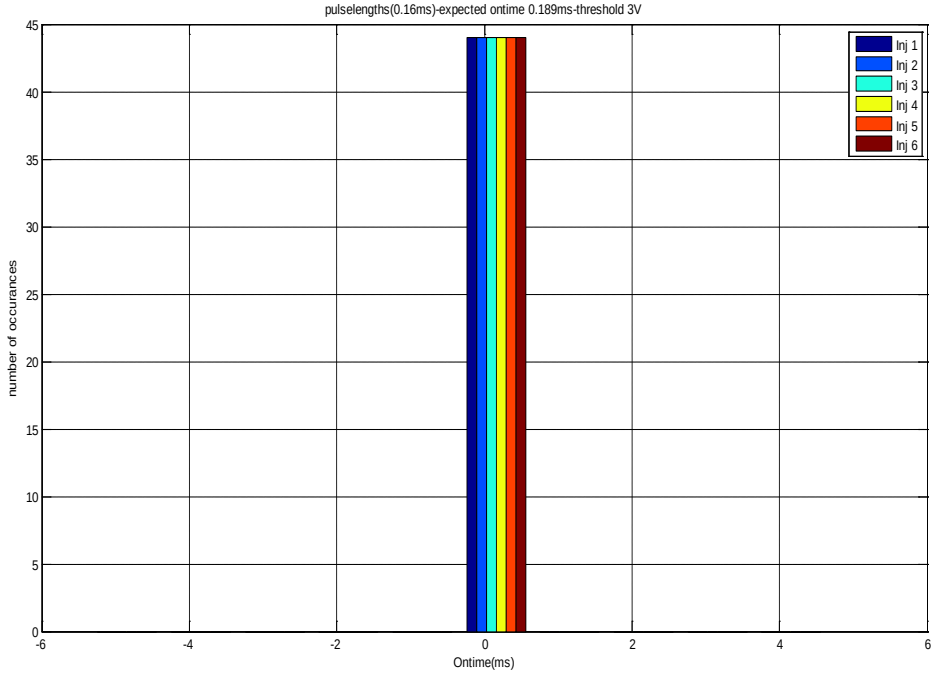

Figure A.31 Histogram of captured ontime (ms) with injectors with threshold at 3V

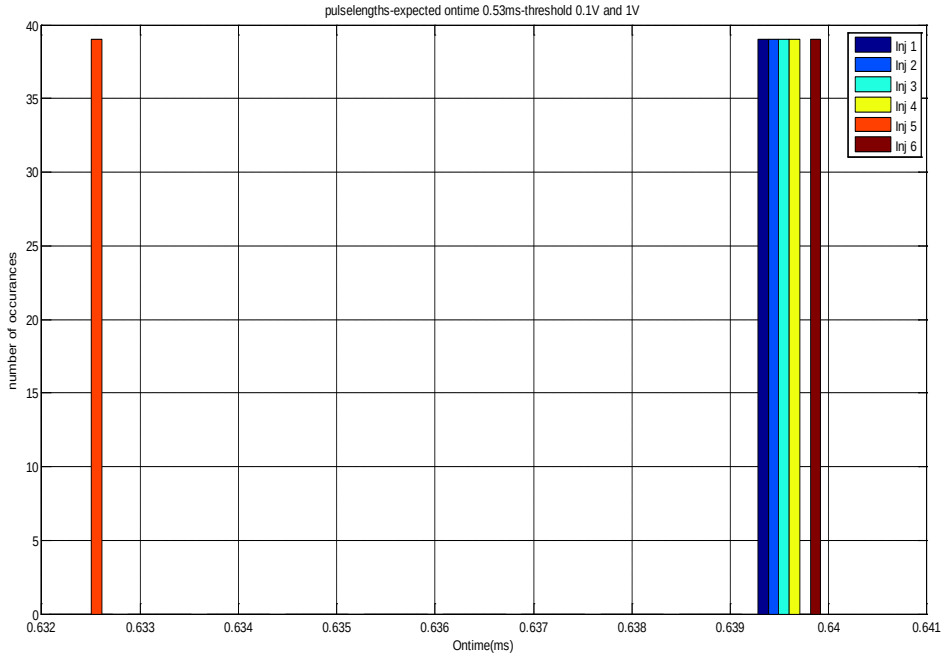

Figure A.32 Histogram of captured ontime (ms) with inductors with threshold at 0.1V and 1V

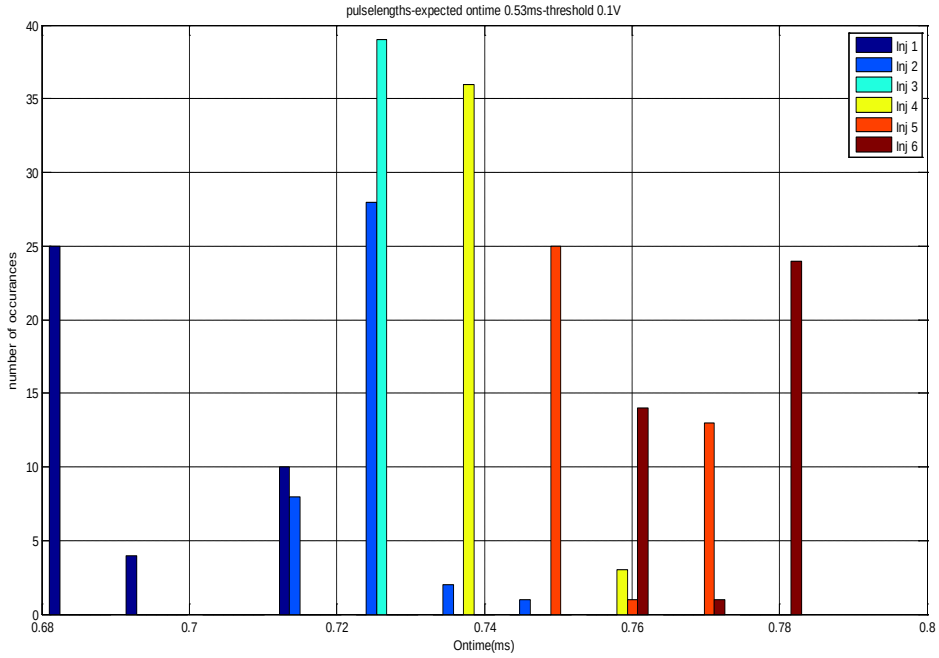

Figure A.33 Histogram of captured ontime (ms) with inductors with threshold at 0.1V

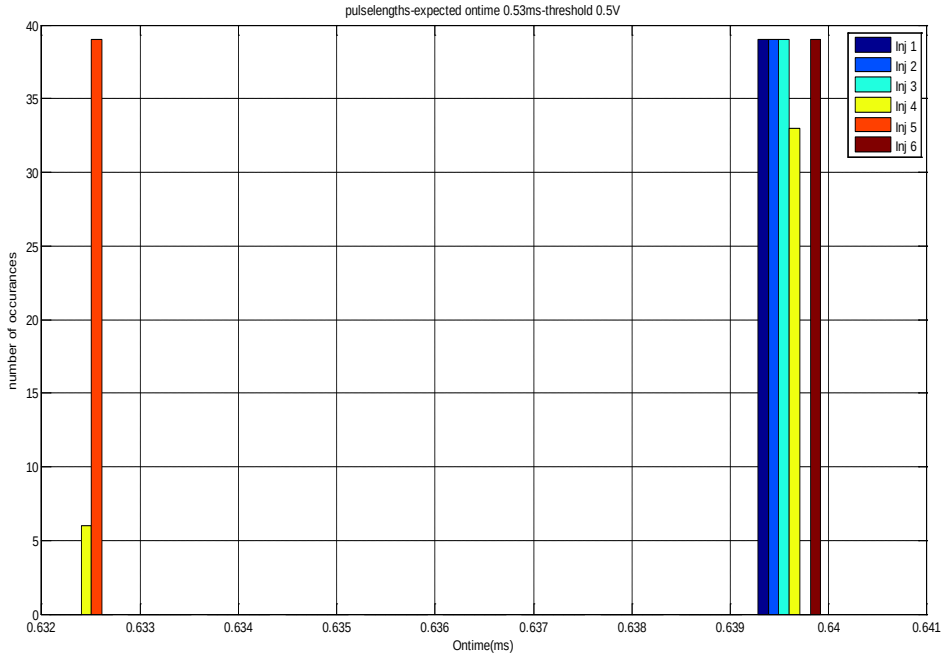

Figure A.34 Histogram of captured ontime (ms) with inductors with threshold at 0.5V

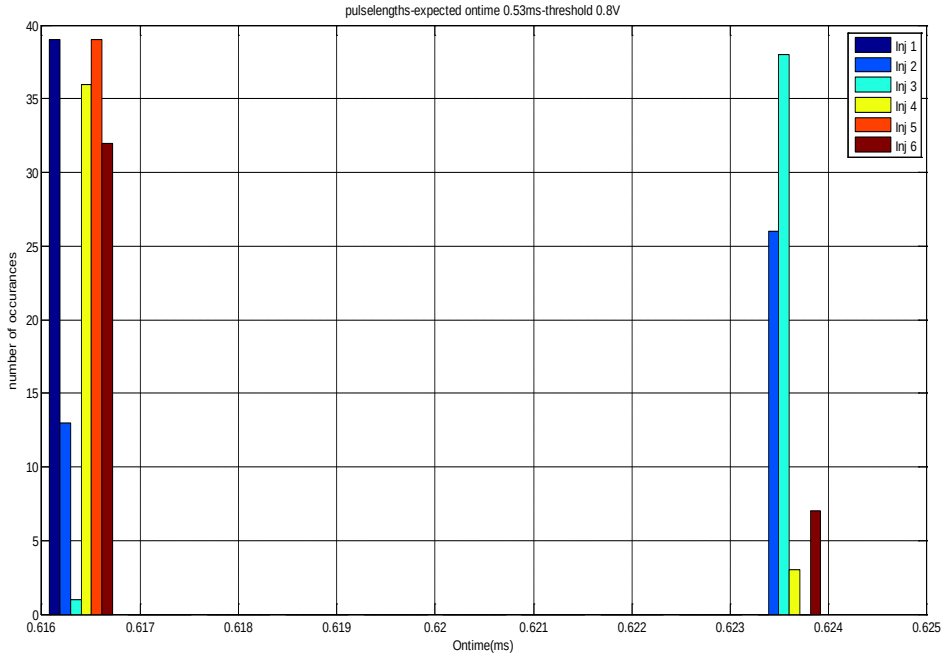

Figure A.35 Histogram of captured ontime (ms) with inductors with threshold at 0.8V

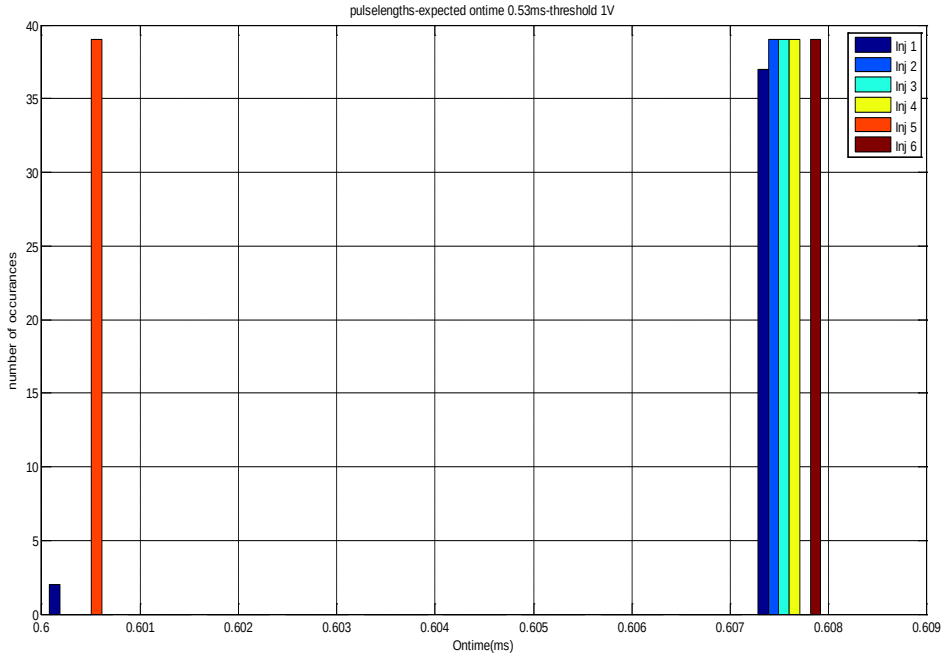

Figure A.36 Histogram of captured ontime (ms) with inductors with threshold at 1V

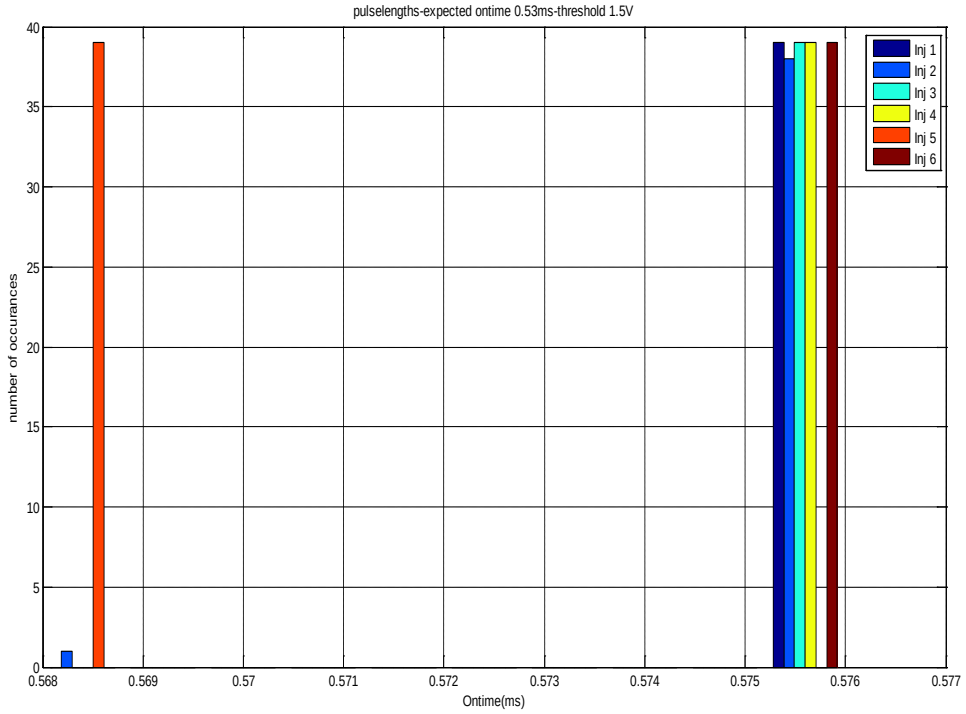

Figure A.37 Histogram of captured ontime (ms) with inductors with threshold at 1.5V

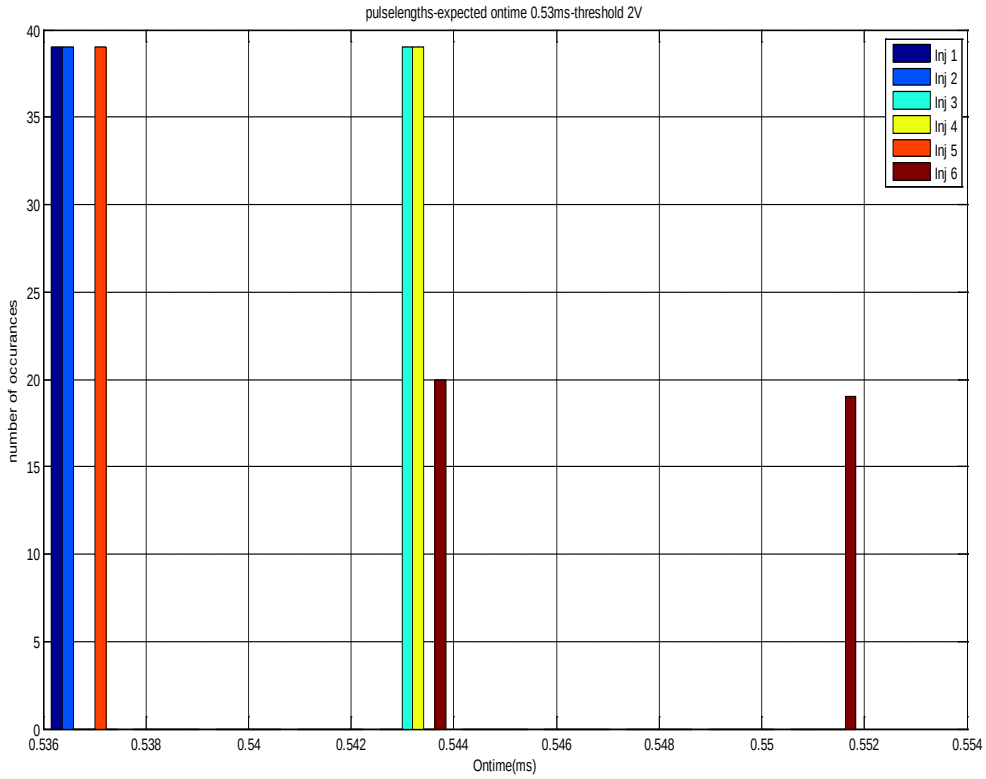

Figure A.38 Histogram of captured ontime (ms) with inductors with threshold at 2V

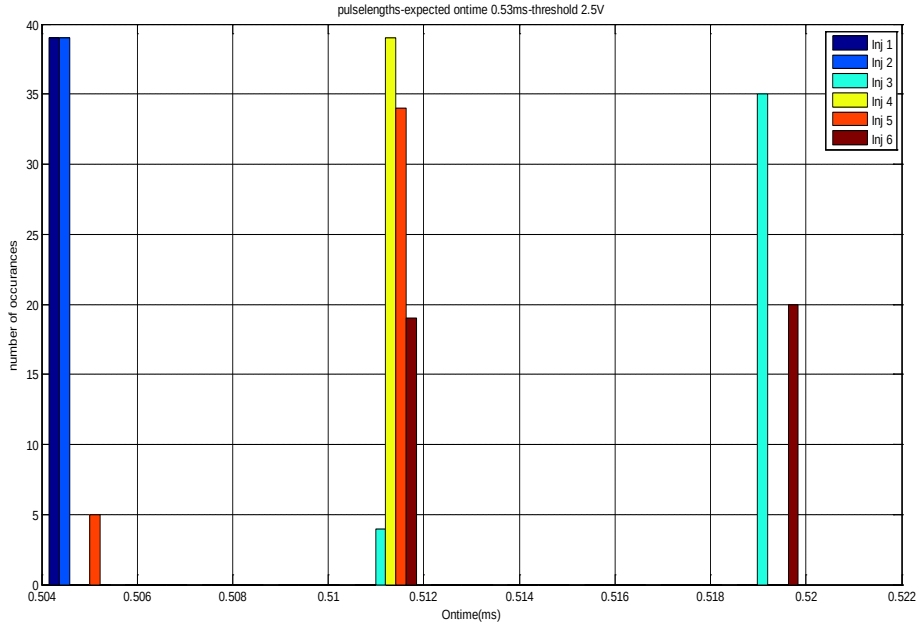

Figure A.39 Histogram of captured ontime (ms) with inductors with threshold at 2.5V

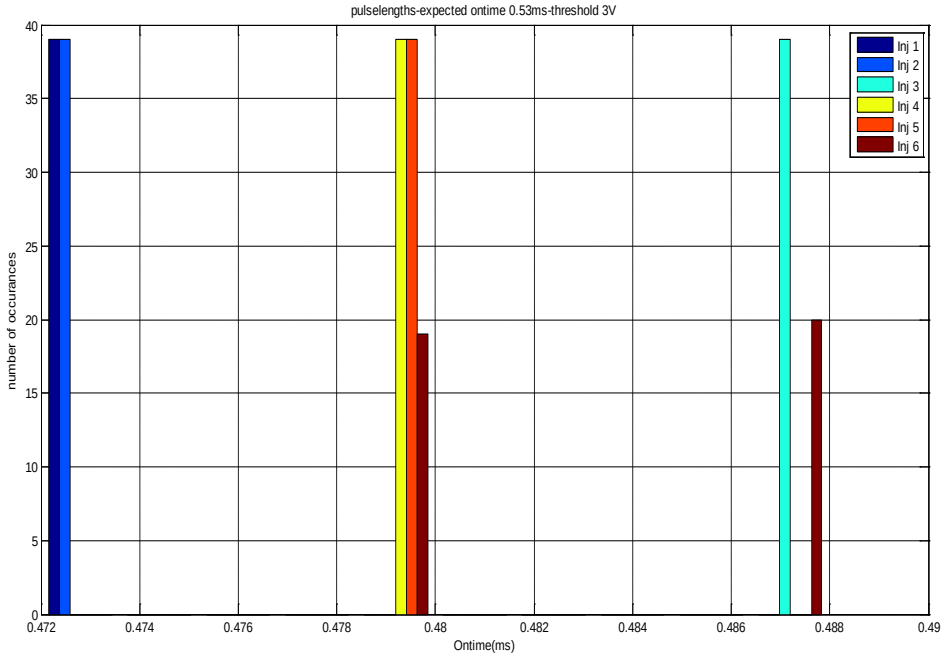

Figure A.40 Histogram of captured ontime (ms) with inductors with threshold at 3V